Microfabricated devices for the spatial and temporal control of the cellular and tissue microenvironment

BY

ELLY SINKALA
B.S., Vanderbilt University, 2008

THESIS

Submitted as partial fulfillment of the requirements for
the degree of Doctor of Philosophy in Bioengineering in the
Graduate College of the University of Illinois at Chicago, 2013

Chicago, Illinois

Defense Committee:

Dr. David Eddington, Advisor
Dr. Jun Cheng
Dr. Richard Magin
Dr. Mitchell Roitman, Psychology
Dr. David Featherstone, Biological Sciences

ACKNOWLEDGEMENTS

To my family. You are a source of love, guidance, and unlimited support.

TABLE OF CONTENTS

LIST OF TABLES

LIST OF FIGURES

LIST OF ABBREVIATIONS

PDMS	Polydimethylsiloxane
PS	Polystyrene
PEG	Polyethylene Glycol
PtOEPK	Platinum (II) octae-thylporphyrin ketone
mmHg	Millimeters of mercury
PtTFPP	Platinum porphyrin
I	Intensity
I_o	Intensity without quencher
MDCK	Madin-Darby canine kidney cells
FSCV	Fast-scan cyclic voltammetry
mFC	Macro flow cell
μFC	Micro flow cell
V	Volts
E_{app}	Applied potential
GUI	Graphical user interface

SUMMARY

The cell microenvironment is an integral component of cellular behavior. At a given moment, a cell is bombarded by signals and cues from the environment, which all are processed and integrated into specific behaviors. It is difficult examine how a particular cue affects a cell in its natural environment due to the interference of other signals. Therefore, the ability to control the microenvironment of cells and tissues is necessary to study cell interactions. Towards this end, four different devices were developed to aid in the study of cell and tissue behavior.

Oxygen-sensitive microwells are microfabricated polystyrene circular wells that are embedded with an oxygen responsive dye for the purpose of measuring the oxygen tension of isolated cell clusters. Here, both cell-cell interactions and oxygen levels are controlled or monitored by the device. Oxygen is critical in a number of cell pathways, but is often overlooked in cell culture. The device is a simple and quick method to measure the oxygen levels without disturbing the cells in culture. The microwells parameters such as depth and width are adaptable to specific experimental conditions, and the microwells are compatible with high-magnification modalities such as confocal microscopy.

The second device is a calibration tool for fast-scan cyclic voltammetry (FSCV), a commonly used analytical tool to measure chemical species. The microfluidic flow cell (μFC) is a tool that utilizes microfluidics to improve the electrode calibrations for FSCV. The μFC is simple device that switches between buffer and buffer with a known concentration of the analyte of interest – in this case dopamine - in a Y-channel. The ability to quickly switch solutions

yielded electrode calibrations with faster rise times and were more stable at peak current values. The μFC reduced the number of external electrical components previously needed for this calibration and produced linear calibrations over a range of concentrations. For proof of concept, an electrode calibrated with the μFC was used to measure changes in dopamine concentration of a rat undergoing behavioral tasks.

The last two devices stem from a common idea – the ability to precisely control chemical delivery to cells and tissues. The first device automates the delivery of chemicals to gain spatially and temporally control. Having this degree of control is important for a variety of studies from yeast chemotropism to neurotransmitter release. The device consists of six valve-actuated channels that are constructed with vias to allow chemical access to the environment. The program LabVIEW is used to determine the duration, repetition, and delay of chemical release. The device was utilized for the study of yeast chemotropism on agarose and was able to produce a consistent gradient that caused orientation of yeast cells towards the higher concentration end of the gradient.

Lastly, the final device is an expansion of the automated chemical delivery device. Instead of six vias for chemical access, the expanded device has an array of 192. This provides an even higher degree of control and allows for several chemicals to be studied in combination. A multiplexor is utilized to increase the number of vias to 192 while only requiring 24 off chip valves for control. A MATLAB GUI allows each individual via to be independently accessed and chemical delivery be independently controlled.

SUMMARY

Although these devices are look different on the surface, they share the common design principles such as laminar flow, spatial definition, and diffusion to exert specific constraints on the cell and tissue environment.

I. CHAPTER 1: OXYGEN-SENSITIVE MICROWELLS

1.1 Introduction

1.1.1 Microwell cell culture: controlled, high-throughput analysis of cell behavior

Microwell cell culture allows precise control of cellular microenvironments by physically isolating a defined number of cells in discrete wells. The number of cells trapped is dependent on microwell diameter, depth, and the seeding density. Microwell popularity is attributed to its relatively simple fabrication and the ability to conduct high-throughput analysis down to the single-cell level. Several biological studies utilize microwell cell culture to address a variety of unknown cell behavior and properties[1-5].

Microwells have been implemented as a technique to produce standardized embryoid bodies (EB) from embryonic stem (ES) cells. ES cells are of interest since they can differentiate to a number of cell types, which can be used for a variety of therapies[1, 2]. The elements in the microenvironment such as the cell-cell contacts or growth factors determine ES differentiation and previous methods to differentiate ES cells yielded non-uniform EBs[6]. Microwells can standardize these factors allowing more control over the process of differentiation and to determine the components necessary to produce optimal results.

Microwells are also utilized for high-throughput screening since the high volume of wells allows many experiments to be performed in parallel and the ability to image and track individual cell behavior over time. Areas that require high-throughput screening include drug toxicity studies[3, 4] where a large library of parameters are tracked and monitored and the cellular responses are recorded.

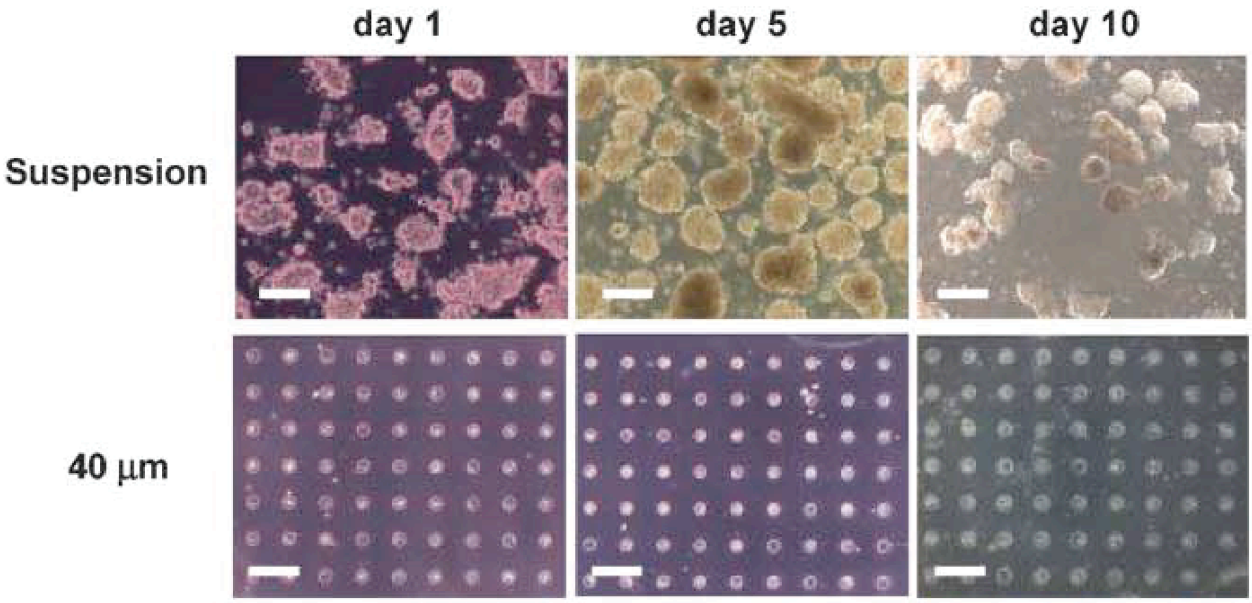

Figure 1.1 A comparison of EBs formed in suspension and in 40 micron microwells. The EBs produced in microwells exhibited near uniform shape and size. (reprinted from Karp et al., Lab Chip, 2007)

While the studies in the previous two examples are not related, they require similar specific conditions that are met with the implementation of microwells. These conditions are what distinguish microwell cell culture from standard cell culture.

1.1.2 Standard cell culture vs. microwell cell culture

Standard cell culture produces measurements that are averages of millions of individual responses and can provide misleading information on individual cell behavior due to cell heterogeneity even amongst cells of the same type [7]. In reality, a population of cells can provide a variety of distributions in cell behavior even when exposed to the identical environment. For example, a bimodal response may not be apparent if it analyzed as a population instead of on the single cell level as shown in Figure 1.2. Studying the cells at a singular level is essential for determining cells that are outliers in a population, which can be studied further to examine the cause of their differences.

Microwells simplify the analysis of individual cell response compared to standard cell culture by reducing the number of cell-cell contacts and limiting the number of cells in close proximity. Controlling these interactions is vital for applications ranging from tissue engineering to drug resistance [8, 9], where the efficacy of potential therapies are tested on relevant cell lines.

1.1.3 Previous iteration of microwells

Microwells have been constructed from a multitude of materials including but not limited to polydimethylsiloxane (PDMS) [10, 11], hydrogels [12-14], polystyrene (PS) [11, 15, 16], and photoresists [10, 11, 13]. PDMS is optically transparent, non-toxic, biocompatible, and moldable

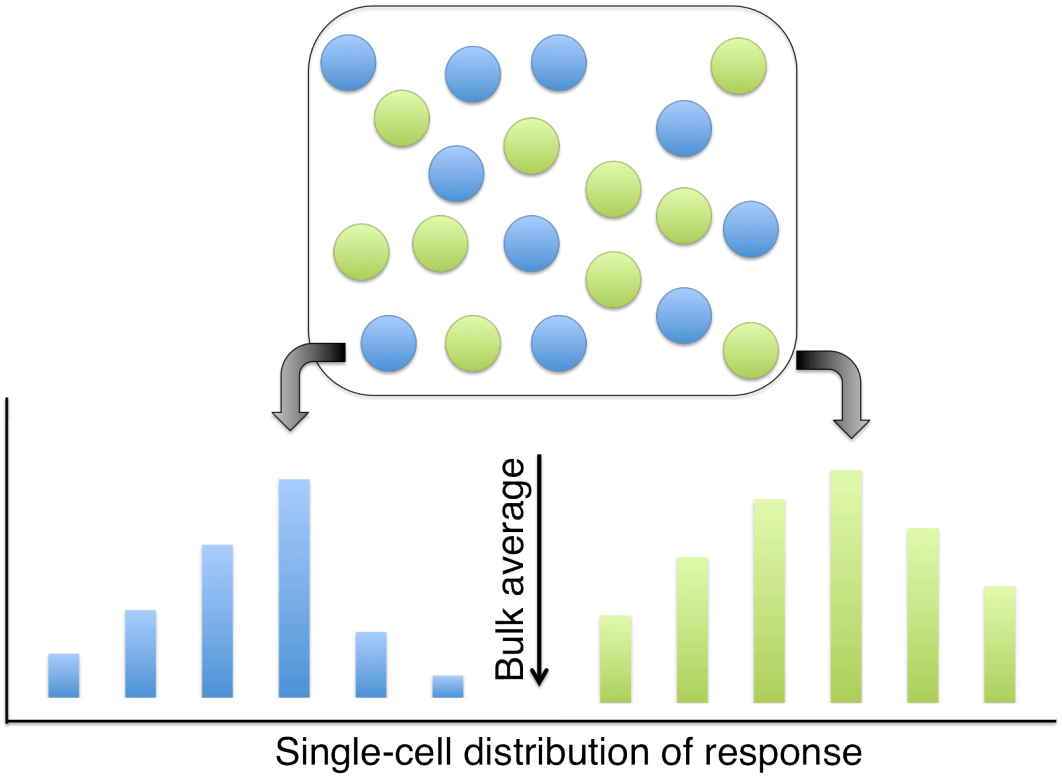

Figure 1.2 A population of cells of the same type can exhibit heterogeneous behavior. This schematic shows a population of cells represented as blue and green circles. If the population's response is average, the bimodal behavior of the population shown in the chart is lost.

making it suitable for microwell fabrication [17]. The microwells can be formed directly from a photoresist master, or a PDMS microstamp is used to form wells in uncured PDMS [10, 11]. The microwell array size and the individual diameters are tunable with the photoresist mold. However, PDMS is not an ideal substrate for cellular investigations due to the polymer's hydrophobicity, which absorbs many bioactive compounds present in the cell media[18]. Poly ethylene glycol (PEG) hydrogels are another popular microwell material composed of PEG-DA prepolymer that is molded into microwell arrays by PDMS stamps and subsequently crosslinked by UV light[12, 13]. PEG microwells can also be fabricated by selectively crosslinking PEG using a photomask [14]. PS is another substrate that is increasingly used in microwell work due to its extensive use in cell culture and is the standard material in cell culture dishes. The PS microwells can also be surface-treated similarly to standard culture dishes. Hot embossing thick PS films with a PDMS master under a load creates patterned microwells [11]. Pre-stressed polystyrene sheets can also be heated to create molds for PDMS or PEG microwells [15]. Although the microwells have various methods of construction, the commonality is the ability to provide a uniform environment and to exert spatial control over cells.

1.1.4 Oxygen monitoring in culture

The ability to monitor oxygen is an important yet often overlooked aspect of cell culture. Oxygen consumption is one indicator of metabolism and can reveal changes in the cell and its environment. Cell metabolic rate also influences other processes such as the production of reactive oxygen species and proliferation. Cells are usually exposed to ambient air or about 21%

oxygen during standard biological studies. However, cells normally do not experience oxygen tensions this high. This is particularly true for primary cells. It is common to see oxygen tensions of 90-110 mmHg (12-14%) O_2 for the brain[19], 27-49 mm Hg(3.6-6.4%) O_2 for bone marrow[20], and 30-90 mmHg (3.9-12%) O_2 for liver[21] in vivo. Figure 1.3 shows the growth suppression that occurs when cardio fibroblasts are exposed to three levels of oxygen (3,20,21) [22]. As the oxygen levels rise, the growth rate of the cells is reduced. When the cells that were previously exposed to 21% oxygen are exposed to 3%, growth rates were recouped as shown with the white bar. Incorporating oxygen sensors into cell culture substrates would provide a real time analysis of oxygen levels, which can relay the cell's condition. Measuring oxygen levels is also important as oxygen tensions vary dramatically between tissue types in vivo. It is essential to characterize various tissues' oxygen tensions when conducting oxygen-dependent experiments for the in vitro cells to exhibit behavior similar to in vivo. Furthermore, monitoring oxygen tension in cell culture is useful to determine if the cells are exposed to the appropriate oxygen levels, which can have an effect on the experimental outcome.

There are several variations of *in situ* oxygen sensors. Clark electrodes were previously used to measure oxygen tension of cell monolayer[23]. Unfortunately, these probes consume oxygen, which change the oxygen tension exposed to the cells. Also, the probes are not easily integrated into the cell culture setup for continuous measurement and the selective membrane is prone to fouling due to repeated cell exposure. Currently, commonly used sensors involve oxygen sensitive fluorophores embedded in a substrate. One method incorporates platinum porphyrin dye (PtTFPP) into PDMS thin films that are sandwiched between Teflon and another

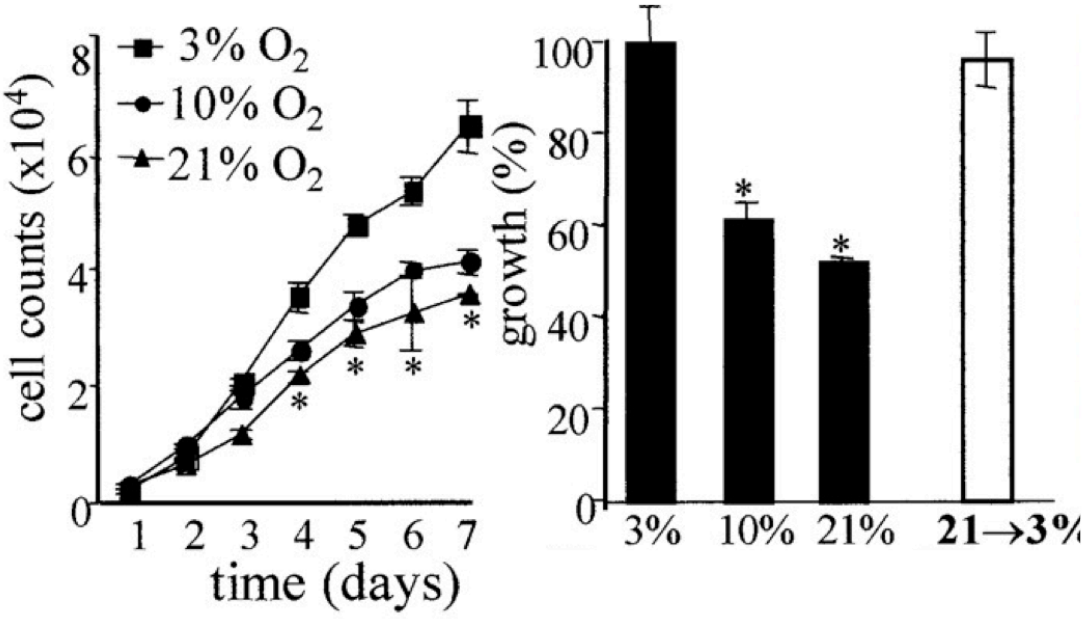

Figure 1.3 Cardio fibroblasts were cultured for seven days at 3,10, and 21 percent oxygen. The cells exhibited slower growth rates at higher oxygen concentrations. (reprinted from Roy et al., Cir Res, 2003)

layer of PDMS. The sensor detects changes in the oxygen tension through the PDMS layer where cells are attached[24].

Others have used nanosensors composed of oxygen–sensitive ruthenium (II) embedded in polystyrene nanobeads, which are attached to cells to monitor oxygen consumption directly[25]. For our oxygen-sensitive microwells, PtOEPK, a fluorophore that is quenched in the presence of oxygen reducing the intensity, is used as the oxygen sensor that is embedded in PS for immobilization[26] and is embossed with a PDMS stamp to form the microwells. PS becomes the cell substrate. PtOEPK is already commonly used in the food industry to determine the oxygen levels in prepackaged food such as produce or processed meat. A PtOEPK sensor placed in the food packaging and exposed to fluorescent light is a quick method to measure oxygen concentration to determine the rate of ripening or lipid oxidation of food[27].

We produced oxygen-sensitive microwells that house cells for culture and detect oxygen in a format compatible with high-resolution imaging as these wells were made on a coverglass substrate. Well depth was varied by changing the concentration of solvent in the PS solution. PS in contact with the PDMS master reduces the sensor thickness to approximately 75 μm making it compatible for high-resolution microscopic imaging of cells. The microwell design produced areas between the wells that were not in contact with the cells, which prevented fouling of the sensor. The sensors have the ability to monitor changes with a limited number of cells as a function of oxygen over a large area simultaneously.

1.2 Methods and materials

1.2.1 Fabrication of the PDMS embossing mold

A 3" silicon wafer was rinsed with acetone, isopropanol, and methanol and dried under nitrogen. Negative photoresist (SU-8 2150, MicroChem, MA) was spincoated to a thickness of 250 μm. The photoresist was prebaked at 65°C for 10 minutes and 95°C for 65 minutes. Photoresist was exposed to UV light of 390 mJ/cm^2 through photomask. Photoresist was post exposure baked at 65°C for 5 minutes and at 95°C for 25 minutes. Photoresist was developed in SU-8 developer, rinsed with isopropanol, and dried with nitrogen resulting in circular wells of a particular diameters ranging from 200-500 μm (Figure 1.4a). Developed photoresist was silanized with (Tridecafluoro 1, 2,2-tetrahydroctyl)-1-trichlorosilane (United Chemical Technologies, PA) vapor in a desiccator for 2 hours to facilitate PDMS casting and removing the many cast PDMS pillars from the many SU8 wells. PDMS prepolymer (Sylgard 184, Dow Corning, IL) was mixed 10:1(polymer:curing agent), degassed, and was poured onto the master (Fig. 1.4b). PDMS was cured on a 75°C hotplate for 2 hours. PDMS was removed from the SU-8 master to create a stamp to emboss PS/PtOEPK (Fig. 1.4c).

1.2.2 PS/PtOEPK patterning

A 35% w/w PS/toluene solution was composed of PS pellets (200,000 MW, Sigma-Aldrich, MO) dissolved in toluene (Sigma-Aldrich, MO). The solution was tightly sealed in a glass bottle to prevent toluene evaporation and was placed on a shaker for 24 hours for complete dissolution. PtOEPK was added at 1 mg/ml of PS/toluene solution and was dissolved. A coverglass was cleaned with acetone, methanol, and isopropanol and dried under nitrogen. A 400

μL volume of solution was pipetted onto a circle coverglass with a diameter of 25 mm and was set aside for 24 hours for complete toluene evaporation (Fig1.2.1d). The PS/toluene solution was exposed to light during the evaporation process to reduce the extent of photobleaching during experiments. The PDMS stamp was placed in contact with the PS-coated coverglass and placed on a 100^{o}C hot plate for 15 minutes. A weight of 3.0 kg was placed on the stamp to press the PDMS into the heated substrate (Fig.1.2.1e). The PDMS was cooled to room temperature and removed, revealing the microwells (Fig. 1.2.1f). The microwells were then released from the coverglass (Fig.1.2.1g). Microwells were prone to curling after removal. To create a flat substrate, the microwell discs were placed on an 85^{o}C hotplate and gently flattened. Next, the wells were plasma treated with a corona discharge device (BD-20AC, Electro-Technic, IL) to promote cell attachment; however, this step can be skipped if non-adherent cells will be used. For ease, the microwells were placed in a 6-well plate. A milliliter of PDMS was added to the bottom of the 6-well plate to "glue" the microwells to the plate and prevent movement. The microwells were sterilized in 70% ethanol for 20 minutes and were exposed to UV light at 254 nm in a biosaftey cabinet for at least 15 minutes prior to use in cell culture experiments.

1.2.3 Cell culture and staining

Madin-Darby Canine Kidney (MDCK) cells (ATCC, MD) were cultured in Dulbecco's Modified Eagles Medium (DMEM, Gibco) supplemented with 10% (vol/vol) Fetal Bovine Serum (Thermo Scientific HyClone, UT) and 1% of penicillin (10,000 U) and streptomycin (10mg/mL) (Sigma-Aldrich, MO). The cells were incubated at 37^{o}C with 5% CO_2. Cells were seeded by pipetting a concentration between 0.5-1$\times 10^7$ cells/mL on a square coverglass the width

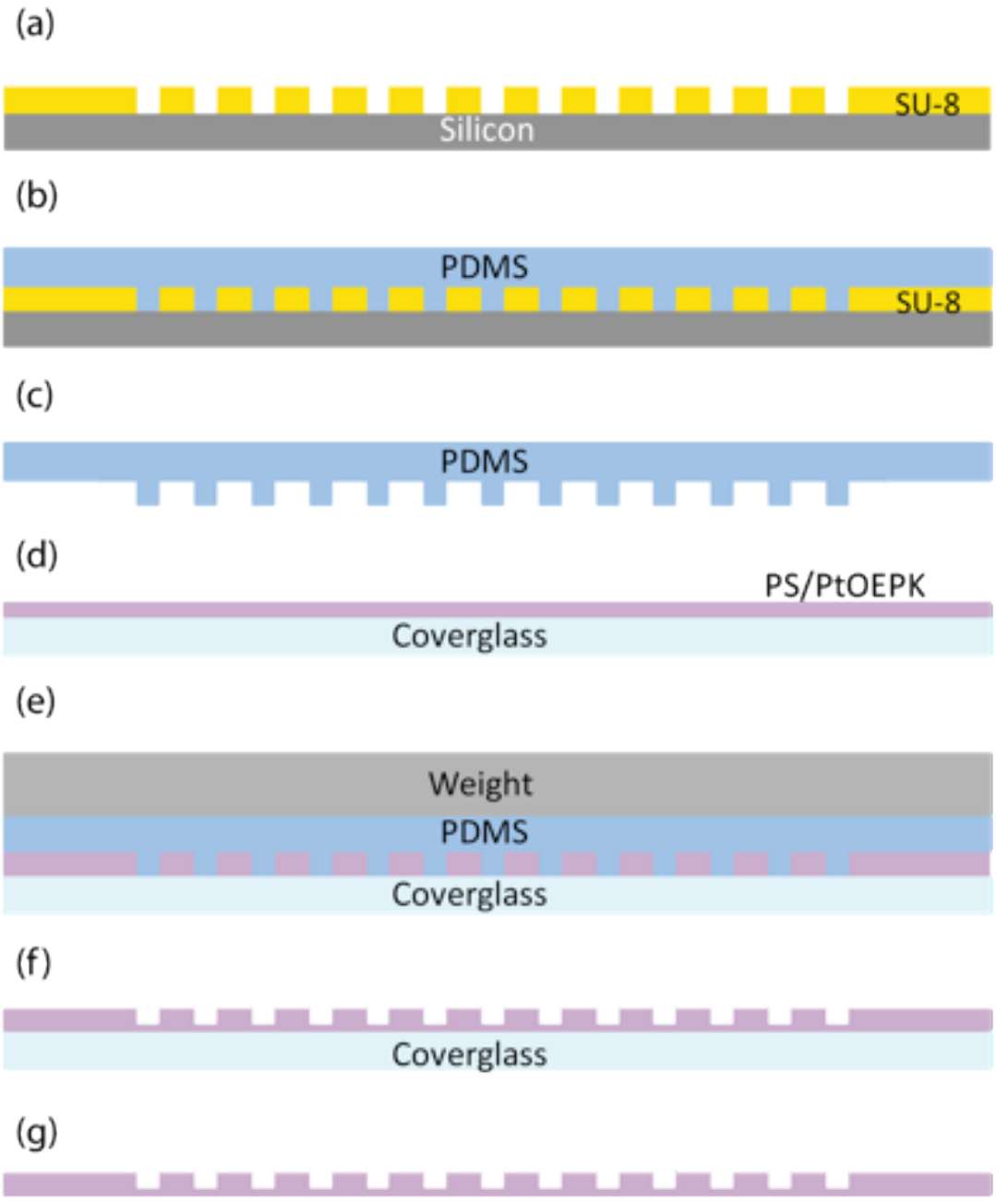

Figure 1.4 The fabrication process for the oxygen-sensitive microwells.

of the substrate. A cell loading technique was utilized to seed cells into the wells while removing excess cells from the surface. Wells containing media and cells were then placed into the incubator and subsequent media was not added until the cells attached to prevent dislodgement. Hoechst dye (Sigma-Aldrich, MO) was added at a concentration of 3 μg/μL to stain and count cells trapped in microwells. PtOEPK cytotoxicity was evaluated with a live/dead viability/cytotoxicity assay (Invitrogen, CA). MDCK cells were stained with a Rhodamin-phalloidin (Invitrogen, CA) to image the actin cytoskeleton.

1.2.4. Oxygen sensor calibration and microscopy

Oxygen sensitive microwells were calibrated by determining the corresponding fluorescent intensity at a particular oxygen level. Gases containing 21%, 10%, and 0% O_2 (100% N_2) were exposed to the microwell surface during fluorescent image acquisition, and the intensities were recorded. Images were obtained at the junction between four wells (Figure 1.3.1) to measure intensity changes. Ten measurements were made at various locations on a coverslip of microwells. An inverted fluorescent microscope (Olympus IX71, NY), a Hamamatsu camera (C8484-03001, Japan) fitted with a filter with an excitation/emission of 595/760 nm with a 620 nm dichroic mirror (Chroma, VT), and Metamorph (v7.63.10) were used for image acquisition and analysis. To determine sensor sensitivity, a Stern-Volmer plot was produced.

The Stern-Volmer relationship determines how the presence of one chemical species affects the decay rate of another chemical species. This is described by a simple equation below:

$$A^* + Q \rightarrow Q + A \quad \text{Eq. 1}$$

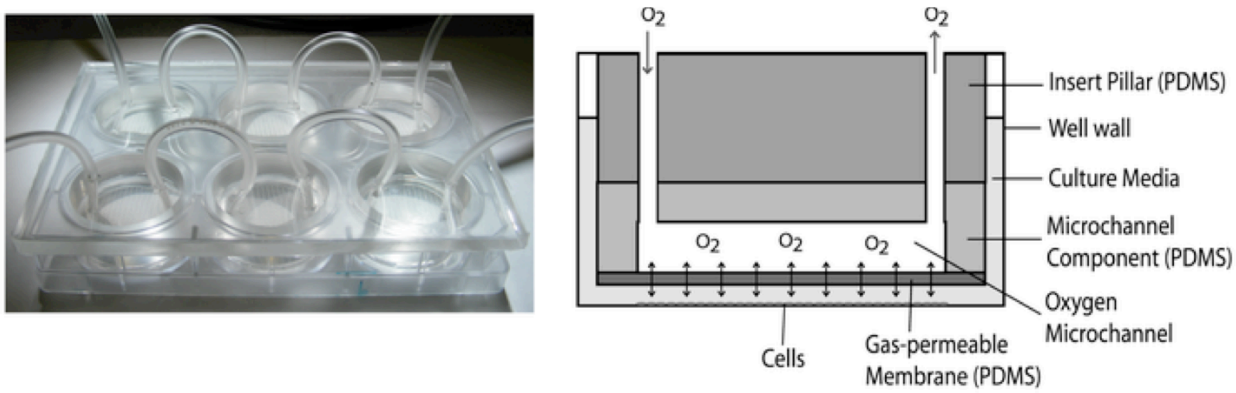

Figure 1.5 PDMS oxygen insert was used to calibrate the PtOEPK microwell sensors. Different concentrations of oxygen and their corresponding fluorescent intensities were used to determine the calibration curve.

where A* is a chemical species in its excited state. Q is the quencher that affects the decay rate of A, and A is the chemical species at its steady state. For the microwells, A* is the PtOEPK sensor in the absence of oxygen, which is the quencher (Q). The equation describing the kinetics of the quenching is:

$$\frac{I_f^o}{I_f} = 1 + k_q \tau_o \cdot [Q] \quad \text{Eq. 2}$$

where I_f^o is the intensity of the sensor without oxygen, I_f is the intensity of the sensor in the presence of oxygen, k_q is the quencher rate coefficient, τ_o is the fluorescence lifetime of A, and $[Q]$ is the concentration of oxygen present.

Since conditions can vary, the sensor sensitivity to oxygen is experimentally determined. Known concentrations of oxygen were exposed to the microwells using the 6-well PDMS oxygen inserts[28]. In Figure 1.5, the insert has a microfluidic gas network with a gas permeable membrane at the bottom. Gas is then flowed through the device to the network where the gas is diffused through the membrane. The PtOEPK sensor sitting on the opposite side of the network is exposed to the diffused gas. Subsequently, the fluorescent intensity is measured and the data was linearly fit to create the concentration curve.

1.3 Results

1.3.1 Microwell patterning with PDMS mold

PtOEPK-embedded PS was utilized when creating the microwell sensor. Figure 1.6a shows a brightfield image of 500 μm diameter microwells on a glass cover slip with the inset

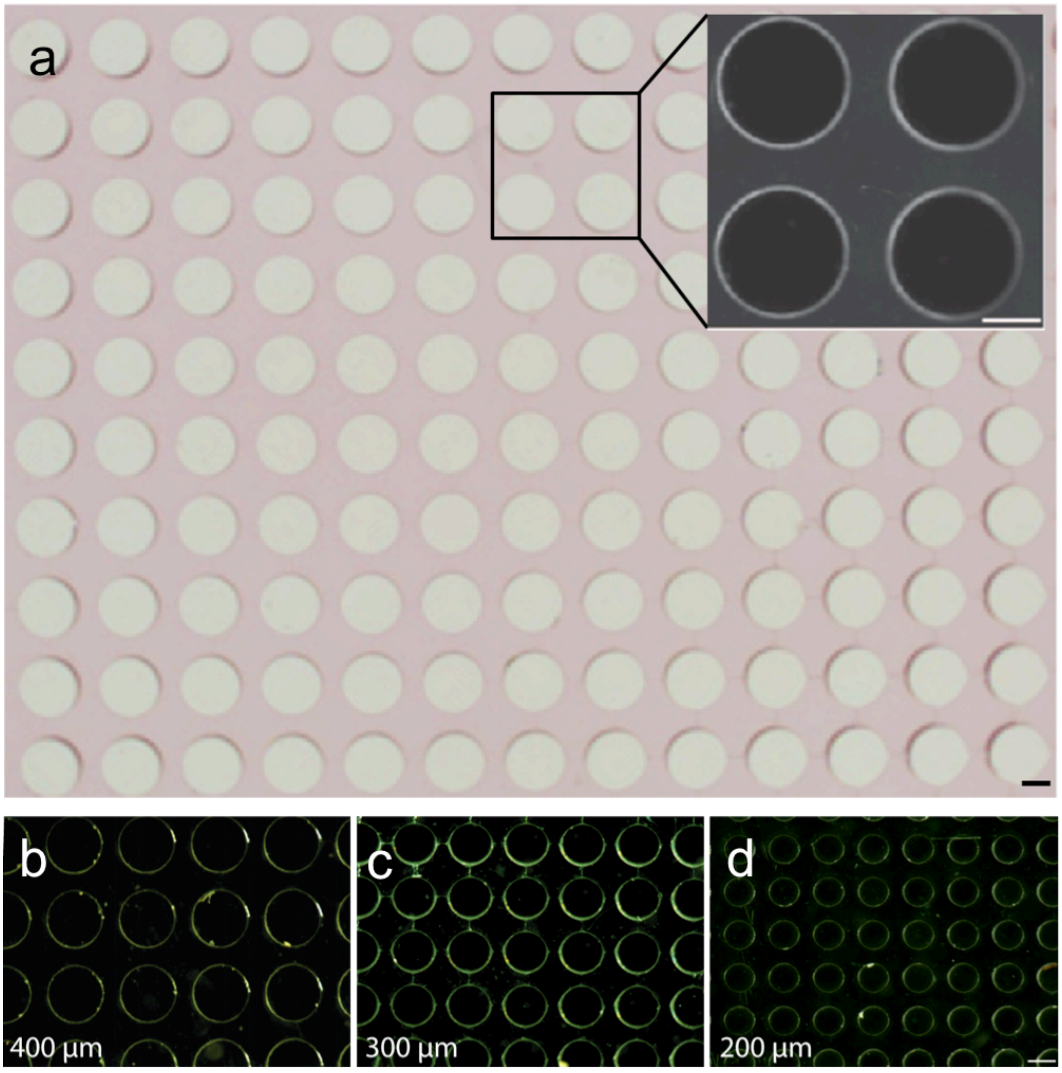

Figure 1.6 PS/PtOEPK thin films were embossed to form uniform 500 µm diameter microwells. (a) A brightfield image of the oxygen-sensitive microwells. Scale bar is 1 mm. The insert is a view of the same well fluorescing under 21% oxygen. Well diameters vary by changing the PDMS stamp diameter depending on the application. Wells of (b) 400 µm, (c) 300 µm, and (d) 200 µm are shown.

showing the fluorescence of these microwells at 595 nm excitation and 760 nm emission at 21% oxygen. PtOEPK/PS embossing is a flexible technique and can be adapted to specific experimental conditions. To demonstrate this, well sizes were altered by using PDMS stamps of different diameters ranging from 100-500 μm. The patterning technique reliably produced wells down to 100 μm. However, microwells produced at diameters lower that 100 μm became inconsistent. The posts of the microwells were about 300 μm tall. As the diameter of the microwell reduced, the aspect ratio increased, and it became more difficult to produce the wells since the higher aspect ratio posts were more likely do deform under pressure and heat. Varying the concentration of PS dissolved in toluene altered sensor thickness. Higher PS concentration resulted in deeper wells, and conversely, lower PS concentration produced shorter wells. Figure 1.7 shows the corresponding well depth for a particular PS concentration. PtOEPK/PS is only 75 μm thick at the bottom of wells, which maintains a transparent surface necessary for microscopy. High magnification modalities, such as the confocal microscope, require thin cover slips to mount specimens, and the coat of PS/PtOEPK at the bottom is minimal thickness making it compatible with high-resolution microscopy.

1.3.2 Cellular experiments with microwells characterization

Depending on the experiment conducted, the required number of cells trapped in an individual microwell can vary. Studying the heterogeneity of a population usually requires single cells to be deposited into each microwell so that differences in the subsequent progeny can be measured and compared. Where as the production of cell clusters, as seen when creating embryoid bodies or islets, need a larger number of cells trapped for cluster formation. To

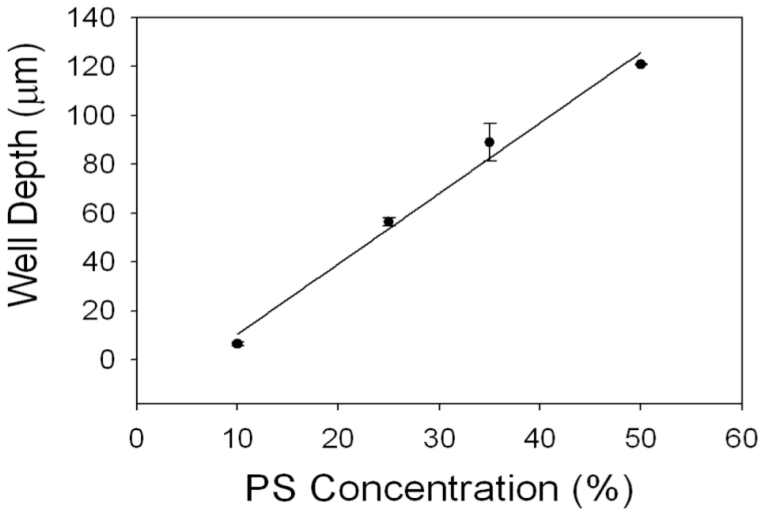

Figure 1.7 The well depths for 10, 25, 35, and 50 percent PS in toluene solution were 6.5 μm, 56.4 μm, 91.8 μm, and 120.9 μm respectively. The data represents the mean of three experiments with error bars representing the standard deviation.

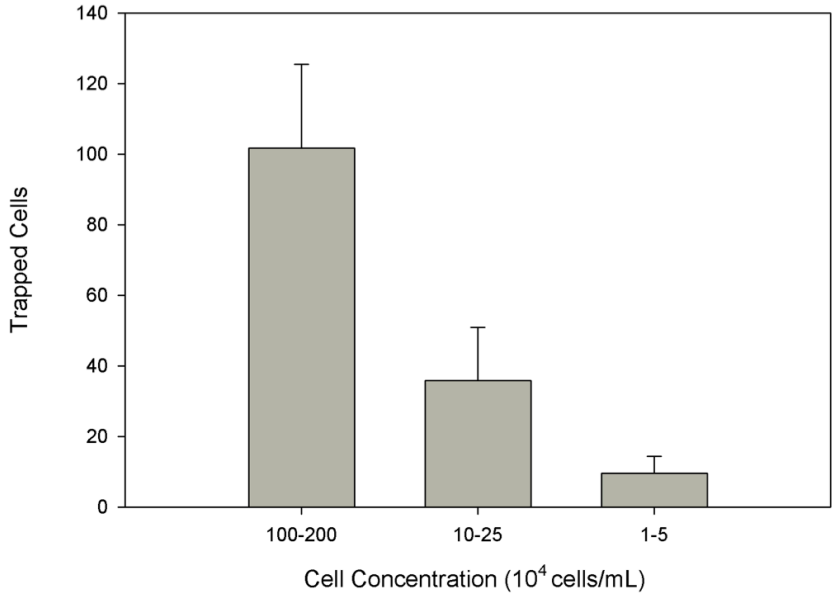

Figure 1.8 Microwells seeded with cell concentrations of 1-5x10^4 cells/mL, 1-2.5x10^5 cells/mL, and 1-2x10^6 cells/mL trapped 101±24, 36±15, and 9±5 cells respectively.

determine the ideal cell concentration for a particular number of trapped cells, different cell concentrations were seeded into the microwells and the number of cells trapped was counted. A separate 25 mm "microwell disk" housing 500 μm diameter microwells was used with each different concentration. The microwells were seeded with a range of cell concentrations and the average number of cells trapped is displayed in Figure 1.8. Concentrations of 1-5x10^4 cells/mL, 1-2.5x10^5 cells/mL, and 1-2x10^6 cells/mL trapped 101±24, 36±15, and 9±5 cells respectively.

The PS in microwells creates a matrix and immobilizes PtOEPK. However, since the cells are in direct contact with the sensor, the biocompatibility of PtOEPK was determined. Trapped cells were monitored and exhibited normal growth and proliferations a confirmed in Figure 1.9a and 1.9b, which displays cells 1 hour and 2 days after seeding (stained with calcein AM). The plasma-treated microwells created a substrate for cell attachment and spreading. For more quantitative analysis of PtOEPK cytotoxicity, a live/dead assay was performed on the cells growing in the microwells. After a week in culture, cells trapped in oxygen sensitive microwells in Figure 1.9c and 1.9d maintained viability confirmed by the uptake of only the calcein AM dye and limited uptake of the EthD-1 dye. A control was created by trapping cells in microwells made without PtOEPK as shown in Figure 1.9e and 1.9f. PtOEPK excitation wavelength overlaps with EtD-1 causing the microwell to fluoresce in Figure 1.9d. Microwells with and without the sensor had 93% and 95% viability respectively, and there was no statistical difference confirming the suitability of wells for short-term cell culture.

The PS thickness at the bottom of the microwell measured 75 μm, which is suitable for high magnification microscopy such as confocal. Figure 1.10a shows a confocal image of

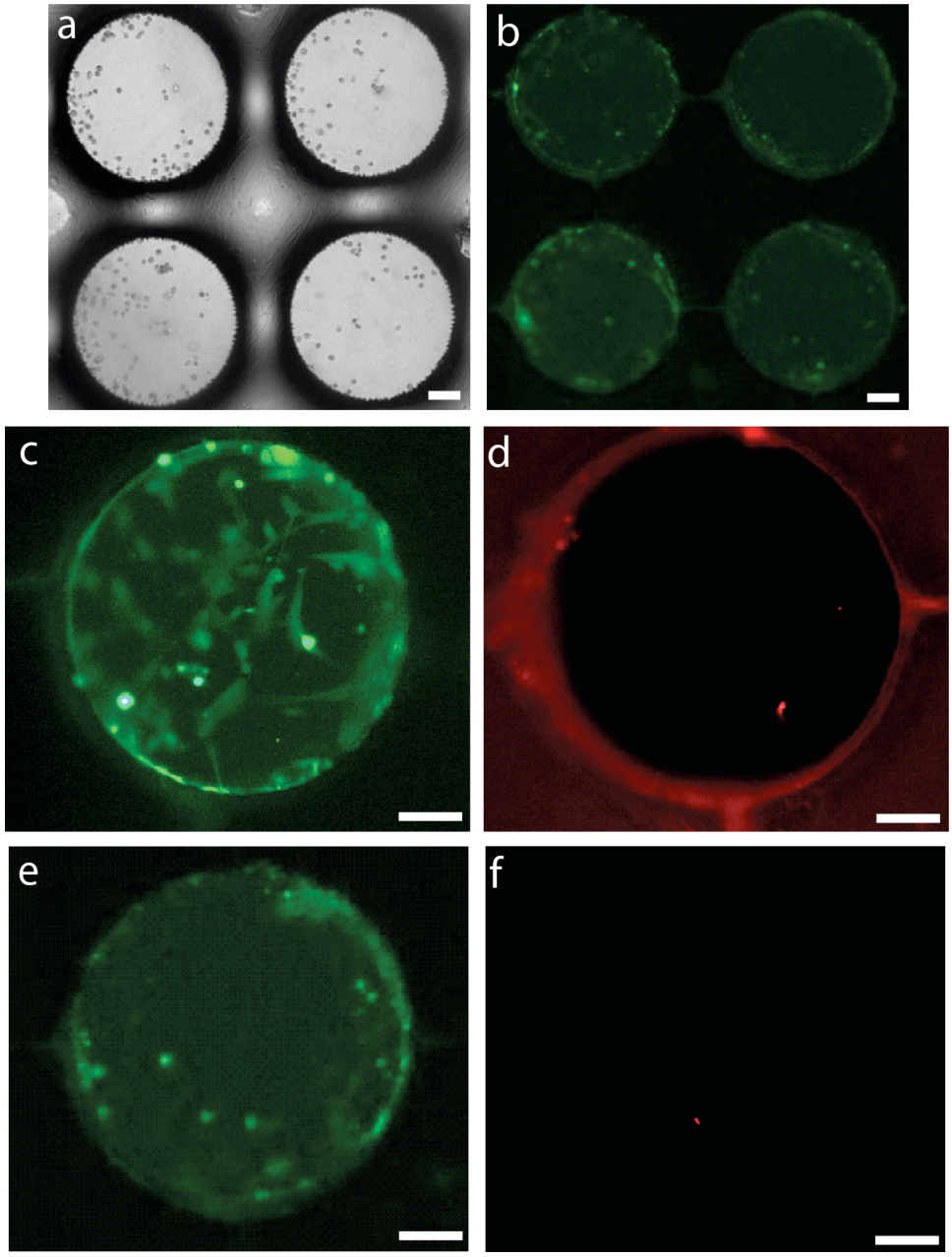

Figure 1.9 Live/dead assay was performed on cells growing in the microwells. Trapped cells were imaged (a) 1 hour and (b) 2 days after seeding. Cells were confined to the wells and exhibited normal growth and proliferation. Scale bar 100 μm. MDCK stained with (c) calcein AM (live) and (d) EtD-1 (dead) in microwells with PtOEPK. A control was created by trapping cells in microwells without PtOEPK and stained with (e) calcein AM and (f) EtD-1. There was limited uptake of EtD-1 confirming PtOEPK's low toxicity is appropriate for short-term cell culture.

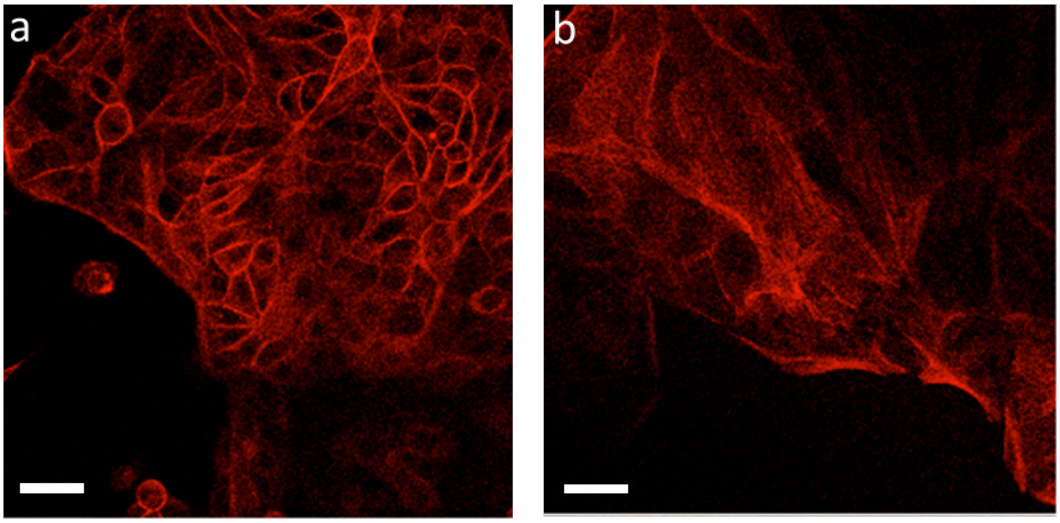

Figure 1.10 The actin cytoskeleton of MDCK cells was stained with with rhodamine-conjugated phalloidin to visualize the actin. Cell undergoing proliferation (Figure 1.10a) and spreading (Figure 1.10b) were imaged. The scale bars are 50 μm and 20 μm respectively.

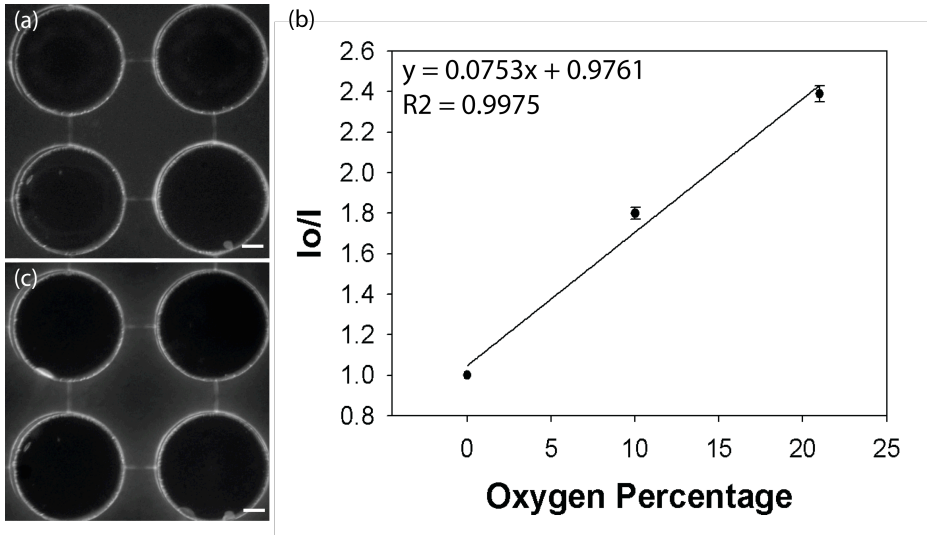

Figure 1.11 Microwells were exposed to (a) 21% oxygen and (c) 0% oxygen (100% nitrogen) and changes in fluorescent intensity were monitored. Oxygen measurements were performed in the center of the four wells. A Stern-Volmer plot describes the relationship between a chemical species (PtOEPK) and its quencher (oxygen) in Fig. 1.3.3b. At 35%, the Stern-Volmer slope was .0753, and a concentration of 21% oxygen yielded a 2.5 increase in the intensity as compared to 0% O_2. Scale bars are 100 μm.

MDCK cells stained with rhodamine-conjugated phalloidin to visualize the actin. Figure 1.10b is a magnified view of the cells in the microwell.

1.3.3 PtOEPK characterization

The sensitivity of the microwells is dependent on two conditions: the concentration of PtOEPK and PS thickness. There is a trade off between sensor sensitivity and PS thickness. A thinner PS/PtOEPK results in higher sensitivity since the PtOEPK dye is more likely to be exposed at surface and interact with the oxygen molecules than compared to thicker films where the PtOEPK is more likely to immobilized[26]. For our application, a 35% (w/w) solution of PS and toluene was used to achieve deeper wells to contain the cells. However, the concentration and the resulting thickness used are dependent upon the size of the cells and application. Figure 1.11a and 1.11c displays changes in fluorescent intensity of 35% (w/w) microwells exposed 0% oxygen (100% nitrogen) and 21% oxygen. Oxygen measurements were performed in the center of the four wells, and ten locations on the microwell chip were measured. A Stern-Volmer plot describes the relationship between a chemical species (PtOEPK) and its quencher (oxygen)[28], and this was used to determine the change in intensity relative to oxygen and PS concentration in Fig. 1.11b. At 35%, the Stern-Volmer slope was .0753, and a concentration of 21% oxygen yielded a 2.5 reduction in the intensity as compared to 0% O_2.

1.3.4 Microwell sensor oxygen measurements

The beginning of the chapter focused on utilizing the microwells as a method to measure exogenous oxygen that is inputted into the system. However since the sensor is sensitive to

ambient oxygen concentration, is it possible for the microwells to detect changes in the microenvironment of the cells in different conditions? To test the microwells' ability to sense environmental changes, the oxygen levels of trapped cells at different concentrations were monitored. One coverslip with 500 μm diameter microwells were seeded with MDCK cells at a high density (330 cells/well) and another coverslip at a low density (20 cells/well). MDCK cells were selected due to their high aerobic activity[29]. Oxygen-sensitive microwells were calibrated as previously described to determine the Stern-Volmer curve. The measurement locations used during calibration were re-measured with the addition of cells. Coverslips were placed in a six well plate and stored in an incubator. Fluorescent images were captured after 12 hours. High-density wells had an oxygen level of 12.6±0.77% where as low density wells exhibited an oxygen level of 19.5±0.47%, which was 35.7% higher than the high density seeding as shown in Figure 1.12. Thus, microwells with a lower cell density resulted in a lower rate of oxygen consumption, which maintained a higher oxygen level.

1.4 Discussion

An advantage of the technique presented is the combination of the sensor and the substrate, which simplifies the fabrication process. Previous methods for combining sensors on substrates deposited multiple layers of the sensor and substrate for cell attachment requiring intricate fabrication or multiple photolithographic steps to fabricate the designs[11]. PS dissolved in toluene made embossing manageable since the solution was easily deposited as a thin film onto a coverglass, and very minimal heat and pressure was required to generate the patterns. Plasma-treated PS is compatible with adherent cell culture eliminating the need to adsorb

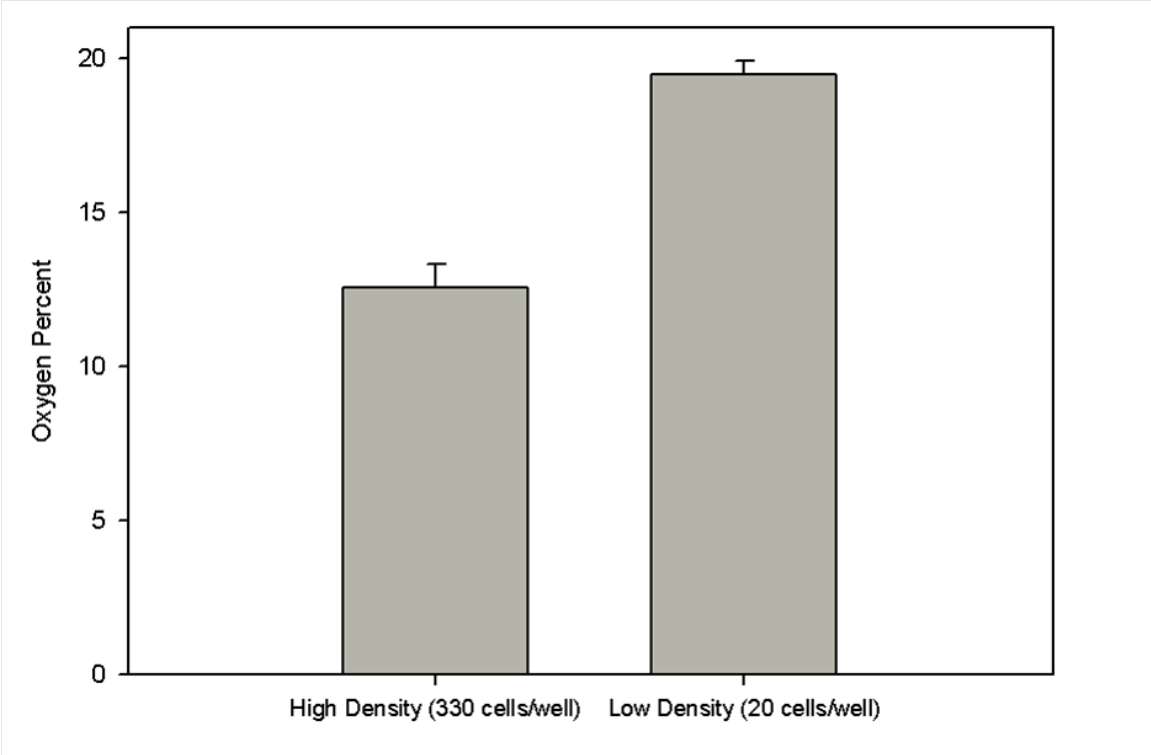

Figure 1.12 The oxygen concentration was measured at the microwells' surface. High-density microwells exhibited an oxygen level of 12.6±0.77% where as low density wells exhibited an oxygen level of 19.5±0.47%, which was 35.7% higher than high density seeding. The heights of the bars are the mean of three independent experiments with 6 oxygen measurements at each experiment with error bars representing the standard deviation.

proteins and other components for cell attachment. In addition, non-adherent cell types can also be used without this plasma treatment step, which will block adhesion to the substrate. MDCK cells seeded in the wells exhibited normal attachment and spreading shown in Figure 1.9c when pretreated with oxygen plasma. Since the cytotoxicity of PtOEPK with direct was unknown, a live/dead assay determined that PtOEPK was safe for a short-term cell culture period of 1 week. However, for experiments longer than 1 week, the PtOEPK may leach out and cytotoxicity would have to be reassessed.

This technique is easily adaptable to various experimental conditions. Well depth was determined by the PS concentration used, and well diameter was varied by the diameter of the PDMS stamp. It is a robust technique, and the PDMS stamp was reused at least 20 times without pattern deterioration. The microwell design created distinct locations for oxygen measurements on the chip between the wells where the sensor is in the proximity (within 500 μm) of the cells without being directly exposed to the cells, which would generate optical interference of the fluorescence intensity. Well depth can be easily adjusted by altering the dissolution conditions for a particular cell type, as larger cells require deeper wells for trapping. This adaptability creates a variety of applications that would benefit from oxygen monitoring ranging from single cell analysis to developing standardized embryoid bodies both of which have been previously demonstrated. Previous studies have also measured the stability of PtOEPK and its low susceptibility to photobleaching, which makes it ideal for extended experiments[30]. While there are certainly other simple microwell fabrication strategies[15] with their unique advantages none combine oxygen sensors on coverglass substrates. Most importantly, the oxygen sensitivity can be locally measured by measuring the intensity between four wells. A 2 cm^2 area on a substrate

contains over a hundred sensor regions, making the ability to gather multiple data points across a large substrate a simple and straightforward task.

A cell's oxygen tension plays a critical role in cell behavior. Thus, measuring oxygen tension can provide additional information about how a cell responds to various oxygen concentrations or how a change in oxygen affects a cell process. This is demonstrated in Fig. 1.12 where MDCK cells at high density had a 35.7% decrease in oxygen tension than low-density wells. The ability to monitor the oxygen tension is especially important in cell processes involving growth and development. As stated previously, experiments are normally performed at ambient air (21% oxygen) can cause cell behavior to deviate from in vivo. Oxygen is an important element in embryonic stem and progenitor cell development where areas of low oxygen tension drive differentiation[31]. For example, oxygen can control the differentiation of mesenchymal stem cells where an oxygen level of 3% maintains their undifferentiated state[32]. In addition, an oxygen-deficient environment also drives vascularization of mammalian embryos[33, 34]. Oxygen-dependent factors such as VEGF and HIF-1 help to produce blood vessels in areas of low oxygen tension [35-37]. A possible application of oxygen-sensitive microwells is monitoring the degree of differentiation at specific levels of oxygenation to determine optimal parameters. This is also applicable for the study of vascularization in an embryo. In addition to the oxygen sensor, the capability of high magnification microscopy due to the thin substrate enables the ability to monitor the cell's intracellular responses to oxygen or monitor any changes in conjunction with oxygen consumption. Microwells suitable for high magnification microscopy could monitor the stem cells phenotypic changes such as the appearance of lipid-filled vacuoles during adipogenic differentiation[38]. The microwells are

compatible for small working distances commonly seen with high magnification modalities such as the confocal microscope. In addition, the microwells are able to simultaneously assess oxygen conditions in addition to other standard cellular fluorescent assays.

1.5 Conclusion

The method reported in this paper provides a simple and efficient way to construct PS is a suitable cell culture material, and PS film thickness is easily adjustable by simply changing the concentrations. The ability to tailor the geometric parameters of the wells while incorporating an oxygen sensor makes it flexible for various experiments and other applications. The microwells allow simultaneous monitoring of oxygen levels during experiments. Oxygen-sensitive microwells could be a simple and useful biological tool that can be incorporated into the standard biomedical research lab.

REFERENCES

1. Thomson, J.A., et al., *Embryonic Stem Cell Lines Derived from Human Blastocysts.* Science, 1998. **282**(5391): p. 1145-1147.
2. Watt, F.M., Hogan, and B.L. M., *Out of Eden: Stem Cells and Their Niches.* Science, 2000. **287**(5457): p. 1427-1430.
3. Fernandes, T.G., et al., *High-throughput cellular microarray platforms: applications in drug discovery, toxicology and stem cell research.* Trends in Biotechnology, 2009. **27**(6): p. 342-349.
4. Kang, G., et al., *Agarose microwell based neuronal micro-circuit arrays on microelectrode arrays for high throughput drug testing.* Lab Chip, 2009. **9**(22): p. 3236-42.
5. Karp, J.M., et al., *Controlling size, shape and homogeneity of embryoid bodies using poly(ethylene glycol) microwells.* Lab Chip, 2007. **7**(6): p. 786-94.
6. Keller, G.M., *In vitro differentiation of embryonic stem cells.* Curr Opin Cell Biol, 1995. **7**(6): p. 862-9.
7. Carlo, D.D. and L.P. Lee, *Dynamic Single-Cell Analysis for Quantitative Biology.* Analytical Chemistry, 2006. **78**(23): p. 7918-7925.
8. Albrecht, D.R., et al., *Probing the role of multicellular organization in three-dimensional microenvironments.* Nat Meth, 2006. **3**(5): p. 369-375.
9. Alberts, D.S., *Tumor heterogeneity and extreme drug resistance: meet your match!* Cancer J Sci Am, 1998. **4**(1): p. 25-6.

10. Rettig, J.R. and A. Folch, *Large-Scale Single-Cell Trapping And Imaging Using Microwell Arrays.* Analytical Chemistry, 2005. **77**(17): p. 5628-5634.

11. Ochsner, M., et al., *Micro-well arrays for 3D shape control and high resolution analysis of single cells.* Lab on a Chip, 2007. **7**(8): p. 1074-1077.

12. Cordey, M., et al., *Enhancing the reliability and throughput of neurosphere culture on hydrogel microwell arrays.* Stem Cells, 2008. **26**(10): p. 2586-94.

13. Lindström, S., et al., *High-Density Microwell Chip for Culture and Analysis of Stem Cells.* PLoS ONE, 2009. **4**(9): p. e6997.

14. Revzin, A., R.G. Tompkins, and M. Toner, *Surface Engineering with Poly(ethylene glycol) Photolithography to Create High-Density Cell Arrays on Glass.* Langmuir, 2003. **19**(23): p. 9855-9862.

15. Nguyen, D., et al., *Tunable shrink-induced honeycomb microwell arrays for uniform embryoid bodies.* Lab on a Chip, 2009. **9**(23): p. 3338-3344.

16. Gallego-Perez, D., et al., *High throughput assembly of spatially controlled 3D cell clusters on a micro/nanoplatform.* Lab on a Chip, 2010. **10**(6): p. 775-782.

17. Sia, S.K. and G.M. Whitesides, *Microfluidic devices fabricated in Poly(dimethylsiloxane) for biological studies.* ELECTROPHORESIS, 2003. **24**(21): p. 3563-3576.

18. Regehr, K.J., et al., *Biological implications of polydimethylsiloxane-based microfluidic cell culture.* Lab on a Chip, 2009. **9**(15): p. 2132-2139.

19. Erecińska, M. and I.A. Silver, *Tissue oxygen tension and brain sensitivity to hypoxia.* Respiration Physiology, 2001. **128**(3): p. 263-276.

20. Lennon, D.P., J.M. Edmison, and A.I. Caplan, *Cultivation of rat marrow-derived mesenchymal stem cells in reduced oxygen tension: Effects on in vitro and in vivo osteochondrogenesis.* Journal of Cellular Physiology, 2001. **187**(3): p. 345-355.

21. Aller, M.-A., et al., *Plasma redox status is impaired in the portacaval shunted rat - the risk of the reduced antioxidant ability.* Comparative Hepatology, 2008. **7**(1): p. 1.

22. Roy, S., et al., *Oxygen Sensing by Primary Cardiac Fibroblasts.* Circulation Research, 2003. **92**(3): p. 264-271.

23. Mamchaoui, K. and G. Saumon, *A method for measuring the oxygen consumption of intact cell monolayers.* American Journal of Physiology - Lung Cellular and Molecular Physiology, 2000. **278**(4): p. L858-L863.

24. Thomas, P.C., et al., *A Noninvasive Thin Film Sensor for Monitoring Oxygen Tension during in Vitro Cell Culture.* Analytical Chemistry, 2009. **81**(22): p. 9239-9246.

25. Kuang, Y. and D.R. Walt, *Detecting oxygen consumption in the proximity of Saccharomyces cerevisiae cells using self-assembled fluorescent nanosensors.* Biotechnology and Bioengineering, 2007. **96**(2): p. 318-325.

26. Nock, V., R.J. Blaikie, and T. David, *Patterning, integration and characterisation of polymer optical oxygen sensors for microfluidic devices.* Lab on a Chip, 2008. **8**(8): p. 1300-1307.

27. Smiddy, M., et al., *Use of oxygen sensors for the non-destructive measurement of the oxygen content in modified atmosphere and vacuum packs of cooked chicken patties; impact of oxygen content on lipid oxidation.* Food Research International, 2002. **35**(6): p. 577-584.

28. Oppegard, S.C., et al., *Modulating Temporal and Spatial Oxygenation over Adherent Cellular Cultures.* PLoS ONE, 2009. **4**(9): p. e6891.

29. Lynch, R.M. and R.S. Balaban, *Energy metabolism of renal cell lines, A6 and MDCK: regulation by Na-K-ATPase.* American Journal of Physiology - Cell Physiology, 1987. **252**(2): p. C225-C231.

30. Lam, R.H.W., M.-C. Kim, and T. Thorsen, *Culturing Aerobic and Anaerobic Bacteria and Mammalian Cells with a Microfluidic Differential Oxygenator.* Analytical Chemistry, 2009. **81**(14): p. 5918-5924.

31. Simon, M.C. and B. Keith, *The role of oxygen availability in embryonic development and stem cell function.* Nat Rev Mol Cell Biol, 2008. **9**(4): p. 285-296.

32. Fehrer, C., et al., *Reduced oxygen tension attenuates differentiation capacity of human mesenchymal stem cells and prolongs their lifespan.* Aging Cell, 2007. **6**(6): p. 745-757.

33. Mitchell, J.A. and J.M. Yochim, *Intrauterine oxygen tension during the estrous cycle in the rat: its relation to uterine respiration and vascular activity.* Endocrinology, 1968. **83**(4): p. 701-5.

34. Rodesch, F., et al., *Oxygen measurements in endometrial and trophoblastic tissues during early pregnancy.* Obstet Gynecol, 1992. **80**(2): p. 283-5.

35. Maltepe, E., et al., *Abnormal angiogenesis and responses to glucose and oxygen deprivation in mice lacking the protein ARNT.* Nature, 1997. **386**(6623): p. 403-407.

36. Ramírez-Bergeron, D.L., et al., *HIF-Dependent Hematopoietic Factors Regulate the Development of the Embryonic Vasculature.* Developmental Cell, 2006. **11**(1): p. 81-92.

37. Iyer, N.V., et al., *Cellular and developmental control of O2 homeostasis by hypoxia-inducible factor 1α.* Genes & Development, 1998. **12**(2): p. 149-162.

38. Pittenger, M.F., et al., *Multilineage potential of adult human mesenchymal stem cells.* Science, 1999. **284**(5411): p. 143-7.

II. CHAPTER 2: ELECTRODE CALIBRATION WITH A MICROFLUIDIC FLOW CELL FOR FAST-SCAN CYCLIC VOLTEMMETRY

2.1 Introduction

2.1.1 Fast-scan cyclic voltammetry as an analytical method for chemical detection

Fast-scan cyclic voltammetry (FSCV) is a common analytical electrochemistry tool that has more recently been applied to investigate the role of neurotransmitters in awake and behaving subjects[1-3]. Its ability to detect chemical changes with high temporal and spatial resolution accounts for its prevalence in measuring neurotransmitters such as dopamine (DA) in awake and behaving animals (*in vivo*)[4, 5]. FSCV is an integral tool for understanding drug mechanisms and animal models involved with dopamine release[6].

The sub-second temporal resolution of FSCV is attributed to the interaction between the carbon-fiber microelectrode and the dopamine in solution. A driving voltage is rapidly applied to a carbon fiber electrode that is exposed to DA in solution. DA that is adsorbed on the electrode surface undergoes oxidation and reduction, which produces a current that is measured[7]. The production of the current is described in Figure 2.1 where the release of electrons is produced during the oxidation-reduction process.

Electroactive species are identified by their current by voltage plots; for the neurotransmitter DA, the current at the potential that evokes peak oxidative current is directly proportional to concentration[1]. Electrodes are used acutely and must be calibrated after use to relate concentration to observed current. The calibration process involves a carbon fiber electrode that is exposed to several concentrations of DA and the corresponding current responses are recorded

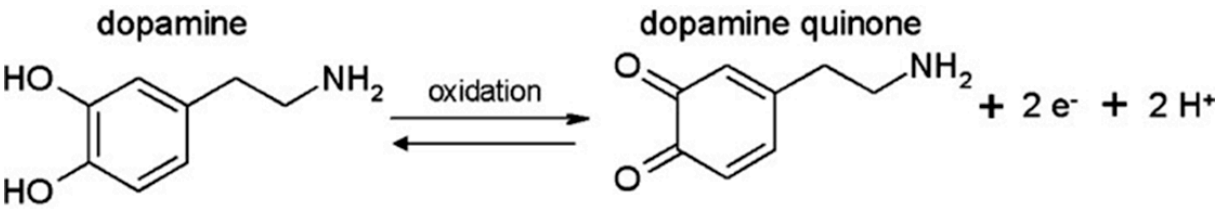

Figure 2.1 The oxidation of DA produces electrons that are adsorbed onto the surface of the electrode tip, which produces an increase in current. As the electrode is exposed to the negative voltage ramp, dopamine quinone is reduced back to dopamine [8]. (reprinted from Bernsmann et al., Electrochimica Acta, 2011)

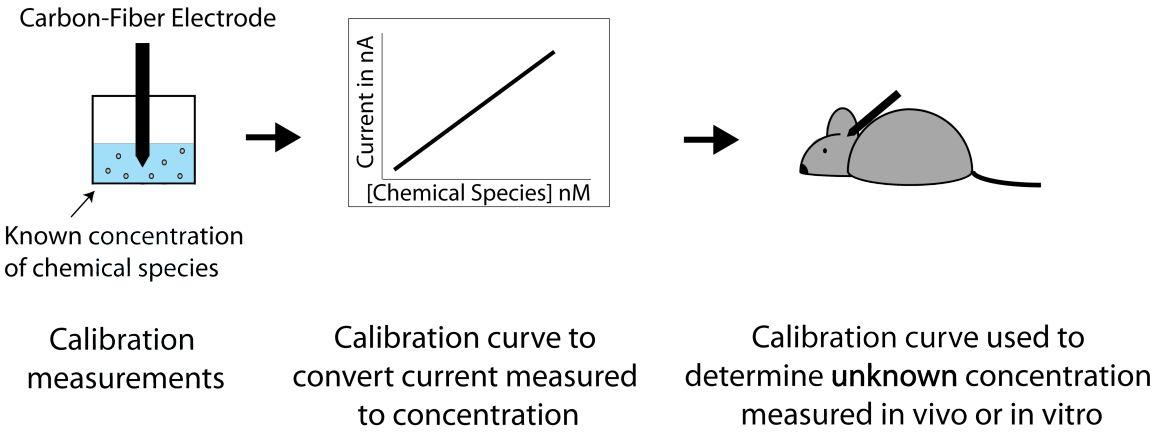

Figure 2.2 The electrode calibration process to convert current to concentration.

to create a calibration curve. This calibration curve is used to determine DA concentrations that are measured in vivo.

2.1.2 Previous and current methods for calibrating carbon fiber electrodes

Commonly, a flow injection apparatus is used to calibrate electrodes[9, 10]. The system consists of a syringe pump and a rotary valve loop injector preloaded with dopamine, and an electrode tip is inserted into the end of the loop injector. A buffer solution (commonly phosphate buffer or artificial cerebral spinal fluid) is continuously pumped through the flow system, and a computer triggers the release of dopamine into the buffer. Thus, the flow injection apparatus briefly exposes the electrode to a known concentration of dopamine before returning to buffer alone. The macro flow cell (mFC), another calibration device, is an adaptation of the flow injection system[11]. Instead of the electrode being inserted in the injector, it is stationary in a flow cell and buffer and dopamine are sequentially passed over the electrode. Buffer is continuously pumped into the system, and an injection apparatus is preloaded with dopamine and injected into the flow cell. In addition, other calibration setups exist that are similar in design and incorporate similar equipment with subtle variations implemented by different laboratories. In all systems the electrode is briefly exposed to dopamine for calibration, but they require multiple components. Electrode placement in the flow injection apparatus is tedious and requires a micromanipulator, and there is a risk of the electrode breaking during placement. The macro flow cell simplifies the electrode placement by using an in-house manipulator that easily docks the electrode into the flow cell. However, due to the large chamber volume, the macro flow cell slowly switches between solutions, creating a slow rise time in the calibration curve, which does

not stabilize at a peak current value. A large contributor to these injector issues is attributed to the large volume used for the buffer solution. This and other issues are addressed with the implementation of microfluidic devices.

2.1.3 Important properties of microfluidics

Microfluidics is the area of study where fluids are controlled and manipulated at the microscale level. There are a number of advantages in microfluidics including: a reduction of reagents required to run specific processes, the relatively low cost of production, and specific characteristics that emerge with fluid at the microscale[12]. These advantages contributed to its incorporation in the area of analytical chemistry where these properties were exploited for high-throughput screening and detection. A particularly interesting phenomenon occurs to fluids at this scale is the production of laminar flow due to a low Reynolds's number, usually less than one. Laminar flow is the parallelization of fluid streamlines, which do not mix except for diffusive mixing. Laminar flow has been essential in the separation of reagents, the formation of droplets[13-15], and the study of cell and developmental processes. Laminar flow was key in the improvement in the design conventional flow injectors.

2.1.4 Microchip-based flow injectors

Microchip-based flow injectors have been developed to address the issues associated with conventional flow injectors[16-20]. Commonly, these chips commonly utilize two separate streams of the buffer and sample of interest. Off-chip switching either using electrokinetic focusing or an injection valve can determine which stream is exposed the microelectrode. The

on-chip measurements improve on the previous methods since there is minimal dilution of the sample of interest. These devices however require separate equipment to drive the switching between solutions.

2.1.5 Microfluidic flow cell

To improve on these methods a microfluidic flow cell (μFC) was developed which borrows from the mFC and builds upon previous microchip-based flow injectors. The μFC houses the electrode in a plastic manipulator that is docked into a polycarbonate Y-channel allowing the electrode access into the channel. The device contains inlet and outlet ports for buffer and buffer with a known concentration of dopamine, and a reference electrode (chlorinated silver wire) is included to perform FSCV.

The ability to quickly change the fluidic interface between two solutions in a Y-channel is exploited as previously demonstrated for other microfluidic applications[21, 22]. When two fluids in a microfluidic Y-channel combine, laminar flow is dominate. Therefore, the two streamlines do not mix except through diffusion at the interface between the liquids. Changing the flow rate of the fluids can change where the fluidic interface is positioned in the channel. It is the changing of the interface that creates the quick switching between dopamine and buffer solutions on the electrode, which creates a step-like current response. The μFC simplifies the electrode calibration while improving the rise times and its stabilization at peak current values.

2.2 Materials and Methods

2.2.1 μFC Fabrication and Calibration Setup

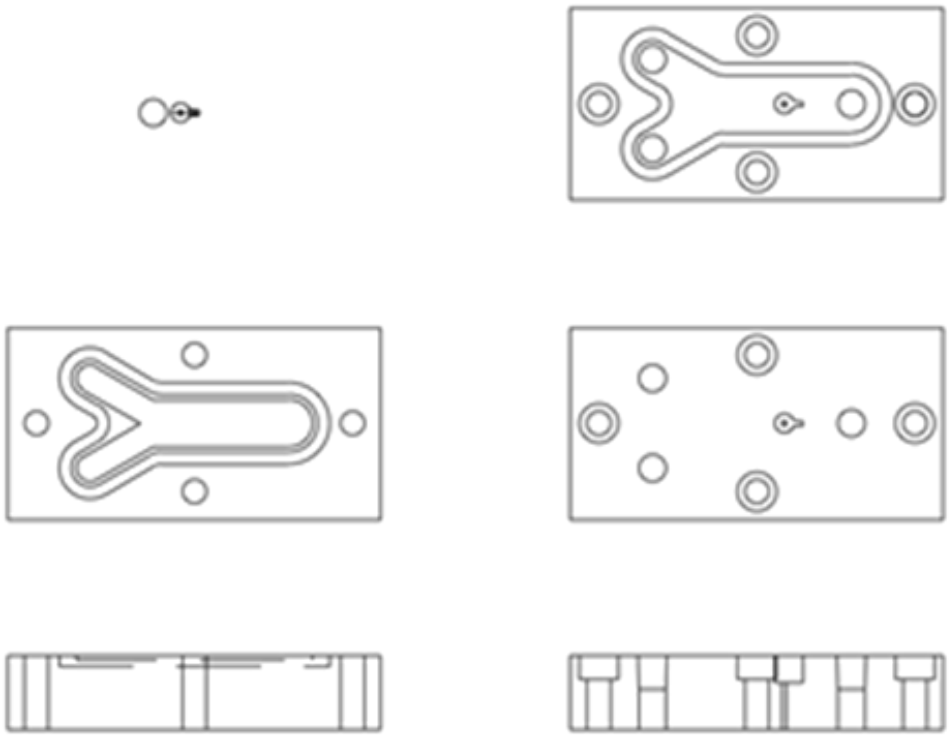

Figure 2.3 An AutoCAD diagram of the two acrylic blocks composing the microfluidic flow cell. **(**Courtesy of Eric Schmidt at Research Resources Center)

The μFC was designed in AutoCAD (Figure 2.3) and machined from two acrylic blocks measuring 2.8cm l × 5.5cm w × 1.2cm h by Eric Schimdt and Matthew Schuck at the Biologic Resources Center at UIC. The top half housed the molded Y-channel and manipulator insert to allow the electrode access to fluid in the channel. A silicone rubber O-ring was placed in the insert to prevent the leaking of solution into the manipulator. Inlets and an outlet were drilled for fluid flow, and a reference electrode, composed of chlorinated silver wire (Ag/AgCl), was inserted into a hole drilled perpendicular to the outlet and sealed with epoxy. The two parts were assembled together with screws to seal the channel. Connectors (#13160; World Precision Instruments) were inserted into the inlets and outlet and connected to Tygon tubing (R-3603, ID 1/16", OD 1/8"; Cole-Parmer). The design of this channel can be easily fabricated by any machine shop with basic CNC milling machine capabilities.

Gravity perfusion was used to drive fluid through the device. Two open 60 ml syringes (BD Syringe) were hung 0.45m above the device, and flow was controlled with intravenous (IV) dial flow regulators (Wolf Medical Supply) and 1way stopcocks (Cole- Parmer).

For all experiments artificial cerebral spinal fluid (aCSF) was used as buffer and contained (in mM): 125 NaCl, 4 KCL, 1.3 $CaCl_2$, 1 $MgCl_2$, 0.66 NaH_2PO_4, 2 Na_2HPO_4, 1 glucose; termed buffer solution). For calibrations, dopamine hydrochloride (Sigma Aldrich) was diluted in the buffer solution (termed dopamine solution). Buffer and dopamine solutions were filled into separate syringes. A manipulator introduced the carbon-fiber electrode into the channel. Flow rate determined which input was exposed to the electrode by shifting the fluidic interface between the input streams in the channel. The buffer solution was continuously

delivered at a rate of 1 ml/min, and when on, the dopamine solution was delivered at a rate of 1.5 ml/min which caused the fluidic interface to shift and exposed the electrode to the dopamine solution. All bubbles were removed before calibrations to prevent interference with the signal measured.

2.2.2 Voltammetric Recordings

Procedures for FSCV recordings are identical to those previously described[11, 23]. Briefly, electrodes were made by aspirating a carbon fiber into a glass pipette, which was pulled in a vertical micropipette puller. These electrodes, which had a length of carbon fiber protruding from the glass seal, were examined under light microscopy and the fiber was cut to 75-100 μm using a scalpel. Electrodes were then loaded into custom-made manipulators (UIC Biologic Resources Center). Using these manipulators, which are designed to interface with the guide cannula implanted in the brain of experimental rat subjects, electrodes were lowered into the channel of the μFC. Electrodes were held at −0.4 V against Ag/AgCl between voltammetric scans and then driven to +1.3 V and back at 400 V/s. This triangle waveform causes oxidation and reduction of chemical species at the electrode resulting in a large background current. Background current is digitally subtracted so that changes in current produced by the oxidation/reduction of transient signals (e.g. neurotransmitter) can be identified. Dopamine is electroactive within this potential range and is identified by plotting current against the applied potential used to produce a background-subtracted voltammogram color plot.

2.2.3 Subjects

Adult male Sprague-Dawley rats (Charles River; ~350 g) were housed in plastic cages (26.5 x 50 x 20 cm) in a temperature (22°C) and humidity (30%) controlled environment on a 12/12 h light/dark cycle (lights on at 7:00 am). Rats were food restricted to ~95% of their ad libitum body weight with free access to water during training and testing but not during recovery from surgery. Animal care and use was in accordance with the National Institutes for Health Guide for the Care and Use of Laboratory Animals and approved by the Institutional Animal Care and Use Committee at the University of Illinois at Chicago.

2.2.4 Surgery

Surgical procedures were identical to previously described[11, 23]. Briefly, rats were anesthetized with ketamine hydrochloride (100 mg/kg) and xylazine hydrochloride (10 mg/kg) and mounted in a stereotaxic frame (David Kopf Instruments). A guide cannula directed at the nucleus accumbens core (mm from Bregma: +1.3 anterior, -1.5 lateral), a chlorinated silver wire reference electrode in the contralateral cortex, and a bipolar stimulating electrode in the ventral midbrain (mm from Bregma: -5.2 anterior, -1.0 lateral), were implanted and affixed to the skull using dental cement. Rats were allowed at least a week of recovery before FSCV recordings took place.

2.3 Results and Discussion

2.3.1 Minimized components for electrode calibration

The mFC required multiple instruments for operation. Two images of the mFC and μFC calibration setup are displayed in Figure 2.3. In the mFC, a gravity flow was used to

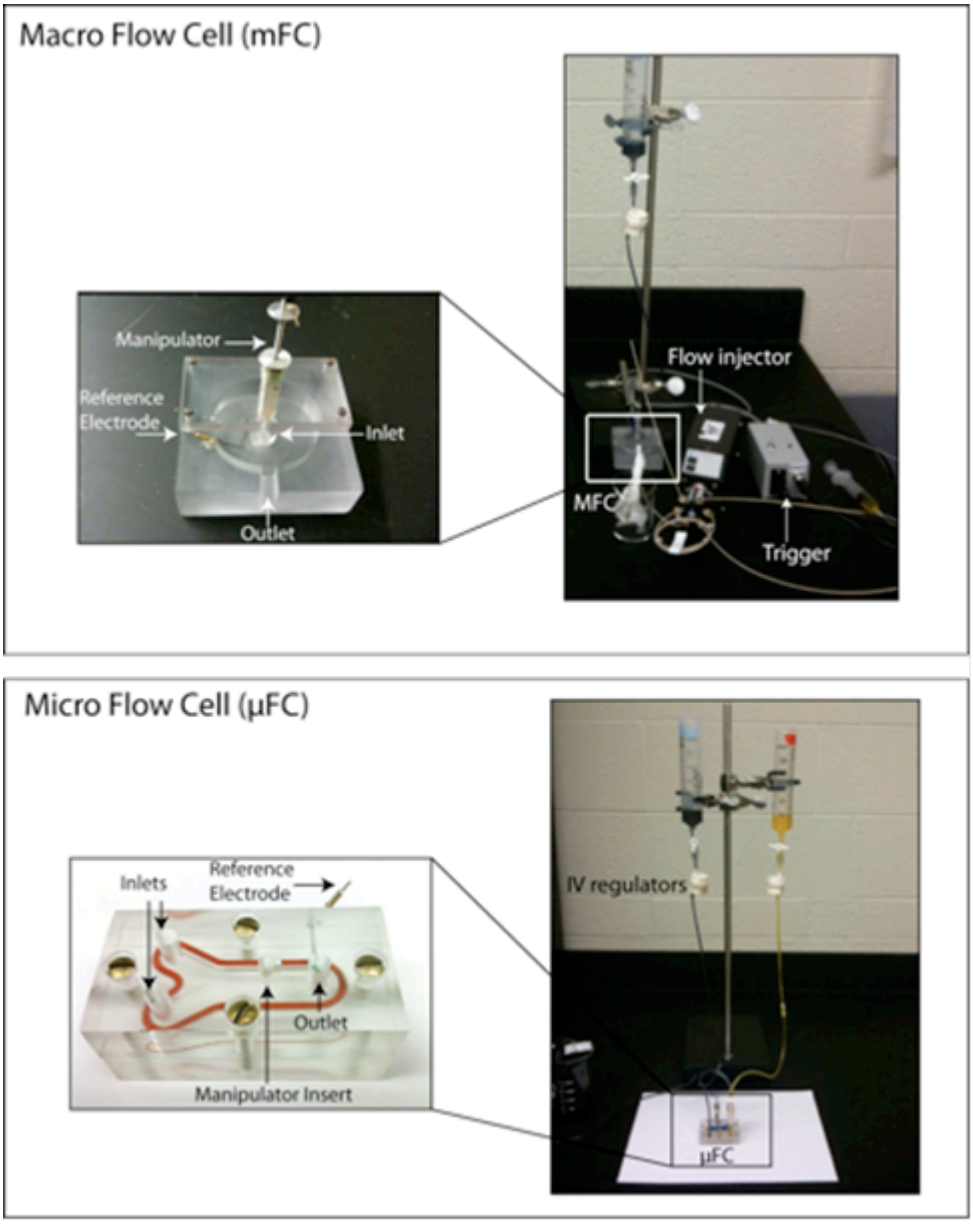

Figure 2.4. The macro flow cell (mFC) requires multiple components for operation. The mFC is connected to a syringe pump which continuously perfuses buffer into a bath through the inlet. A flow injection apparatus injects buffer+dopamine into the bath where the carbon fiber electrode, housed in the manipulator, and the reference electrode come into contact with the solution for current measurements. A trigger and computer (not shown) controls the duration the buffer+dopamine is introduced into the solution. The microfluidic flow cell eliminates the need for external instruments. It consists of a Y-channel with an opening in the center of the channel to accommodate a carbon fiber-microelectrode housed in a manipulator. The electrode is lowered by the manipulator into contact with fluid flow. A gasket is placed in the insert to block fluid from entering the manipulator, and a reference electrode is placed in the side for contact with the outflow. The microelectrode and reference electrode are used in conjunction to measure the changes in current in the system.

continuously perfuse the buffer solution. A flow injection apparatus injected the dopamine solution into the bath where the carbon fiber electrode, housed in the manipulator, and the reference electrode, came into contact with the solution for measurements. A trigger and computer (not shown) controlled the duration the dopamine solution was introduced. Multiple calibrations were tedious since the flow injection apparatus could only preload 300 µl of dopamine solution at a time. Lastly, the additional components occupy a larger amount of bench space.

The µFC addressed problems with the mFC by introducing the carbon fiber electrode directly in the center of a microfluidic Y-channel. As before, the electrode's position in the channel was controlled by the manipulator it was housed in, and a reference electrode was added for current measurements. Gravity perfusion through two open syringes was used to drive the solution. Characteristics of a Y-channel were exploited to switch the electrode between the buffer and dopamine solutions. Altering the flow rate of each solution determined which input was exposed to the electrode. Additionally, the µFC removed the need for external electrical components.

2.3.2 Rapid switching between buffer and dopamine and reduced variability in current response

A step-like current response was achieved by rapidly switching the solution that the electrode was exposed to from buffer to dopamine. In Figure 2.4, food dye was used to color each solution and shows the rapid change in fluidic interface in the device, which is achieved by altering the flow rates. Initially, the flow rate for the buffer solution (blue) was set to 1 ml/min to fill the channel. The dopamine solution (yellow) was introduced into the channel at a rate of 1.5

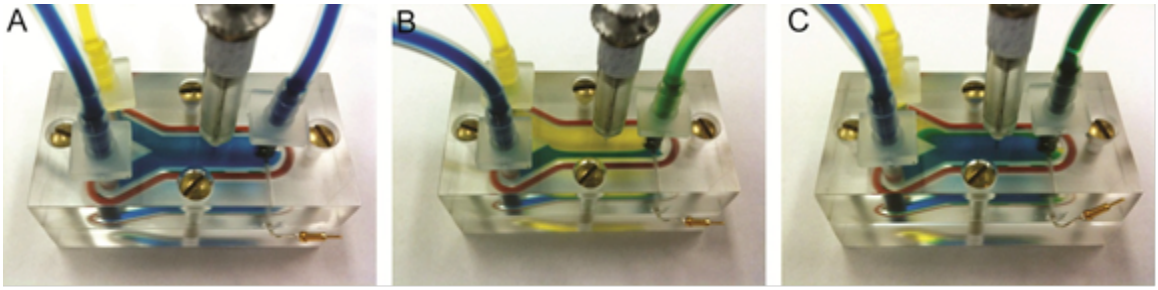

Figure 2.5 The µFC allows for rapid switching of fluids in the microfluidic channel. (A) Initially, only the blue fluid was flowing at 1 ml/min. (B) When on, the yellow stream filled a majority of the channel due to its faster flow rate of 1.5 ml/min. (C) The blue stream recovered when the yellow stream was off.

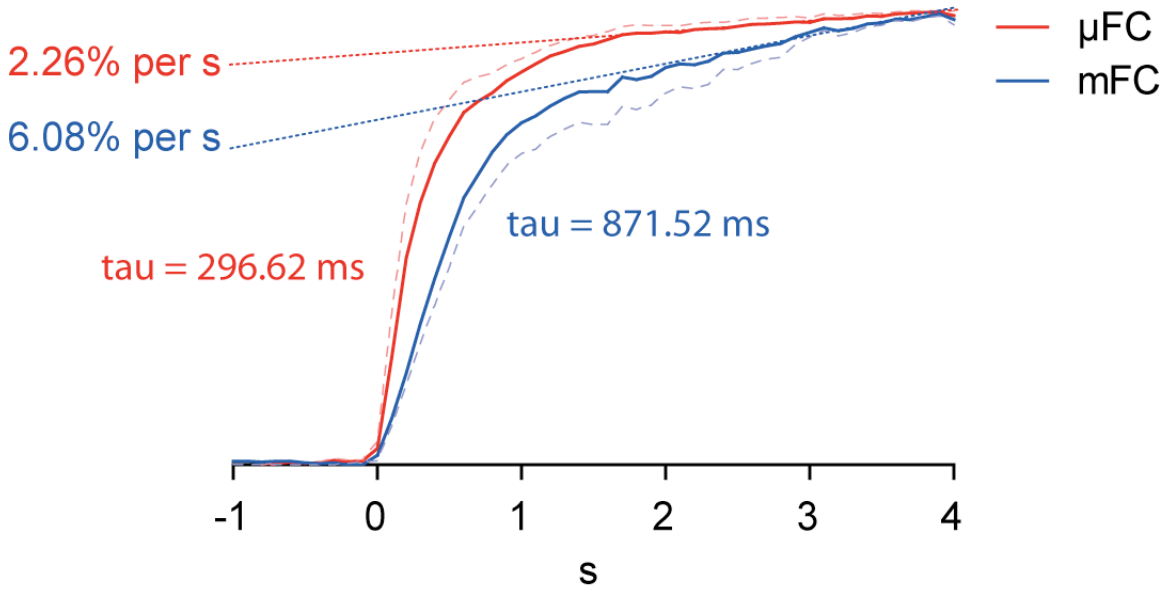

Figure 2.6 The current responses between the macro flow cell (mFC, blue) and µFC (red) were compared. The µFC exhibited a faster rise time and flatter peak. A standard first-order exponential was fitted to the early part of the response. Tau of the rise time, was less in the µFC (296.62 ms) than the mFC (871.52 ms). In addition, slope gradient of the late phase (dotted lines) for the µFC (2.26% per second) was less than for the mFC (6.08% per second). The dashed lines show the upper range of the standard error for the µFC and the lower range for the mFC.

ml/min to displace the flow of the buffer solution and the electrode was briefly exposed to dopamine for ~5 seconds. Last, the flow of the dopamine solution was stopped and the buffer solution was returned to the electrode.

Additionally, the μFC simplified multiple successive calibrations since a large reservoir of the dopamine solution was maintained allowing for many repetitions of switching between solutions, which cannot be achieved in the mFC.

Relative to the mFC, the μFC produced current responses that exhibited faster rise times and plateaued quicker near the peak current value as displayed in Fig 3. Normalized current responses evoked by 1 μM dopamine solution were compared between the μFC and mFC. A first-order exponential was fitted to early phase of both responses and revealed that the rise time was ~3 times shorter in the μFC than the mFC (tau: 296.62 ms vs. 871.52 ms). In addition, when the late phase of the response was fitted with a linear function (dotted lines), the response in the μFC was ~2.5 times flatter than in the mFC, i.e. the slope was shallower (slope: 2.26% per s vs. 6.08% per second). The dashed lines show the upper range of the standard error for the μFC and the lower range for the mFC. The shallower slope as the μFC response reaches its maximum current value indicates that, relative to the mFC response, it is closer to stabilizing at the peak concentration; this provides more confidence when determining the corresponding current value to concentration which means the data gathered and calibrated with this method will be more accurate.

A likely factor accounting for the stabilization of the current response in μFC is the constant level of dopamine solution at the electrode surface during applications. In addition, a large chamber volume in the mFC created turbulent movement in the bath. Although the

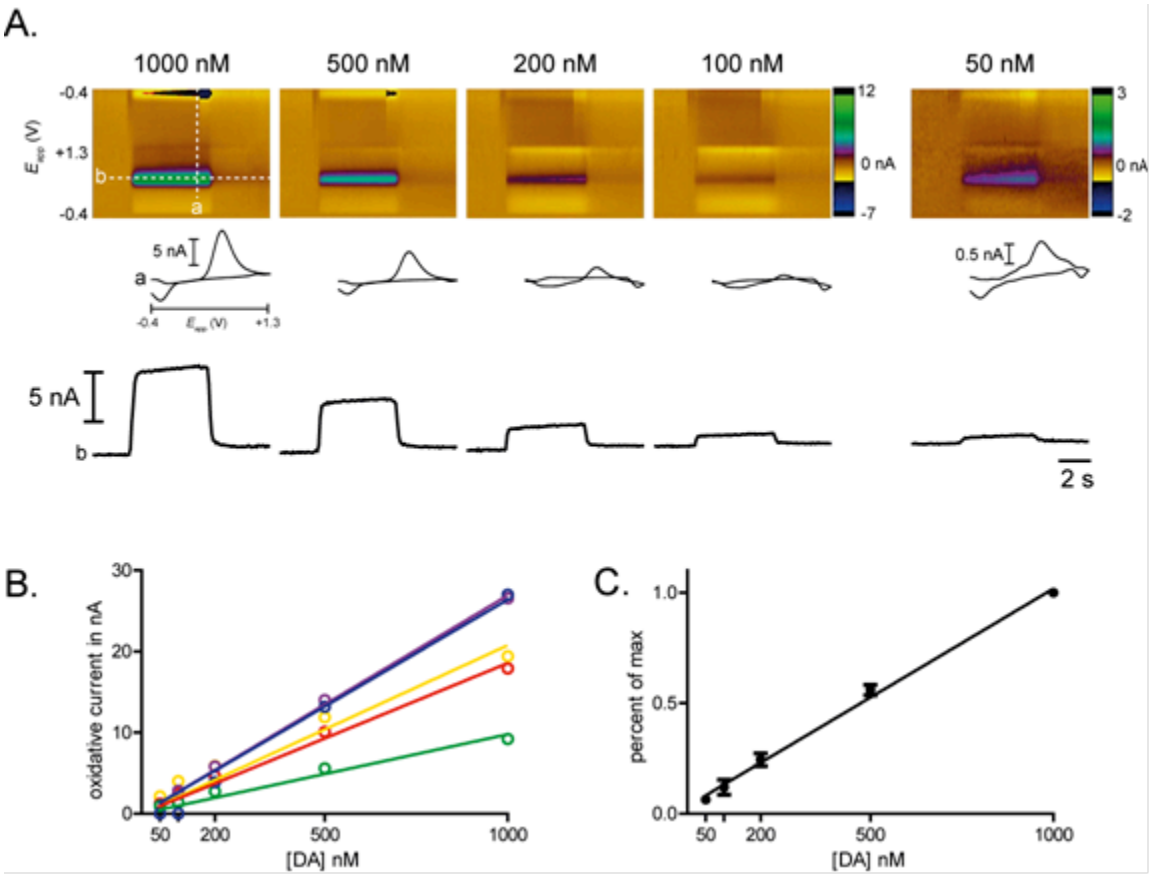

Figure 2.7 Linear calibration curves. (A) We assessed electrode responses in the flow cell to a range of dopamine concentrations (1000, 500, 200, 100, and 50 nM). Shown here are color plots (top panels), cyclic voltammograms (insets) and current by time traces (bottom panels) for a single representative electrode across the range of dopamine concentrations. In the color plots, the x-axis is time (s), the y-axis is applied potential to the electrode (V) and current is coded by pseudocolor (nA, scale on right). The chemical signature of dopamine can be seen as a specific change in current at its oxidation (~0.60 V) and reduction (~-0.21 V) potentials. The dashed white lines in the left-hand color plot show the data from which the cyclic voltammograms (a) and the current by time traces (b) are derived. (B) Data were obtained for five electrodes, shown in different colors. Data are mean ± SEM for three trials at each concentration; errors are too small to be visible. (C) When normalized to account for differences in maximum amplitude, slopes for each electrode were close to 1 (range: 0.918-1.083; mean: 0.985) indicating excellent linearity. Data shown are mean ± SEM for the five electrodes shown in B.

electrode was in contact with the solution near the inlet, turbulent flow still dispersed the dopamine solution creating an inconsistent concentration at the electrode surface. The laminar flow in μFC allowed dopamine to near-instantaneously and continuously interacts with electrode, stabilizing the peak current amplitude and producing faster rise time.

2.3.2 Calibration curves to determine dopamine concentration *in vivo*

Electrode responses in the μFC to different concentrations of dopamine were measured. Figure 2.7A shows the current (represented in color) plotted against the applied potential (E_{app}) as a function of time for dopamine concentrations of 1000, 500, 200, 100, 0 nM. Dopamine was detected at its peak oxidation potential of ~0.6V (green feature). The current monitored at the peak oxidation potential for dopamine are displayed below each 'color plot'. Both the color and current plots exhibit little noise and the current plot retains its step-like shape even at lower concentrations. Figure 2.7B displays current responses obtained from five electrodes in the μFC at concentrations of 1000, 500, 200, 100, and 50 nM. Due to differences in maximum amplitude of the electrodes, the calibration data was normalized (Figure 2.7C). The electrodes exhibited linear slopes that were close to 1 (range: 0.918-1.083; mean: 0.985). The linear slopes confirm that the flow cell is capable of calibrating electrodes over a range of concentrations, which is important when accurately determining concentrations *in vivo*.

The μFC is able to provide accurate calibrations for electrodes used in FSCV studies in awake and behaving animals *in vivo*. The small size of the micro flow cell is an advantage since the calibrations can be conducted in the same cage as the in vivo measurements, which allows for better standardization of the environment between the experiment and the calibrations. Figure 2.8a displays a concentration curve for an individual electrode. As before, the curve shows

excellent linearity and determined that 1 nA corresponds to 48.26 nM dopamine. After calibration, the same electrode was placed in the nucleus accumbens core of a rat, a brain region that receives dense dopamine input and is engaged in behaviors that involve learning about food and other rewards. Current responses across all voltages of the electrode were measured using FSCV in response to sensory stimuli that the rat had been trained to associate with food delivery. Specifically, a compound (tone/light) stimulus preceded the delivery of a rewarding sugar pellet by 3 s. Single dopamine release events, identified by the specific potentials at which oxidative current was observed, were evoked by both the compound cue and the delivery of the sugar pellet and were evident in the color plot (Fig. 2.8b). A scan of the current response against time (monitored at the peak of the oxidative current, 0.65 V) is shown in Fig. 2.8c. An increase in current was apparent at the onset of the compound cue and a second peak in current occurred after delivery of the pellet. In this trial, the cues evoked a greater increase in oxidative current than pellet delivery, consistent with existing literature[24]. Principal component analysis was used with the calibration constant obtained in the μFC to convert the observed current into dopamine concentration[25], and this concentration is plotted in Fig. 2.8c.

Electrode calibrations are essential for studies employing FSCV. While analyte identification can be performed *in situ*, understanding the relationship between observed current and concentration requires electrode calibration. The μFC allows permits accurate calibrations that can be performed before and/or after *in vivo* recordings. Accurate calibrations provide confidence that concentration values assigned to current changes match true concentrations of dopamine encountered in the brain. In addition, the μFC is applicable for other neurotransmitters, chemical species, and the measurement of a solution's pH.

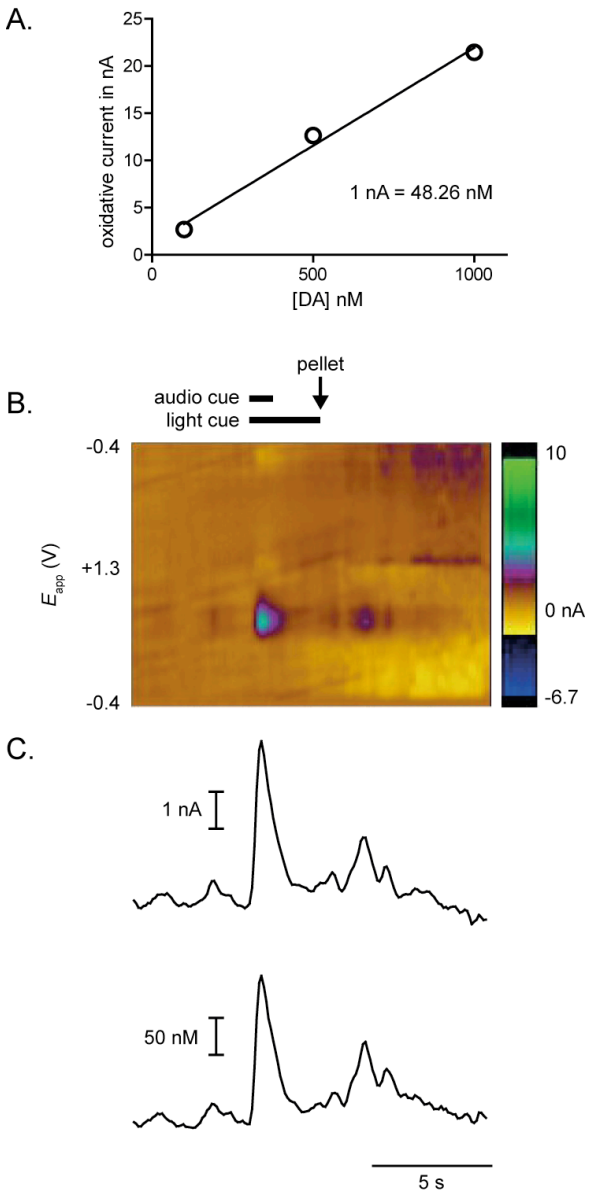

Figure 2.8 Dopamine calibration for *in vivo* measurements. (A) The µFC produced a calibration curve to relate recorded current to dopamine concentration (1 nA= 48.26 nM) for a single electrode. Data shown are mean ± SEM for three trials at each concentration; errors are too small to be visible. (B) This same electrode was lowered into the nucleus accumbens core of an awake, behaving rat and used for *in vivo* measurements. A color plot (as described in detail in Fig. 4) shows dopamine release *in vivo* while the rat responded to food-predictive cues and pellet delivery. (C) The calibration curve is used in conjunction with principal component analysis to derive concentration of dopamine from current produced.

2.4 Conclusion

The μFC is a simple device that permits rapid switching between solutions exposed to electrodes used in analytical chemistry and neuroscience. Relative to other devices, the removal of external components not only simplified, but the reservoirs of buffer and dopamine solutions also allowed for numerous repetitions of calibrations without frequent preloading. Importantly, values obtained in the μFC exhibited faster rise times and a shallower slope near the peak current. The current response of the μFC maintained its step-like shape over a large range of concentrations and produced linear calibration curves, which are essential for accurate modeling of *in vivo* dopamine concentrations. The μFC is a device that can be easily integrated in many laboratory setups and is a simple solution for electrode calibrations.

References

1. Millar, J., et al., *Electrochemical, pharmacological and electrophysiological evidence of rapid dopamine release and removal in the rat caudate nucleus following electrical stimulation of the median forebrain bundle.* Eur J Pharmacol, 1985. **109**(3): p. 341-8.
2. May, L.J., W.G. Kuhr, and R.M. Wightman, *Differentiation of dopamine overflow and uptake processes in the extracellular fluid of the rat caudate nucleus with fast-scan in vivo voltammetry.* J Neurochem, 1988. **51**(4): p. 1060-9.
3. Phillips, P.E., et al., *Subsecond dopamine release promotes cocaine seeking.* Nature, 2003. **422**(6932): p. 614-8.
4. Wightman, R.M., et al., *Real-time characterization of dopamine overflow and uptake in the rat striatum.* Neuroscience, 1988. **25**(2): p. 513-23.
5. Garris, P.A., et al., *Dissociation of dopamine release in the nucleus accumbens from intracranial self-stimulation.* Nature, 1999. **398**(6722): p. 67-9.
6. Robinson, D.L., et al., *Detecting Subsecond Dopamine Release with Fast-Scan Cyclic Voltammetry in Vivo.* Clinical Chemistry, 2003. **49**(10): p. 1763-1773.
7. Millar, J., M. Armstrong-James, and Z.L. Kruk, *Polarographic assay of iontophoretically applied dopamine and low-noise unit recording using a multibarrel carbon fibre microelectrode.* Brain Research, 1981. **205**(2): p. 419-424.
8. Bernsmann, F., J.-C. Voegel, and V. Ball, *Different synthesis methods allow to tune the permeability and permselectivity of dopamineâ€“melanin films to electrochemical probes.* Electrochimica Acta. **56**(11): p. 3914-3919.

9. Kristensen, E.W., R.L. Wilson, and R.M. Wightman, *Dispersion in flow injection analysis measured with microvoltammetric electrodes.* Analytical Chemistry, 1986. **58**(4): p. 986-988.

10. John, C.E., et al., *Neurochemical characterization of the release and uptake of dopamine in ventral tegmental area and serotonin in substantia nigra of the mouse.* J Neurochem, 2006. **96**(1): p. 267-82.

11. Roitman, M.F., et al., *Dopamine operates as a subsecond modulator of food seeking.* J Neurosci, 2004. **24**(6): p. 1265-71.

12. Whitesides, G.M., *The origins and the future of microfluidics.* Nature, 2006. **442**(7101): p. 368-373.

13. Thorsen, T., et al., *Dynamic pattern formation in a vesicle-generating microfluidic device.* Phys Rev Lett, 2001. **86**(18): p. 4163-6.

14. Link, D.R., et al., *Geometrically mediated breakup of drops in microfluidic devices.* Phys Rev Lett, 2004. **92**(5): p. 054503.

15. Anna, S.L., N. Bontoux, and H.A. Stone, *Formation of dispersions using ``flow focusing'' in microchannels.* Applied Physics Letters, 2003. **82**(3): p. 364-366.

16. Fu, L.M., R.J. Yang, and G.B. Lee, *Electrokinetic focusing injection methods on microfluidic devices.* Anal Chem, 2003. **75**(8): p. 1905-10.

17. Fan, L., et al., *Continuous on-line concentration based on dynamic pH junction for trimethoprim and sulfamethoxazole by microfluidic capillary electrophoresis combined with flow injection analysis system.* J Chromatogr A, 2005. **1062**(1): p. 133-7.

18. Moehlenbrock, M.J., A.K. Price, and R.S. Martin, *Use of microchip-based hydrodynamic focusing to measure the deformation-induced release of ATP from erythrocytes.* Analyst, 2006. **131**(8): p. 930-937.

19. Moehlenbrock, M.J. and R. Scott Martin, *Development of an on-chip injector for microchip-based flow analyses using laminar flow.* Lab on a Chip, 2007. **7**(11): p. 1589-1596.

20. Sinton, D., L. Ren, and D. Li, *A dynamic loading method for controlling on-chip microfluidic sample injection.* J Colloid Interface Sci, 2003. **266**(2): p. 448-56.

21. Blankenstein, G. and U. Darling Larsen, *Modular concept of a laboratory on a chip for chemical and biochemical analysis.* Biosensors and Bioelectronics, 1998. **13**(3–4): p. 427-438.

22. Gwo-Bin, L., H. Bao-Herng, and H. Guan-Ruey, *Micromachined pre-focused M × N flow switches for continuous multi-sample injection.* Journal of Micromechanics and Microengineering, 2001. **11**(6): p. 654.

23. Ebner, S., et al., *Depressive-like effects of the kappa opioid receptor agonist salvinorin A are associated with decreased phasic dopamine release in the nucleus accumbens.* Psychopharmacology, 2010. **210**(2): p. 241-252.

24. Day, J.J., et al., *Associative learning mediates dynamic shifts in dopamine signaling in the nucleus accumbens.* Nat Neurosci, 2007. **10**(8): p. 1020-1028.

25. Heien, M.L.A.V., M.A. Johnson, and R.M. Wightman, *Resolving Neurotransmitters Detected by Fast-Scan Cyclic Voltammetry.* Analytical Chemistry, 2004. **76**(19): p. 5697-5704.

III. CHAPTER 3: AUTOMATED CHEMICAL DELIVERY DEVICE FOR THE SPATIAL AND TEMPORAL CONTROL OF CHEMICALS IN THE STUDY OF YEAST CHEMOTROPISM

3.1 Introduction

3.1.1 The role of the microenvironment in cell behavior

In vitro studies are extensively used in experimental biology since the complexities that arise when studying an intact specimen are simplified. Living organisms contain a vast range and number of genes, proteins, and signaling molecules, and the isolation of specific cells or tissue provides a better approach to study the individual components that would be otherwise be lost in the crowd. This idea was the catalyst for the race to grow cells in vitro. Since then, researchers have developed techniques to not only maintain cells in vitro, but to also understand cell behavior. However, since the cells and tissue are not in their native environment, great effort has been taken to mimic the extracellular microenviroment that the cell experiences in vivo. Since the differing environments make it difficult to relate in vitro results to the intact organism, it is important to provide an appropriate analog to the in vivo environment.

Cells are continuously secreting signaling molecules into microenvironment to communicate with neighboring or distant cells. The type, concentration, and location of the molecules secreted can affect the subsequent behavior of the target cell. The next sections will detail the paracrine signaling in yeast. The yeast species *Saccharomyces cerevisiae* is a simple eukaryotic cell and is model organism for the study of eukaryotic behavior. The process of *Saccharomyces cerevisiae* responding and growing in response to chemical gradients is similar to growth of axons in neurons[1]. Thus, studying these interactions can provide more information on axonal growth in mammalian cells.

3.1.2 Yeast chemotropism

Most eukaryotic cells exhibit polarized growth in response to chemical signals. Chemotropism is the process of directional growth due to gradients of chemoattractants or chemorepellents, and this is vital for yeast mating[2, 3]. When yeast are in the haploid state, they are able to mate with other haploid cells of the opposite phenotype. For example, **a** cells secrete a pheromone (a-factor) signaling its presence to α cells in the vicinity. In turn, **a** cells respond to α factor by arresting the cell cycle and develop a polarized growth or a "shmoo" towards the α-cell. The inverse is also true with α−cells[4]. This process is regulated by G-protein-coupled receptors and their corresponding G-proteins.

There are two specific G-protein coupled seven-transmembrane domain receptors that bind to the pheromones, Ste2 and Ste3, which bind to α-factor and a-factor respectively. The production of the receptors increases when exposed to their respective pheromones[5, 6]. These receptors activate a MAP-kinase cascade, which initiates the shmooing of the yeast[7, 8].

While the process of the pheromone binding to the receptor is well understood, how the yeast cells sense the pheromone gradient is unclear. However, the general consensus believes that gradient detection is spatially instead of temporally dependent[9, 10]. When a cell is exposed to a gradient, the concentration of pheromone bound to its receptors is compared between the two sides of the cell. The yeast cell shmoos in the direction with the higher concentration of pheromone, which is the direction of the secreting cell[9, 10].

Yeast chemotropism is either measured directly or indirectly. Direct measurements calculate the angle of the shmoo generated in response to an artificial gradient and is the

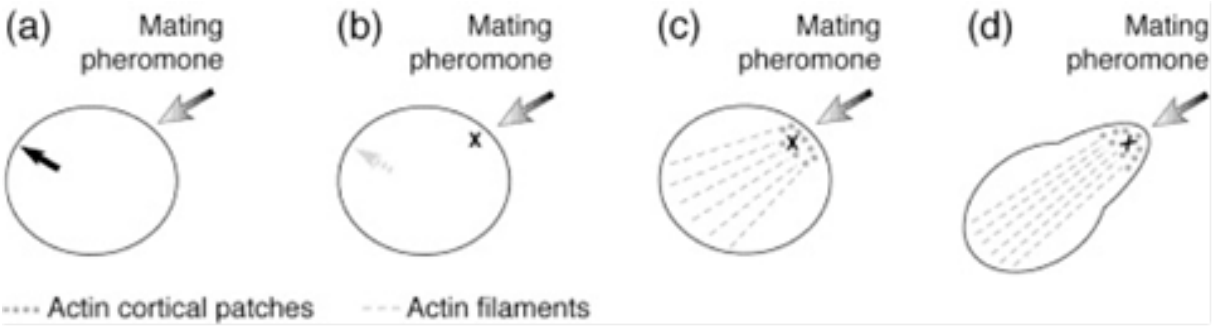

Figure 3.1 A diagram of the directed growth in response to a mating pheromone in the environment.(a) A haploid cell detects a pheromone gradient. (b) Signaling molecules are activated, which initializes cytoskeleton reorganization at point x (c) and a projection is directed towards the pheromone source (d) [3]. (reprinted from Trends in Cell Biology)

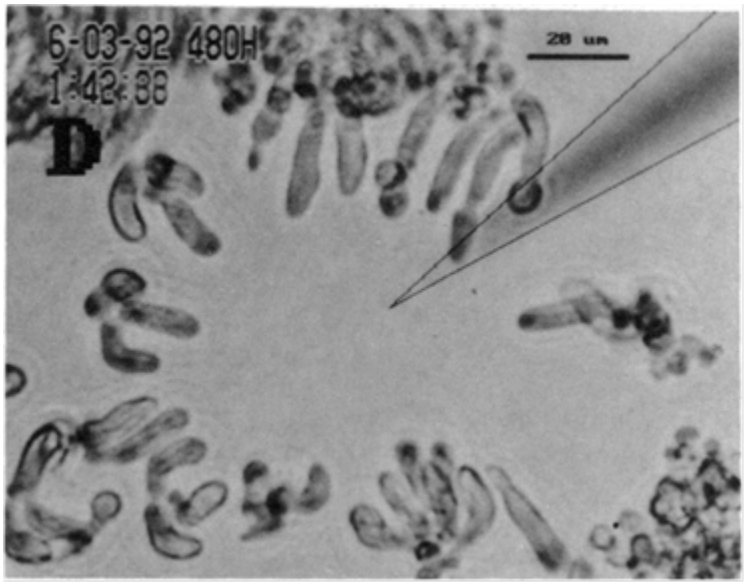

Figure 3.2 Micropipette deposition of pheromone is a common method to establish a point-source gradient. Here, a cells are exposed to α factor pheromone [9]. (reprinted from PNAS)

commonly used approach[9]. The ability of the yeast cell to detect a gradient is highly precise and is able to detect a gradient as shallow as 0.1% per μm, which is only 0.5% in pheromone concentration between the front and back of the cell[11]. In addition, the yeast cells are the most responsive to a gradient that exhibits a steep gradient at low pheromone concentrations[9, 11, 12]. As the slope of the gradient increases, the accuracy of gradient sensing improves, which was initially demonstrated with the micropipette-generated gradient[9]. The accuracy of gradient determination is most optimal when the pheromone concentration approaches the concentration of receptors on the cell[10, 12].

The increasing precision of gradient determination correlates with a previous study that provided a model of how the yeast cells choose which neighboring cell to shmoo towards[12]. A projection is more likely to be produced towards the cell that is releasing the highest amount of pheromone in the vicinity. Here, two indirect chemotropism assays were used. The competition assay was used to determine the strength of mating efficiency between one cell and two mating partners. The mating cells are composed of two types: wild-type and challenger cells that have various genetic modifications. The challenger cell effectiveness in mating with target cell is measured[13, 14]. The discrimination assay tests the target cell's ability to discriminate between two other mating cells of the same type. Lastly, the confusion assay inserts an alpha factor artificial gradient that obscures the pheromone gradients produced by the individual cells. This decreases the ability of a cell to orient and mate with a neighboring cell[15]. A disadvantage of the confusion assay is the possible saturation of the pheromone receptors, which could alter other processes that could interfere with the interaction with the gradient. While indirect studies provide relevant information in regards to chemotropic behavior, it is essential to supplement

these studies with direct measurements, since it simplifies the cell environment. In order to probe yeast sensory mechanism, various methods for pheromone gradient generation have been devised. The commonality between the methods is the creation of a gradient that is positioned in the area. However, the degree of control of the gradients does vary between different methods.

3.1.3 Producing artificial pheromone gradients

Artificial gradients are essential to study yeast chemotropism. The ability to generate artificial gradients simplifies the microenvironment of the yeast, which is necessary for controlling experimental parameters. The first method uses a micropipette to create a point source-radial gradient of pheromone on agarose, a simple and quick way to establish a gradient[9]. The angle between the yeast projection and the pipet are determined to quantify cell orientation. A disadvantage to this method is the lack of consistency during and between experiments. Since the micropipette was handmade, the amount of pheromone released from the pipet was estimated. In addition, this assay does not take into account the pheromone diffusing through the agarose and its concentration change over time.

The advent of microfluidics helped to circumvent the issues in previous gradient studies. As mentioned before, the manipulation of fluids on a small scale allows for more precise control of the diffusion of species, which is important with these studies. The Paliwal group created a device that contained two flow channels containing media with pheromone, the source, and the other housing plain media, the sink[12]. A pheromone concentration profile is established between the source and sink, and since the test chambers that house the cells are different lengths, a variety of profiles can be established. Most importantly, the profiles are stable in the chambers.

This devise was also able to change the direction of the gradient to study the mechanics of reorientation of the yeasts projections. This device was a great progress towards controlling the general vicinity of the gradient. However, the gradient does not move much. At most the Paliwal group was able to flip the gradient by 180 degrees. Brett et al developed a microfluidic device that added the ability of changing the gradient by 90 degrees, which is particularly important for studying reorientation in yeast[16]. The ability to create a dynamic gradient is a great to understand what occurs when yeast mutants are exposed to a gradient.

3.1.4 Automated chemical delivery device

Microfluidics is a platform that is well suited for gradient generation since small volumes of liquid can be precisely controlled, and this precision is due to property of fluids at the microscale environment[17]. As stated in the previous chapter, the fluid flow is laminar, and diffusion becomes the sole form of mixing, which is essential for producing gradients. The previous microfluidic devices dedicated to the study of yeast chemotropism all placed the yeast on a PDMS substrate in side a microfluidic channel. While PDMS is a biocompatible material, it is not an ideal substrate for yeast, which normally are grown on agarose. To circumvent this problem, the automated chemical delivery device (ACDD) was developed. ACDD establishes a pheromone gradient in agarose allowing yeast to grow in an environment which is familiar to standard protocols. The device is composed of four distinctly patterned layers of PDMS bonded to a glass slide. Starting from the bottom, the first and second PDMS layers consist of circular valves that are covered by a 30 μm thin membrane. The valves control the timing and delivery of the pheromone to the yeast and are actuated by applying air or vacuum to deflect the membrane.

The third layer consists of the channels with vias that are responsible for chemical delivery. Lastly, the final layer holds the agarose and yeast. This device allows for the study of yeast chemotropism in an appropriate environment while having control over the pheromone gradient.

3.2 Methods

3.2.1 ACDD fabrication

Standard photolithography techniques were used to create the SU-8 masters for the three patterned layers. PDMS prepolymer (Sylgard 184, Dow Corning, IL) was mixed 10:1(polymer:curing agent) and degassed. The uncured PDMS was poured to a thickness of 2 mm onto the bottom valve layer master that had 150 μm tall features. The PDMS was baked at 85^{o}C for 90 minutes. To create the flexible membrane layer, a clean silicon wafer was dehydrated at 125^{o}C for 15 minutes. Once cooled, the wafer was silanized under a vacuum with 30 μl of (Tridecafluoro 1, 2,2-tetrahydroctyl)-1-trichlorosilane (United Chemical Technologies, PA) vapor in a desiccator for 30 minutes to facilitate membrane removal. The membrane layer is created by spincoating a solution of PDMS and hexane (3:1) on a silicon wafer at 1000 RPM with an acceleration of 100 for 30 seconds. The membrane was cured at 85^{o}C for 10 minutes. The channel layer was made by spincoating PDMS on a patterned SU-8 master for 30 seconds at 700 RPM. After mixing and degassing the uncured PDMS, it was set aside at room temperature for 3 hours to produce a thicker membrane when spincoated. The PDMS was removed from the top of the posts with a directed gentle stream of compressed air to ensure the vias were produced in the channels. The top chamber layer was also constructed from PDMS. Uncured PDMS was poured onto the patterned substrate and cured for 90 minutes at 85^{o}C. Once cured, the PDMS

was removed from the wafer and the inlets, outlet, and chambers were made. The chamber was cleaned with isopropanol (IPA), dried under nitrogen, and cleaned with tape to remove any dust and debris. The channel layer, still on the wafer, was also cleaned with tape, and both layers were plasma treated with a corona discharge device (BD-20AC, Electro-Technic, IL) and bonded. The bonded devices were placed on an 85^{o}C hotplate for 10 min with a 3 kg weight. While these layers bonded, the valve layer and membrane was bonded in same manner as previously stated. Next, the non-feature side of the valve layer was bonded to a glass slide and set aside. The combined chamber and channel layer was cut and removed from the wafer, and holes are made in the same positions where the inlets and outlets are in placed in the chamber layer. A small piece of transparency covered the valves and its corresponding on the channel layer was also covered while plasma treated to prevent bonding between the valves and channels. Lastly, the transparencies were removed and the two combined layers were aligned with under a microscope and bonded. The final device was place on the hot plate at 85^{o}C for 10 minutes. The device was removed, and an 18-gauge needle was used to puncture the membrane in the valve inlets to allow air and vacuum access. The valves were opened with a syringe to prevent any subsequent bonding from the heat of the hotplate.

3.2.2 Integrating solenoid valves to PDMS valves

To automatically actuate the PDMS valves on the ACDD, solenoid valves (LHLA_21211H, Lee Company, CT) were utilized. The solenoid valves are three-way valves that have three port connections and two valve seats. One valve seat always remains open and the other seal is closed in the de-energized mode. When the coil is energized, the orientation is

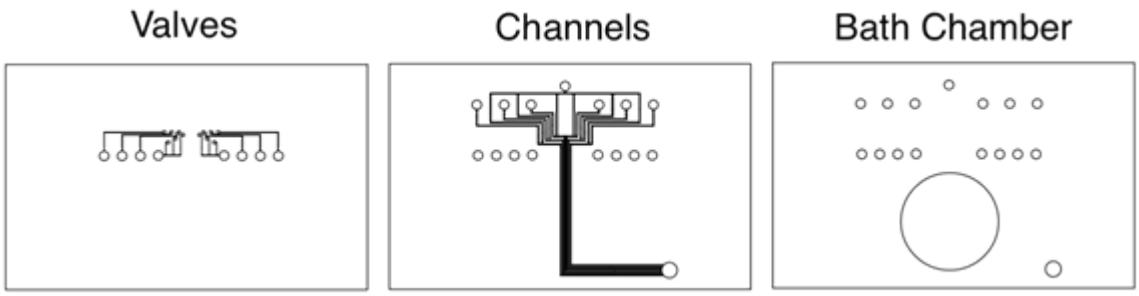

Figure 3.3 AutoCAD drawings of the three patterned layers of the ACDD The first patterned layer is one component of the valves. The feature side faces up on the device and the addition of a thin membrane completes the valve assembly. The second layer is a patterned PDMS membrane that houses the channels for fluid delivery. The third layer is the bath chamber which contains all the ports and an area to hold the agarose.

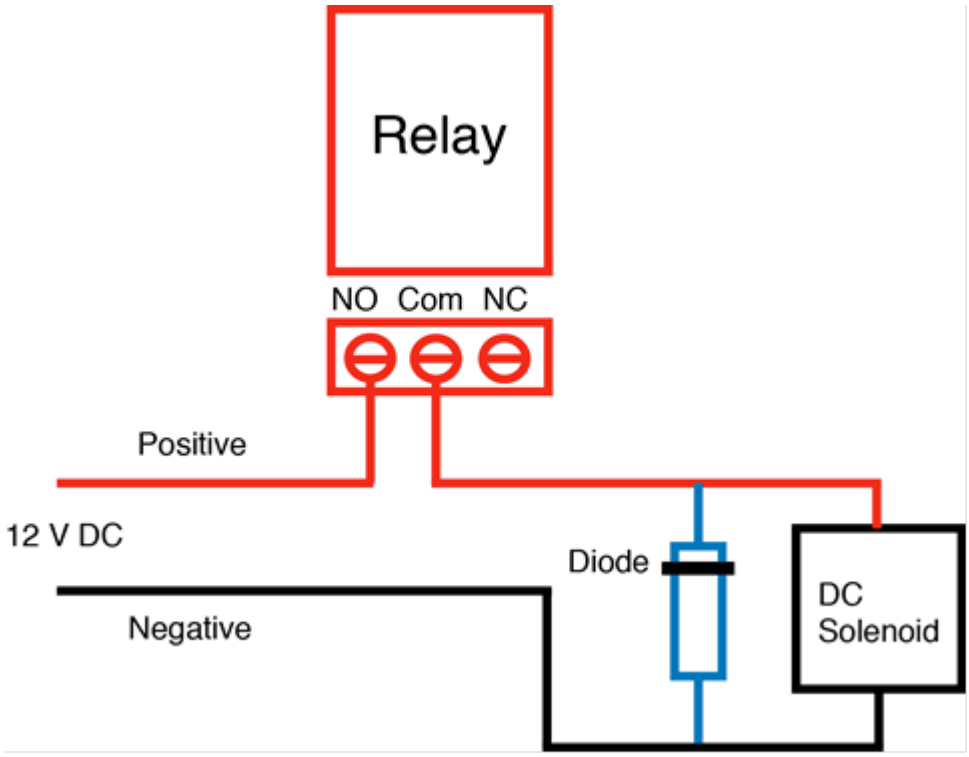

Figure 3.4 The solenoid configuration on the breadboard. A 12VDC power source was connected to the normally open (NO) connection on the TTL-driven relay board. The common (Com) was wired to the diode and solenoid valve, which were placed in parallel. The diode provided protection against back EMF generated by the solenoid valve.

reversed. Eight solenoid valves were used to actuate the twelve PDMS valves on the device. The solenoids were connected to a breadboard, which connected to a 10amp TTL-driven relay board (SimpleCircuitBoards.com). A DAQ Card (USB-6008, National Instruments) interfaced with the TTL board to provide the TTL signal necessary to operate the board. The DAQ card was configured for digital output such that a high signal (+5.8) would activate a relay and a low signal (+0.8) would inactive the relay. Figure 3.3 shows the assembled configuration of the solenoid and relay on the breadboard. A diode (IN4005, RadioShack) was placed in parallel with the solenoid to prevent the electromagnetic field (EMF) from damaging the solenoid. Solenoids can produce back EMF and generate a voltage due to the removal of a current that is passing through an inductor. A 12 V DC power supply was utilized to power the solenoids and TTL-driven relay board.

An air and vacuum were used to actuate the PDMS valves. Both the vacuum and air lines were split into eight individual lines for the eight solenoid valves. Tygon tubing (R-3603, ID 1/16", OD 1/8"; Cole-Parmer) connected air to the port with that was normally open to ensure the closure of the PDMS valves at rest. The vacuum line was connected to the normally closed port. The middle port, which has access to the air or vacuum depending on the solenoid state, connected the solenoid to the PDMS valve. Figure 3.5 shows an image of the final setup with the DAC card, TTL-driven relay board, solderless breadboard, and solenoid valves all in view.

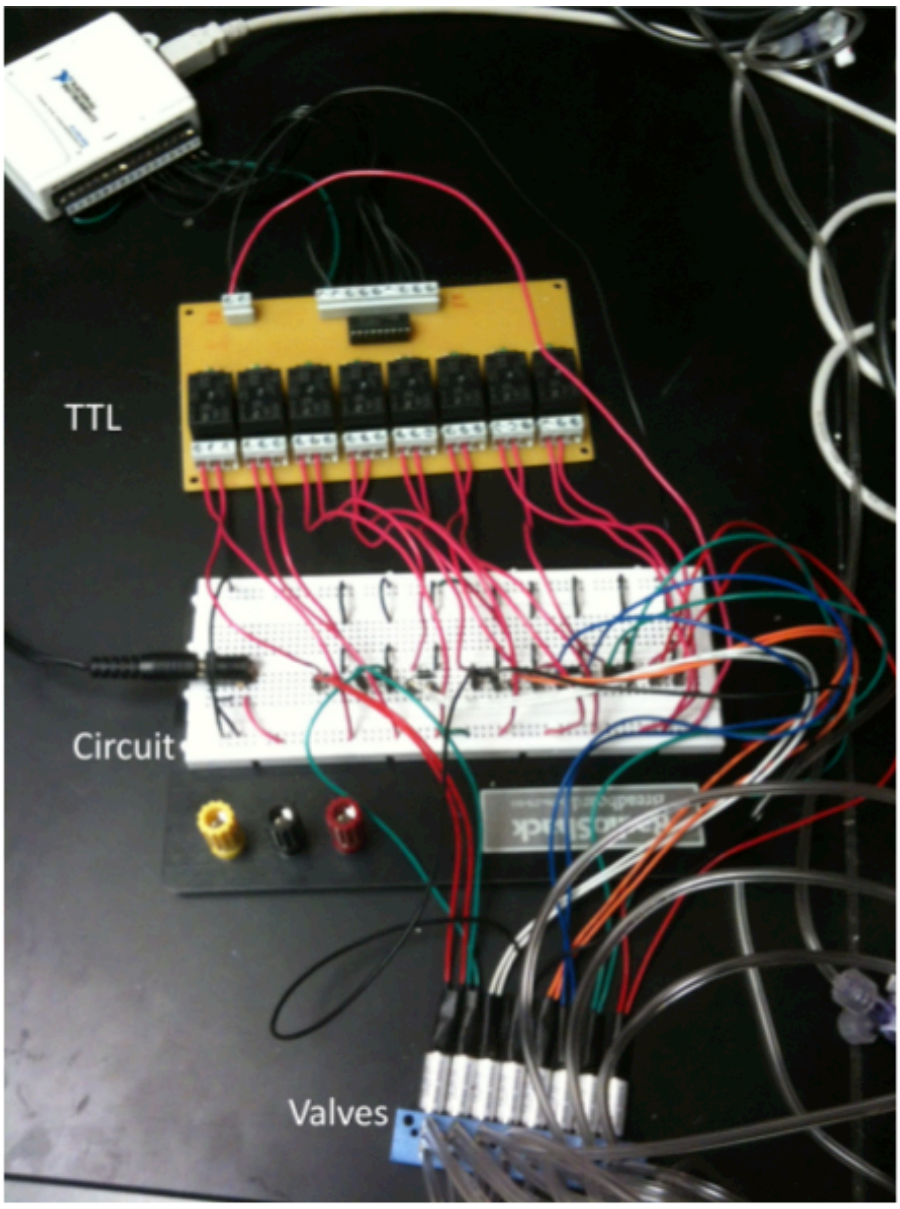

Figure 3.5 The setup to integrate the solenoid valves with the on-chip PDMS valves. A DAQ card (shown in white at the top left) sends +5.8V to active the TTL-driven relay. The relay and solenoids are all powered by a 12VDC power supply. The TTL signals are relayed through the breadboard and connected to the solenoid valves. Depending on the TTL signal, the valves can be at rest (valve closed) or energized (valve open).

To deliver air and vacuum to the on chip valves, the single air line and vacuum line were each both split into eight separate lines using nine 3-way stopcocks to control the flow and connectors to connect tygon tubing. Polytetrafluoroethylene (PTFE) tubing was chosen to connect the valves ports since it required less spac, and a connector and flexible tubing connected the PTFE to the tygon tubing attached to the solenoid valves. The air line was connected to a rotometer (FL-5511G-NV, Omega, CT) first to regulate the air flow going into the PDMS valves.

3.2.3 LabVIEW program to control valves

A LabVIEW (National Instruments) program and graphical user interface (GUI) was constructed to control the timing of the valves and therefore the fluid in the channels. The outputs of the program are the TTL signals of the DAQ card, and the user inputs are: 1) the time the valve is open, 2) the time the valve is closed, 3) the number of times the valve cycle is repeated, and 4) how long a valve is delayed before it is opened. Figure 3.6 shows the GUI that the user operates for valve control. The timing is controlled by the timing component of the computer, which is sufficient for this work since the valves are not operating at very high speeds. Appendix A details the code used to create the GUI.

3.2.4 Device characterization experiments

The device's ability to deliver chemicals of interest was characterized with several different dyes including food coloring, Fluorescein isothiocyanate (FITC), and

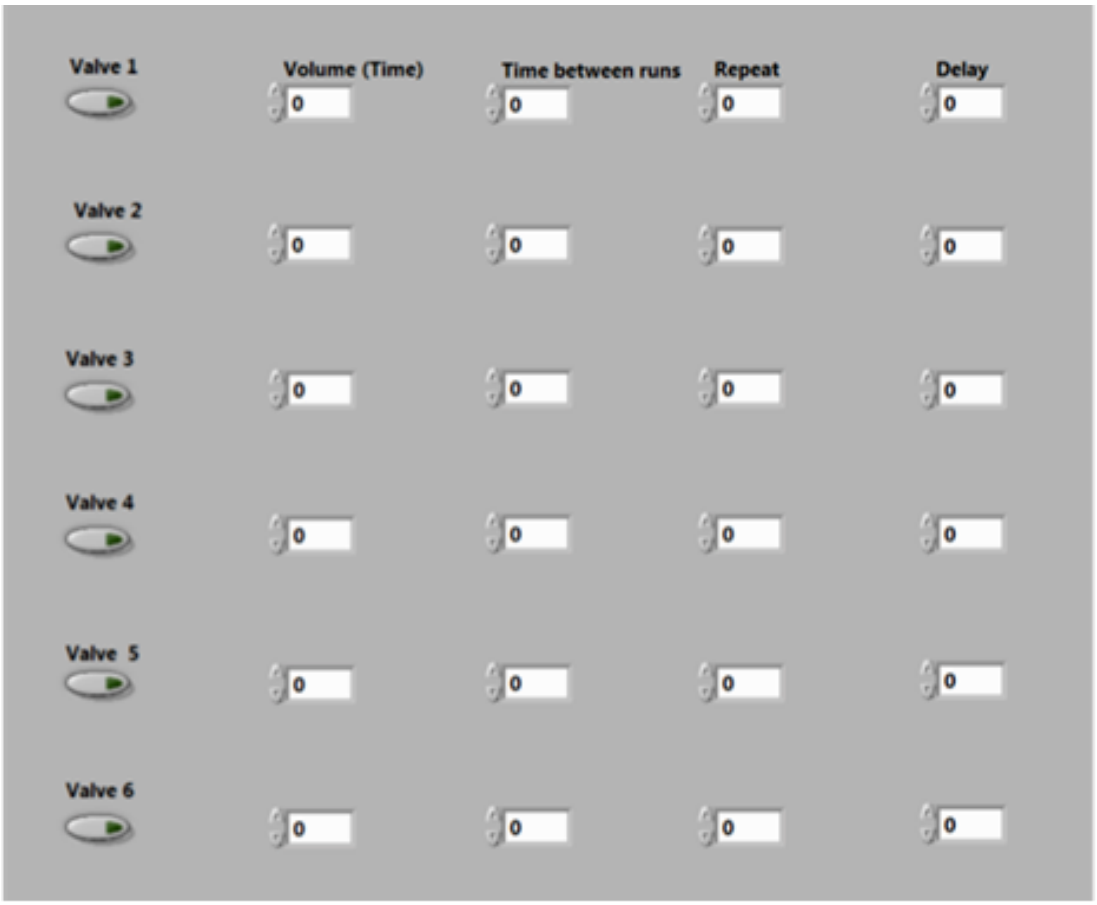

Figure 3.6. A screenshot of the LabVIEW based GUI to operate the PDMS valves on ACDD. Six different valves were available and independently controlled. The other two valves were reserved for actuating the buffer valves, which were held constant. The time the valves were open and close, the repetition of a valve cycle, and the delay were all controllable.

Sulforhodamine 101 (SR101), which all utilized a common setup. As stated previously, gravity perfusion was used to drive fluid through the channels. The dye was placed in 10mL open syringes. A connector was attached to the top of an intravenous (IV) dial to control the flow rate. Tygon tubing was connected to the bottom of the IV dial and inserted into the fluid ports of the ACDD with connectors. The open syringes hanged about 3 feet above the device. To operate the PDMS valves, the tubing from the solenoid valves were inserted into the ports on the device. A non-inverted macroscope (MVX10, Olympus, PA) was utilized for the characterization studies. A brightfield color camera (type, place) was used for the food color characterization, and a fluorescent camera (Hama type, place) was used for the FITC and SR101 studies.

3.2.4.1 Food coloring device characterization

Six open 10 mL syringes were filled with food coloring. Red and blue food color was placed in alternating syringes resulting in 3 blue food color syringes and 3 red food color syringes. One open 10 mL syringes was filled with buffer (distilled water). The channels on the device were perfused with alternating red and blue dye, and the buffer channel was filled. The IV dial regulated the flow to 5 mL/h. The valves were set to a cycle of 2 seconds open and 3 seconds closed to show the control the valves have over the perfusion of the dye into the channels, and the valves controlling the buffer channels were opened after each cycle to wash out the dye in the channels. Figure 3.9 depicts the channels first perfused with dye and subsequently rinsed with buffer with the opening of the buffer valves.

3.2.4.2 FITC Characterization

FITC was used to visualize the valve control of the fluid into the bath chamber through the vias. Five milliliters of 50 mM concentration of FITC was placed in the open syringes as previously stated. The flow rate was set to 5 mL/h, and the valves were programmed to open for 10s and close for 5s for each consecutive channel. Line-scans where drawn in line with the vias to measure the intensity of FITC that exited the vias into the bath.

3.2.4.3 SR101 characterization for yeast chemotropism experiments

A series of experiments were conducted to determine which parameters produced sharp and stable gradients in the agarose pad. The number of vias used, puffing rates, and the positioning of buffer channels were tested to determine the most optimal settings. The motivation for the different tests is detailed further in the results. The optimal parameters used for the yeast studies are presented below.

SR101 was used to simulate the pheromone gradient in an agarose pad. Four of the six channels were utilized. Sterile water was flowed through the first device, and 0.0025 mg/mL and 0.00125 mg/mL of SR101 was placed in the second and third channels respectively. Lastly, the fourth channel also had water perfused through. Perfusing the previously mentioned fluids through the channels until they exited the vias downstream prefilled the four channels. A 2% w/w concentration of agarose (BP1360-100, Fisher Scientific)/yeast peptone dextrose (YPD) was autoclaved and poured into the bath chamber and cooled for two hours before experimentation.. The valves for the buffer-filled channels (1 and 4) were programmed to open for 10s and close for 240s, and the valves for the SR101-filled channels (2 and 3) opened for 10s and closed for

300s for the duration of the 6 hour experiment. Line-scans where drawn above the vias to measure the intensity of SR101 in the agarose pad.

3.2.5 Yeast chemotropism experiments

The yeast chemotropism experiments used a similar procedure as stated in the previous section. As before, four of the six channels were utilized. YPD, the media for yeast, was placed in channels 1 and 4 and acted as a buffer to flank the injected dye. YPD with 400 nM α factor and YPD with 200nM α factor was placed in the second and third channels respectively. The channels were prefilled with the YPD until they exited the vias downstream. A 2% w/w concentration of agarose/YPD was autoclaved and poured into the bath chamber and cooled for two hours before experimentation. The valves for the YPD-filled channels (1 and 4) were programmed to open for 10s and close for 240s, and the valves for the YPD+pheromone-filled channels (2 and 3) opened for 10s and closed for 300s for 2 hours to establish a gradient at the surface of the agarose pad. A 28 mm coverslip was placed over the solidified agarose to prevent extensive drying and shrinkage. An overnight culture of MATa haploid-type bar- *S. cerevisiae* was position on the agarose pad with a PDMS stamp with 500 μm post 1.5 mm center to center spacing. The yeast were positioned above the vias in the device, and a 18 mm coverglass was placed on the yeast for high magnification imaging at 40x. The perfusion of the YPD and pheromone was restarted, and an image of the yeast was taken every hour for five hours.

3.2.6 Determination of yeast orientation to gradient

To determine if the established artificial gradient produced directed cell growth, the angle of orientation was determined by marking a line from the pheromone source to the center of the cell's base and a second line starting at the center of the cell's base through the middle of the cell's mating projection. A cell that had a projection directly towards the pheromone source had an angle of 0^{o}, and a cell that had a projection directly away from the pheromone gradient had an angle of 180^{o}. The mean, standard deviation, and standard error of mean were calculated for each set of orientation angles and each experiment was conducted three times.

3.3.1 Results

3.3.2 Automation, valves, and vias provide a higher degree of fluid control

PDMS on-chip valves upstream of the vias were essential for controlling the perfusion of fluids into the bath chamber area. Air pressure was used to ensure closure of the normally closed valves and prevented the vias from leaking. A vacuum was used to open the valves by deflecting the membrane downwards and allowing fluid to pass under the PDMS block that was once obstructing the fluid and exit out the vias as shown in Figure 3.7a and 3.7b. Normally closed valves were initially chosen since the time the fluid was being delivered was much less than the time the fluid was not delivered. In addition, it required less energy and resistance to keep a valve closed than the normally open on-chip valves, reducing the incidence of device failure. The on-chip valves were 300 μm in diameter to aide in the alignment with the channel layer above. It was important for the valve to sit directly underneath the disjointed segment of the channel and having the valve be significantly wider than the width of the channel allowed for margin of error

when hand aligning the PDMS layers. The buffer valves, which corresponded with the buffer channels that intersected the main fluid channels, varied slightly from the main channel valves. Here, one solenoid valve actuated three PDMS valves in contrast to the one to one configuration that was used for the main channel valves to reduce the number of solenoid valves.

The ability to automate the state of the valves allowed for a higher degree of control that is difficult to create with pipettes or other methods of delivery. Solenoid valves were used to actuate the on-chip valves through the use of a TTL-driven relay, DAQ board, and a LabVIEW GUI. The state of the valve either delivered a vacuum to open the valve or an air source to close it. The valves had a fast operation speed (50 ms), which was essential to have almost instantaneous action after GUI input. The key aspects of actuating the valves with the LabVIEW program were the 5V TTL signals and the timing mechanism on the computer processor. For our application, the computer's timing was sufficiently accurate to operate the valves. However, for extremely fast valve actuation (< 100 ms), different National Instruments hardware that is capable of time keeping on the order of milliseconds must be used for high accuracy.

Figure 3.6 shows the LabVIEW program, which has four user control inputs for the operation of the valves. These inputs were the time a valve were open (volume), the time a valve was closed, the number of times a cycle (the opening and closing of the valve) was repeated, and the time a valve was delayed before beginning a cycle. The timing was in seconds, and each of the valves was independently controlled. This configuration was important for the end user to have a variety of options to suit specific experimental needs. Appendix I shows the LabVIEW code and comments in detail.

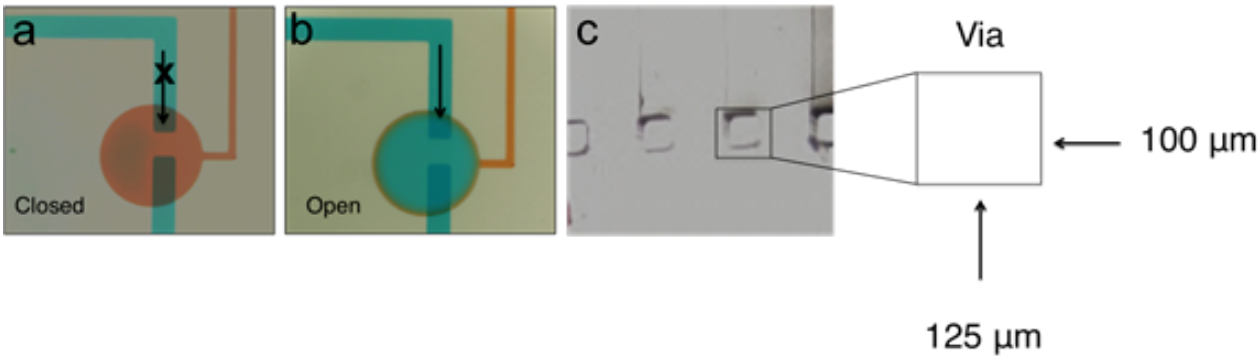

Figure 3.7 On-chip PDMS valves (red food coloring) were used to control the fluid dispersed from the vias downstream. (a) Initially, air was delivered to the PDMS valves to ensure closure of the valve. This blocks fluid upstream of the valve from passing to the lower segment of the channel (blue food coloring). (b). When a vacuum was applied to the valve, the membrane deflected downwards, which allowed fluid to pass under the PDMS obstruction and flow to the vias. (c). Vias were placed downstream of the valves for fluid access into the bath chamber. The vias measured 125 x 100 µm.

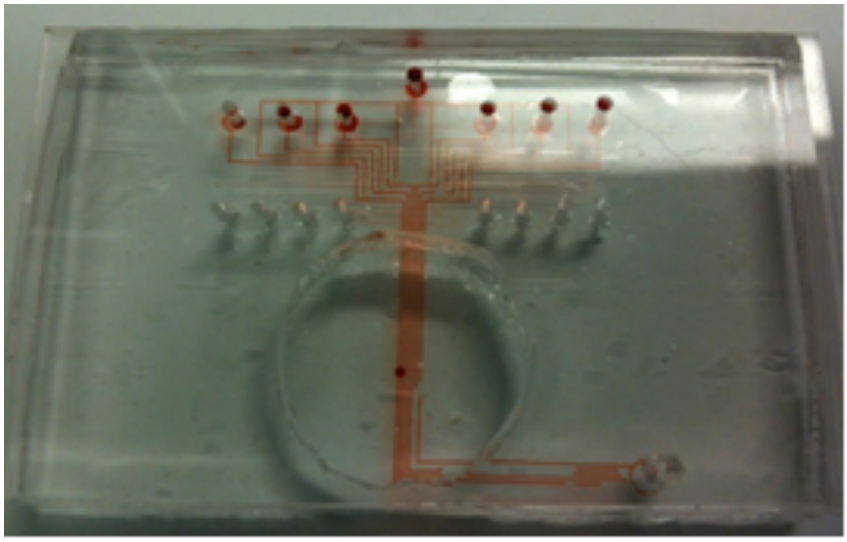

Figure 3.8 The ACDD was constructed from four layers of PDMS. The channel layer is highlighted in red.

The vias in Figure 3.7c were essential for constricting the area in which the fluid was deposited, which was essential for spatial control. The vias' dimensions of 125 W x 100 L microns was chosen to create a small opening for fluid dispersion and to have a robust SU-8 master that was able to endure many PDMS castings. The posts must be sufficiently tall to prevent PDMS coverage of the posts when spincoated, which is required to form a hole in the channel. Since the height of the posts were about 120 μm and the width were 125 μm, the posts had a ~1:1 aspect ratio. Constructing SU-8 posts with a smaller width would result in higher aspect ratios, which causes the posts to become more susceptible to breaking with each PDMS casting.

3.3.3 Characterization of the ACDD with color and fluorescent dyes

The ACDD, shown in Figure 3.8, was filled with red food coloring to highlight the six main channels and the intersecting buffer channels. The top seven ports were used for fluid input, and the bottom eight ports were for air or vacuum input to operate the valves. Vias were placed downstream in the center of the bath chamber and an exit fluid port was placed at the end of the channels. The exit port was places to redirect extra fluid that was not expelled from the vias. This was more commonly seen when a substance was sitting on the vias. In Figure 3.8, the vias were occluded to fill the lower portion of the channels with red food coloring for visualization. The bath chamber was filled with agarose for the yeast experiments, which are detailed in the following sections.

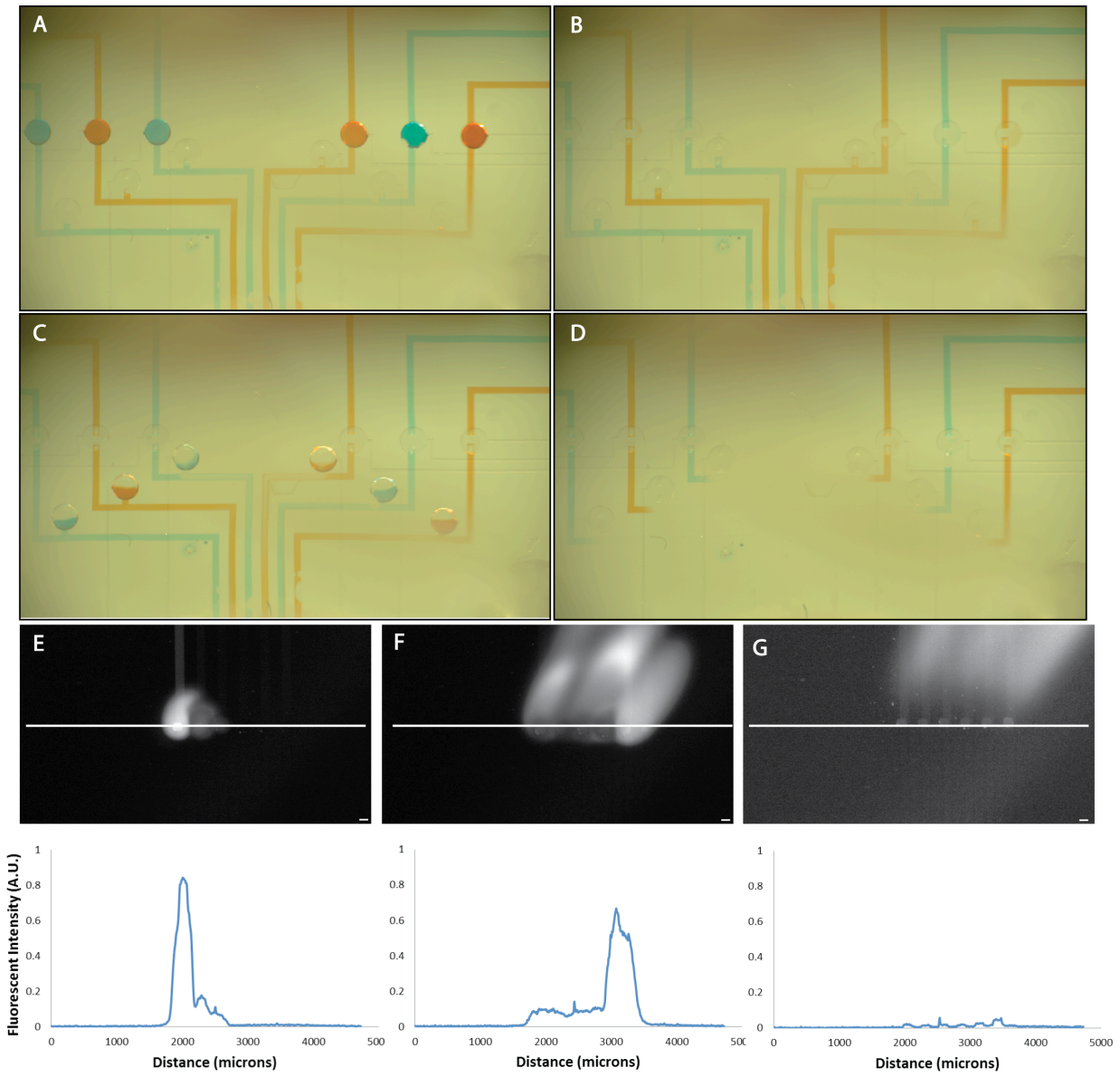

Figure 3.9 The ACDD controls the delivery of chemicals to the tissue. In panels A-D, the top valves control the dye, and the bottom valves control the buffer. (A)Initially, all the top valves are open and the bottom valves are closed. (B) The top valves close blocking the fluid flow while the bottom valves remain closed. (C) The top valves remain closed, and the bottom valves open to wash out the dye. (D) Both sets of valves are closed after all the dye is removed from the channels. FITC was used to visualize the puffing of chemicals into the bath chamber filled with water. The top six valves were sequentially opened in succession. The bottom three panels show the changing profile as the valves open and close after (E) 10s, (F) 30s, (G) and 60s. The FITC line profiles are displayed below shows the change in profile over time.

In Figure 3.9, the channels were filled with alternating blue and red food coloring. Since each channel was individually accessed, multiple chemicals or multiple concentrations of a chemical can be delivered and subsequently patterned on a substrate through the vias. Figure 3.9a-d shows the mechanisms involved during the operation of the main (top) and buffer (bottom) channel valves. In Figure 3.9a, the main channel valves were open allowing fluid to pass to the lower part of the channels towards the vias. The buffer channels, perfused with water, were closed. The solenoid valves switched to the air source closing the main channel valves (Figure 3.9b). Although it appears that the dye was filling the valves, the appearance of the dye in the circular valves was attributed to the food coloring occupying the void area between the membrane and channel once the valve was deflected. In Figure 3.9c, the buffer valve opened, and they briefly were filled partially with dye due the pressure of the fluid. However, water was quickly perfused into channels resulting in clearing the dye that once occupied the channels (Figure 3.9d).

The bottom three panels show the controlled release of FITC into the bath chamber filled with water. FITC was used as an example of a possible chemical that is delivered into the environment in this case the bath chamber. The top six valves were sequentially opened in succession and a line profile shows the intensity of FITC as the valves were opened and closed. Since FITC was deposited into the bath, the intensity of FITC in bath rapidly decreased after a valve was closed due to diffusion. The bottom three panels show the changing FITC profile after (E) 10s, (F) 30s, (G) and 60s. The ability to control the timing of chemicals into the bath chamber is essential for the development of gradients that is detailed further in the next section.

3.3.4 Gradient characterization for yeast chemotropism studies

To determine the pheromone gradient profile on the agarose, gradient characterization was performed with SR101, which has an excitation and emission of 585/605 nm. The red fluorescent dye was selected due to its similar diffusion coefficient (4×10 −6 cm2 s −1) to alpha factor in water. This similarity allowed for an estimation of gradient location that would be most like the pheromone gradient used in the studies.

A schematic of the dye delivery process is shown in Figure 3.10. The porosity of the 2% w/w agarose pad was favorable to the diffusion of dye and pheromone. The dye was perfused into the channels and exited at the via where it diffused through the ~2 mm thick agarose pad to the surface where the yeast cells were seeded.

Establishing a linear and stable gradient in the agarose was essential for the yeast chemotropism experiments with pheromone. To accomplish this, an optimal timing of the valving cycle was determined. It was important to find cycle that did not overwhelm and saturate the agarose, but was also capable of not losing the stability of the gradient produced. Initially, one via was perfused with SR101 (.01 mg/mL) as a starting point to determine the shape of the gradient profile. A valving cycle of 5s on and 30 minutes off was used as a starting pointing. We determined that the gradient produced while linear was changing to rapidly over time. Figure 3.11a shows the profile widening as the dye was perfused for 6 hours. This change was too large for the yeast studies and could not be utilized. Several other combinations were tested but most resulted in a widening profile. It was finally determined that a valving cycle of 10s on and 5 minutes off produced a profile that was stable after 2 hours but did not flood the agarose pad as

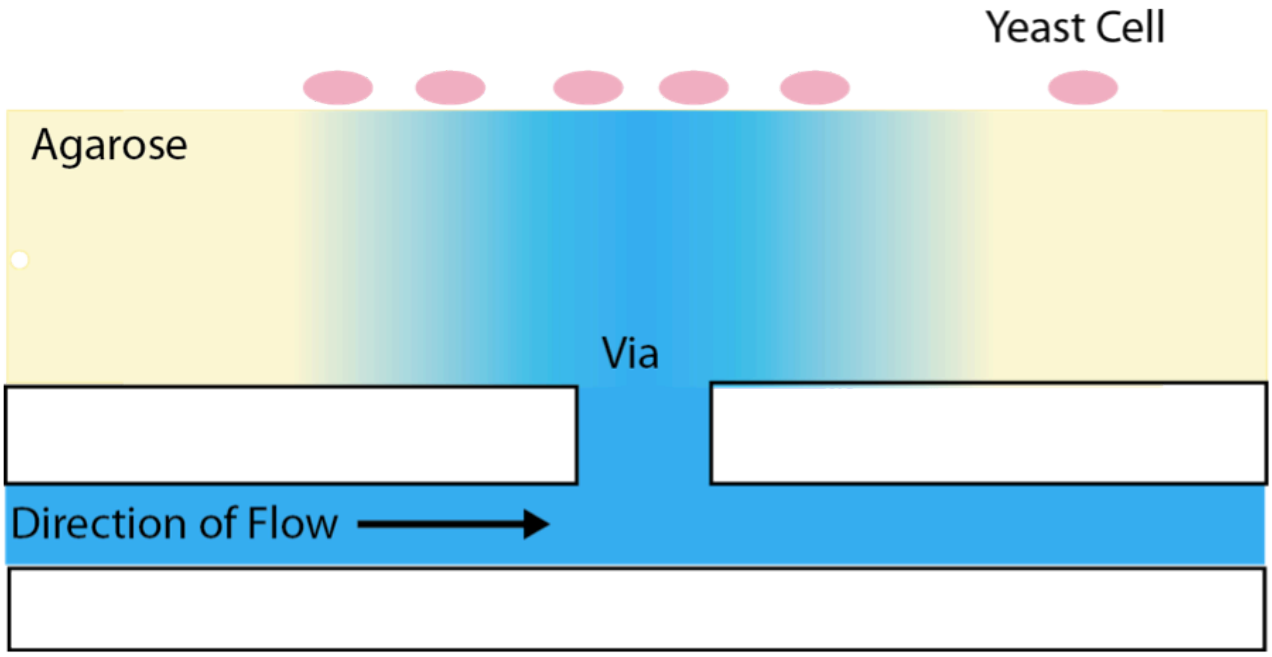

Figure 3.10 The schematic is a representation of the exiting of the dye from the channel via and its diffusion into the agarose pad. Yeast cells that were seeded at the surface were exposed to the gradient produced in the agarose pad.

shown in Figure 3.11b. Once the timing was determined, we focused creating a sharper linear gradient at the side of the profile.

Next, we used a high concentration of SR101 (.0025 mg/mL) one channel and a low concentration of SR101 (.00125mg/mL) to establish a sharp gradient difference. The overall concentrations of the SR101 was reduced from the previous single via trials to reduce the incidence of oversaturation in the images. The slope of the linear portion of the gradient profile was sharper however spreading at the top of the profile and the end were still apparent.

The final step to create a sharp linear profile was to flank the SR101 vias with channels filled with buffer. The rates of puffing the buffer was also optimized. The time the valve remained open was constant at 10 s. Only, the time the valves were off were changed. Initially, a puffing rates of 2 and 3minutes off were used, but this disturbed the profile of the original gradient instead of sharpening it. When longer times were used (5 and 6 minutes off), the profile did not exhibit a change. It was determined that a puffing rate of 10s on and 4 minutes off produced a sharp and stable gradient. The line profile of this configuration is shown in Figure 3.11c.

The final parameters used for the yeast studies are as follows. A linear gradient was established in the agarose by flowing a high concentration of SR101 (.0025 mg/mL) in channel 2 and a low concentration of SR101 (.00125 mg/mL) in channel 3. Channels 1 and 4, filled with sterile water, served as buffer channels to blunt the profile and created a sharper slope. In addition, the optimal valving cycle for a stable gradient was determined to be 10s open and 5 minutes closed for channels 2 and 3, and 10s open and 4 minutes closed for channels 1 and 4. The outside channels

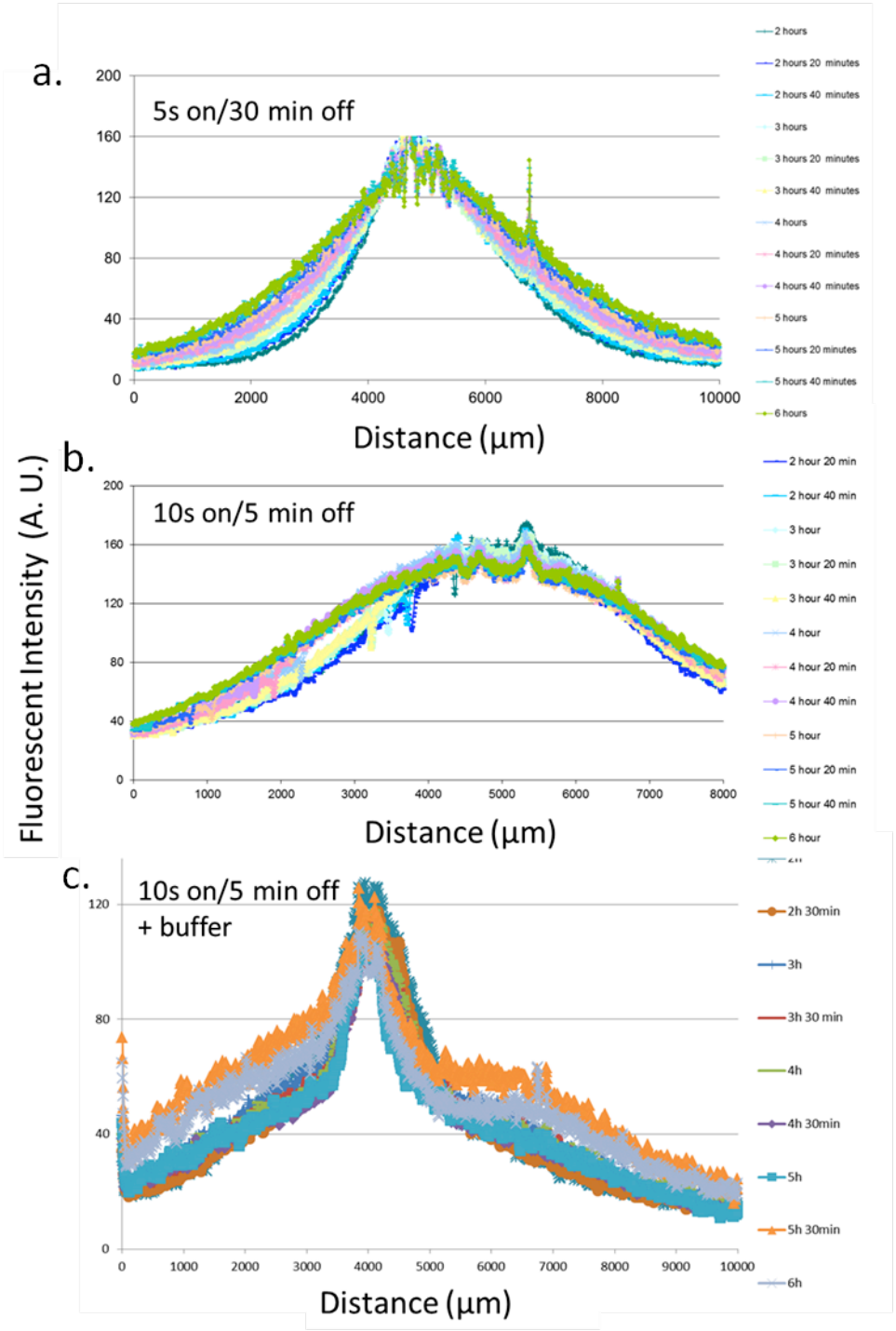

Figure 3.11. Line profiles of valve cycles (a) 5s on/30 minutes off, (b) 10s on/5 minutes off, and (c) 10s on/ 5 minutes off with buffer and pheromone were compared.

were perfused faster to create a sharper slope in the gradient. Figure 3.12 shows the change in intensity of the agarose pad between 0 minutes (3.12a) and just after 30 minutes (3.12b) of perfusion, and the profile of SR101 in the agarose after two hours is shown Figure 3.12c.

3.3.5 Pheromone gradient for yeast chemotropism studies

The SR101 studies gradient experiments provided an approximation of the pheromone gradients produced for the orientation studies. A linear pheromone gradient was established similarly to the SR101gradient in the agarose by flowing a high concentration of pheromone (400 nM) + YPD in channel 2 and a low concentration of pheromone (200 nM) + YPD in channel 3. Channels 1 and 4, filled with YPD without pheromone, served as buffer channels. Since the gradient stabilized after 2 hours, the yeast were placed onto the agarose pad with a PDMS stamp after this time point (Figure 3.13). The stamp ensured that a small number of yeasts and more importantly single yeast cells were deposited onto the agarose. The yeast cells were imaged every hour for 5 hours to track the development of shmoos in response to the artificial gradient. Using criteria stated in the methods, the angle of orientation was measured for single yeast cells. Table 3.1 shows the results from the studies. Out of 62 eligible cells, 36 were shmooed, and the average angle of orientation was 62.2 degrees with an SEM of 6.8 degrees. This confirmed that the cell were able to recognize the gradient and orient preferentially towards it.

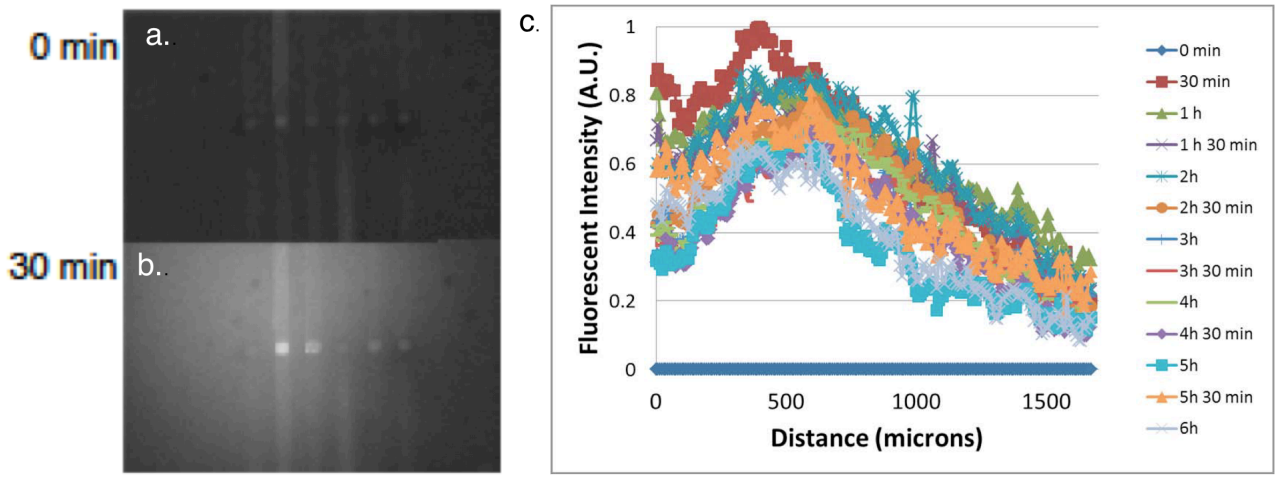

Figure 3.12 SR101 was used to visualize the gradient profile in the agarose before perfusion (a) and 30 minutes after perfusing the dye (b). After 30 minutes, a noticeable increase in intensity was observed. (c). An intensity profile was collected after 2 hours of perfusion and it exhibited a stable and linear profile.

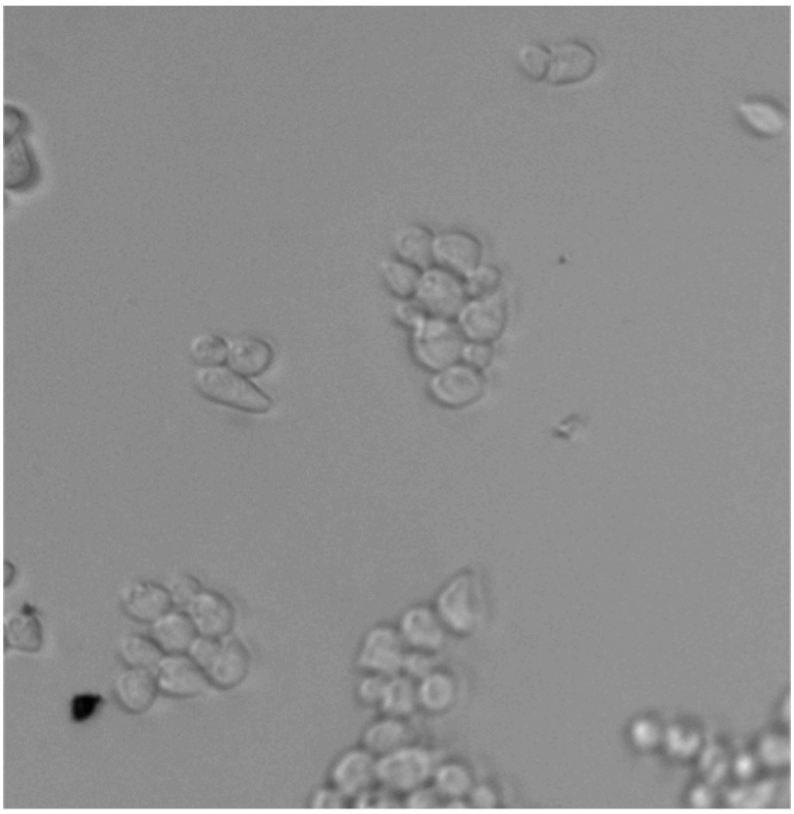

Figure 3.13 Yeast cells arresting in their cell cycle and shmooing in the presence of a gradient.

# of eligible cells	64
# of shmooing cells	36
Average angle of orientation	62.2 degrees
Standard Deviation	40.8 degrees
SEM	6.8 degrees

Table 3.1 The yeast cells average angle of orientation.

3.4.1 Discussion

The automated chemical delivery device is a platform that can establish gradients in tissues and other constructs. Here, we created a pheromone gradient on agarose for the study of yeast chemotropism. While the construction of the device and its corresponding setup required many components, the device was not difficult to operate after assembly and the end user simply required gravity perfusion and the LabVIEW GUI for operation. An advantage of the device was the ability to seed cells on agarose. There are previous microfluidic devices that are able to expose yeast to pheromone gradients. However, the yeast in these devices sit on PDMS, which is not ideal for pheromone studies. PDMS is hydrophobic and readily absorbs small molecules into the bulk. Therefore, the concentration of pheromone that is perfused through the device may not be the same concentration that is seen by the cells. The ACDD reduces this problem by limiting the time the pheromone is in the device. Once the pheromone has exited the via and is diffused into the agarose, the pheromone is no longer in contact with the PDMS. Since the yeast are seeded on agarose, it allows for any assays conducted on agarose to be performed on the device.

The gradient profile can be adjusted to fit experimental needs. For the chemotropism experiments, the optimal valve cycle and pheromone concentrations created a profile suitable for our studies. However, any of these parameters are flexible and can be altered for other studies. For example, to create a steeper gradient, a larger difference between the pheromone concentrations (400 nM and 200 nM to 400 nM to 50 nM) or faster perfusion of the buffer channels could be implemented. The ability to create a stable gradient in agarose is important since an added dimension comes into play. Most microfluidic devices can be treated as 2D since there are little changes in the z-direction. While ACDD itself is microfluidic, how it delivers the

chemicals to the yeast is not and the z-direction must also be considered since the pheromone has to diffuse through the agarose. This was a factor in the SR101 gradient characterizations since it was difficult to isolate the plane at which the dye was fluorescing. Although a stable gradient was produced, the light emitted by the dye may have been at other planes of the agarose even though the surface was in focused for images. An agarose pad thickness of ~2mm was chosen since it was thin enough to limit the diffusion of the pheromone while hindering the shrinking of the agarose pad over the course of the experiment.

The chemotropism experiments confirmed that the yeast were sensing a gradient, and they preferentially shmooed in the direction of the gradient. There were initial concerns over the ability of the yeast to shmoo since the gradient was essentially underneath the cells and although the yeast cannot burrow in the agarose, it was unsure if they would respond to a planar gradient below them. However, the angle of 62.2^{o} that was calculated from the experiments falls in line with other microfluidic devices that had an average angle of orientation of about 60^{o}. One issue that arose was the number of cells that were shmooing in the gradient. In standard yeast culture with α factor, approximately 80% of the cells were shmooing. On the device, a much lower concentration of cells about 30% were shmooing. Several factors could contribute to the discrepancy. Although a PDMS stamp was used to place cells onto the agarose pad, a large number of cells were aggregated together. This may affect the cells' ability to recognize the gradient due to cells in close proximity. In addition, as with all cell types, the yeast have heterogeneous behavior, and it is possible that the concentrations used (400 and 200 nM) do not produce a gradient sharp enough to trigger shmooing in some cells. As stated before, cells respond to a very steep gradient, so increasing the slope may increase the number of cells that

shmoo. Future experiments, detailed in the next section, will explore the limits of the gradient production to improve both angle of orientation and the number of cells shmooing.

3.5.1 Future direction

While a 60^{o} angle of orientation coincides with the angles stated in literature, it is ideal to produce a smaller angle of orientation. As stated before, cells are heterogeneous even amongst cells of the same type so it is unreasonable to expect all the cells to orient perfectly towards the gradient. However, changing the current system may reduce the angle of orientation. Future studies will address this by increasing the slope of the gradient by changing the pheromone concentrations and increasing the buffer perfusion.

After the orientation experiments, the next step is to induce reorientation in the yeast. This is performed by change the direction of the gradient so a 90 or 180 degrees change moves the initial shmoo towards the direction of the newly established gradient. The current device is not wel1-suited gradient change, but the device detailed in chapter 4 has 192 vias, which increases the possibilities for more complex gradient profiles.

The ability to control chemicals of interest, in this case pheromone, to study cellular behavior is a translational tool to other cell and tissue types. The next section details how the same concept of chemical control is also vital for neurobiological studies.

References

1. Bennett, M.K. and R.H. Scheller, *The molecular machinery for secretion is conserved from yeast to neurons.* Proceedings of the National Academy of Sciences, 1993. 90(7): p. 2559-2563.
2. Follette, P.J. and R.A. Arkowitz, *Chemotropism During Yeast Mating Chemotaxis*, T. Jin and D. Hereld, Editors. 2009, Humana Press. p. 99-110.
3. Arkowitz, R.A., *Responding to attraction: chemotaxis and chemotropism in Dictyostelium and yeast.* Trends in Cell Biology, 1999. 9(1): p. 20-27.
4. Ydenberg, C.A. and M.D. Rose, *Yeast Mating Cell Fusion*, E.H. Chen, Editor 2008, Humana Press. p. 3-20.
5. Hagen, D.C. and G.F. Sprague, Jr., *Induction of the yeast alpha-specific STE3 gene by the peptide pheromone a-factor.* J Mol Biol, 1984. 178(4): p. 835-52.
6. Hartig, A., et al., *Multiple regulation of STE2, a mating-type-specific gene of Saccharomyces cerevisiae.* Mol Cell Biol, 1986. 6(6): p. 2106-14.
7. Dohlman, H.G. and J. Thorner, *REGULATION OF G PROTEIN–INITIATED SIGNAL TRANSDUCTION IN YEAST: Paradigms and Principles.* Annual Review of Biochemistry, 2001. 70(1): p. 703-754.
8. Park, H.-O. and E. Bi, *Central Roles of Small GTPases in the Development of Cell Polarity in Yeast and Beyond.* Microbiology and Molecular Biology Reviews, 2007. 71(1): p. 48-96.

9. Segall, J.E., *Polarization of yeast cells in spatial gradients of alpha mating factor.* Proc Natl Acad Sci U S A, 1993. 90(18): p. 8332-6.

10. Vallier, L.G., J.E. Segall, and M. Snyder, *The alpha-factor receptor C-terminus is important for mating projection formation and orientation in Saccharomyces cerevisiae.* Cell Motil Cytoskeleton, 2002. 53(4): p. 251-66.

11. Moore, T.I., et al., *Robust Spatial Sensing of Mating Pheromone Gradients by Yeast Cells.* PLoS ONE, 2008. 3(12): p. e3865.

12. Paliwal, S., et al., *MAPK-mediated bimodal gene expression and adaptive gradient sensing in yeast.* Nature, 2007. 446(7131): p. 46-51.

13. Nern, A. and R.A. Arkowitz, *A GTP-exchange factor required for cell orientation.* Nature, 1998. 391(6663): p. 195-8.

14. Valtz, N., M. Peter, and I. Herskowitz, *FAR1 is required for oriented polarization of yeast cells in response to mating pheromones.* J Cell Biol, 1995. 131(4): p. 863-73.

15. Dorer, R., P.M. Pryciak, and L.H. Hartwell, *Saccharomyces cerevisiae cells execute a default pathway to select a mate in the absence of pheromone gradients.* J Cell Biol, 1995. 131(4): p. 845-61.

16. Brett, M.E., et al., *A microfluidic device that forms and redirects pheromone gradients to study chemotropism in yeast.* Lab Chip, 2012. 12(17): p. 3127-34.

17. Whitesides, G.M., *The origins and the future of microfluidics.* Nature, 2006. 442(7101): p. 368-373.

IV. CHAPTER 4: THE DEVELOPMENT OF AN EXPANDED AUTOMATED CHEMICAL DELIVERY DEVICE FOR THE DELIVERY OF CHEMICALS TO CELLS AND TISSUES

4.1 Introduction

4.1.1 The development of platforms to control cell and tissue environment

In the United States, the need for transplantable organs far exceeds the supply available. Many people die waiting for compatible donor organs, and this imbalance has driven research to develop methods to construct ex vivo organs and tissues. There are many aspects that one must consider when engineering an organ such as the cell type, materials and scaffolds required for cell growth, and the chemicals and signaling molecules in the microenvironment[1]. While the cell type and scaffolds were initially the focus, it has been shown that the microenvironment plays a large role in cell behavior as seen with cell differentiation[2-4] and cell migration[5-7]. It is essential to have a clear understanding of how cells behave in their microenvironment in order to scale to these interactions to the macroscale of tissues and whole organs. Specifically, there is a need to direct the environment of cells and tissues in a way that is analogous to in vivo behavior.

Microfabrication is a platform that is able to produce devices that can manipulate chemicals, proteins, cells, and other molecules to control the microenvironment. Microfluidics, a smaller segment in the area of microfabrication, is also well-suited for microenvironment control since it can precisely control small volumes of fluid at the sub-millimeter scale[8]. The need for microenvironment control is applicable for the study of many different cell and tissue types. The next sections will detail previous microdevices constructed for the spatial and chemical control

of cell and tissues to explore behavior. The first several sections will detail examples of devices that are capable of patterning of cells and initiating chemical gradients. To show the need for chemical control in tissues, examples of microfluidic devices constructed for the delivery of chemicals to brain slices will also be profiled.

4.1.2 Cell patterning

The use of soft lithography-derived devices for cell patterning has become a popular method in cell biology. Although cell patterning is the common nomenclature, the patterning actually begins on the cell substrate either with proteins[9-13] or a modification of the substrate's surface[14, 15] to enhance cell attachment to specific domains on the substrate. Since it is possible to create micron sized dimensions, PDMS stamps are a simple tool for protein deposition[16]. This method is called microcontact printing, which was demonstrated by Zhang et al. They utilized self-assembling oligopeptides that are recognized by cells for adhesion. Using this method, they were able to pattern a variety of cells which included human carcinoma and mouse fibroblast cells which are shown Figure 4.1[17]. Cell patterning can also occur inside microfluidic devices. Takayama et al. utilized the laminar flow in the microchannels to pattern cell culture media, cell culture substrate, and the cells themselves[18]. They were able to pattern two different cell types as well as control the geometries of the patterns.

The drive behind cell patterning is that tissues are not homogenous. There are multiple cell types in a given organ, and many times, a heterogeneous environment is required for cells to exhibit optimal behavior[19, 20]. A drawback with micro-contact printing is the possibility of an unstable, patterned monolayer depending to the method used[21]. However, these cell-

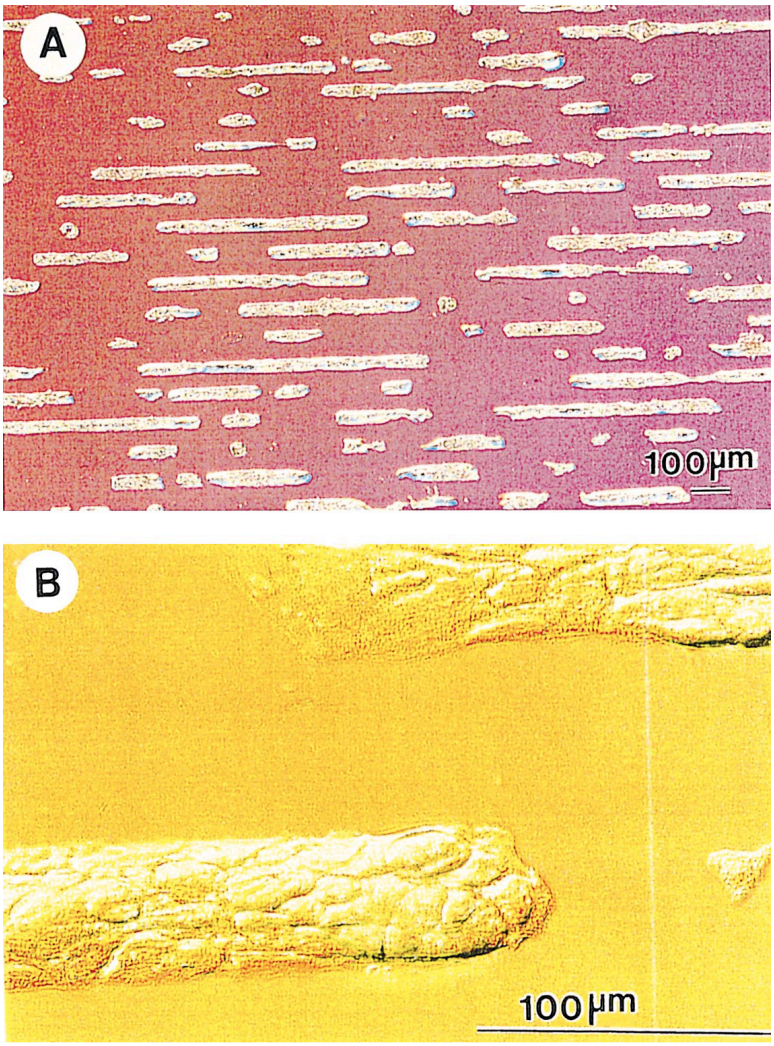

Figure 4.1 Human epidermal carcinoma A431 cells on a linear array pattern at (A) 50X and (B) at 400X**.** (reprinted from Zhang et al., Biomaterials, 1999) .

patterning tools allow the ability to control the positioning of cells and correlate the spatial environment with its behavior in a systematic method that is reproducible for experimentation.

4.1.3 Production of gradients for chemical control

In addition to the spatial control of cells, the chemicals and soluble factors in a cell's environment can determine cellular behavior. Most commonly, these chemicals are produced as gradients in the cell's vicinity. Gradients of soluble factors are involved in a multitude of biological processes including chemotaxis[22-24], development[25, 26], and nerve growth[27, 28]. Due the extensive role of gradients, it is important to accurately reproduce this phenomenon. Microfluidics is valuable tool for gradient generation since, as previously stated, laminar flow restricts mixing to diffusion. This can be manipulated to create gradients in Y-channels (also called T-sensors)[29-31]. Y-channel devices consist of two microchannels that converge into a single channel, and the devices configuration resembles the letter Y or T. Two fluids flowing into the inlets and into the main channel, and since diffusion is the only method of mixing, a gradient is established down the channel. The gradient's properties depend on the flow rate, channel length, size of solute, and other factors. A disadvantage of this method is that signaling molecule produced by the cells are removed due to the constant perfusion of media. In addition, the shear stress from the fluid flow could activate shear-dependent pathways in the cells and effect cell behavior. While there are many variations of gradient producing microfluidic devices, many of them utilize the same properties established in Y-channels.

The following three sections will move from cells to tissues. The ability to control the delivery of neurotransmitters and drugs to brain slices is very important for understanding how

these chemicals interact with the brain. This has driven the development of microfluidic devices for the control of chemicals to brain slice tissue.

4.1.1 Neuronal signaling

Neurons, the cellular component of the nervous system, are one of the few cell types to communicate via electrical signaling. A neuron receives a stimulus and relays this information as action potentials to different neurons or other cell types. With estimates of 100 billion neurons and 100 trillion synapses in the brain, the shear number conveys the intricacy of this system [32]. Neurons are assembled into neural circuits, which are neurons organized to process specific type of information. Neural circuits are scaled up to neural systems (including central, periphery, parasympathic, and sympathetic) creating an interconnected network between the cells. This scaling up culminates in the behavior of the organism, and the need to understand how external cues are processed in these neural circuits and subsequently produce a particular behavior is a large driving force behind the research in psychology. The ability to understand the mechanisms behind behavior is a step towards understanding what has deviated in a variety of disease states such as Parkinson's.

4.1.4 Brain slice preparation is used to study neurons in vitro

Brain slice preparation is an extensively used in vitro technique to study neuron characteristics and behavior[33]. Its popularity is attributed to several factors including the ability to directly image the neural networks, have full control over the slice environment, and easily deliver drug and neurotransmitters without the interference of the blood brain barrier.

While the brain slice preparation is not an exact representation of an intact brain, the maintenance of the neural microcircuits in the brain slice allows for the study of interactions without the extensive experimental setup that is required for in vivo work. Currently, it is common to deliver chemicals to a brain slice by bath application. However, this does not reflect the conditions in vivo. For more control over chemical delivery, another method puffs chemicals onto a slice using a pipette. This method does localize the release, but it is difficult to control the application of the chemicals and only a very small area is stimulated in relation to the circuit.

4.1.5 Microfluidics is well-suited for the area of neurobiology

The present issues can be addressed with the application of microfluidics.. There have been several microfluidic devices designed to control the delivery of chemicals to brain slices[34-36]. One example utilizes the laminar flow and, similarly to Takayama et al., delivers chemicals of interest over a brain slice[34]. Since there is no mixing, different streamlines of chemicals can be delivered to different regions of the brain slice. However, this is still a relatively large area, and a streamline cannot target a small portion of the brain slice. Another design reduces the area of delivery for better control with the application of microposts. The slice sits on a bed of microposts, and a few are connected to ports that deliver chemicals when suction is applied[36]. This increases the spatial control by reducing the area a chemical is applied to the However, only a few posts have chemical delivery, which reduces the possible locations where a chemical can be delivered on a slice. As with cells, it is necessary to create platforms that can highly control chemical microenvironment of tissues.

4.1.6 The expanded ACDD patterns chemicals on a substrate

The expanded ACDD design borrows the valves and vias utilized in the ACDD and expands it to create a grid of 192 vias that are all independently controlled. The device is a combination of the cell patterning and gradient-producing devices previously mentioned. Essentially, the large grid of vias that are coupled to fluid inlets can pattern chemicals of interests onto tissues or substrates for cell culture. The device has three fluid inlets for the patterning of multiple chemicals on a substrate, and the number of vias allows for multiple points of chemical delivery. In addition, the delivery of fluids is also temporally controlled through valve automation. This time-dependent delivery creates a dynamic platform for cells that can change the type and concentration of chemicals on a substrate over time and makes this a unique platform for the study of cell behavior in a dynamic system.

The ability to deliver chemical spatially and temporally is also essential for tissue, especially brain tissue. The timing and location of neurotransmitters or drugs can affect the activity of a slice, and there are many pathways that are not understood very well. The expanded ACDD will allow for multiple points of chemical delivery on a brain slice for an unlimited number of possible of chemical configurations. This chapter details the construction and methodology of the development of the array device.

4.2. Methods

4.2.1 Device fabrication of large array device

4.2.1.1 Fabrication of SU-8 masters for the valve and channel layers

The expanded array device was composed of four PDMS layers. Two of them, the valve and channel layers, were patterned. Figure 4.2 shows the corresponding AutoCAD layers between the ACDD and the expanded device. The master for the valve layer was composed of one SU-8 layer. SU-8 2050 was spun on a 4 inch silicon wafer at 500 RPM for 10s and 2100 RPM for 30s.

The wafer was softbaked at 65^{o}C for 3 minutes and 95^{o}C for 9 minutes. The SU-8 was exposed to UV light at an exposure energy of 215 mJ/cm^2 through a patterned transparency. The wafer was postbaked at 65^{o}C for 2 minutes and 95^{o}C for 7 minutes, and developed in SU-8 developer (MicroChem, PA). To aid in PDMS membrane removal, the wafer was silanized with 50 μL Tridecafluoro 1, 2,2-tetrahydroctyl)-1-trichlorosilane (United Chemical Technologies, PA) in a desiccator for 30 minutes.

The channel master was composed of two SU-8 layers. SU-8 2015 was spun on a 4 inch silicon wafer at 500 RPM for 10s and 2000 RPM for 30s. The wafer was baked at 95^{o}C for 4 minutes and cooled. A maskless photolithography system called MicroPG101 (Heidelberg Instruments, Germany) was used to pattern the SU-8 at an exposure energy of 150 mJ/cm^2. After patterning, the wafer was baked for 5 minutes at 95^{o}C and developed in SU-8 developer for 1 minute with gentle agitation. The final height of the first layer was 25 μm. The second layer consisted of posts that would eventually become vias in the channels. Before spincoating the second SU-8 layer, tape was used to cover the alignment marks for better alignment in the MicroPG. SU-8 2100 was spun at 500 RPM for 10s and 2000 RPM for 30s. The tape covering the alignment mark was removed, and the wafer was baked at 65^{o}C for 5 minutes and then at 95^{o}C for 25 minutes. The wafer was patterned in MicroPG at an exposure energy of 250 mJ/cm^2

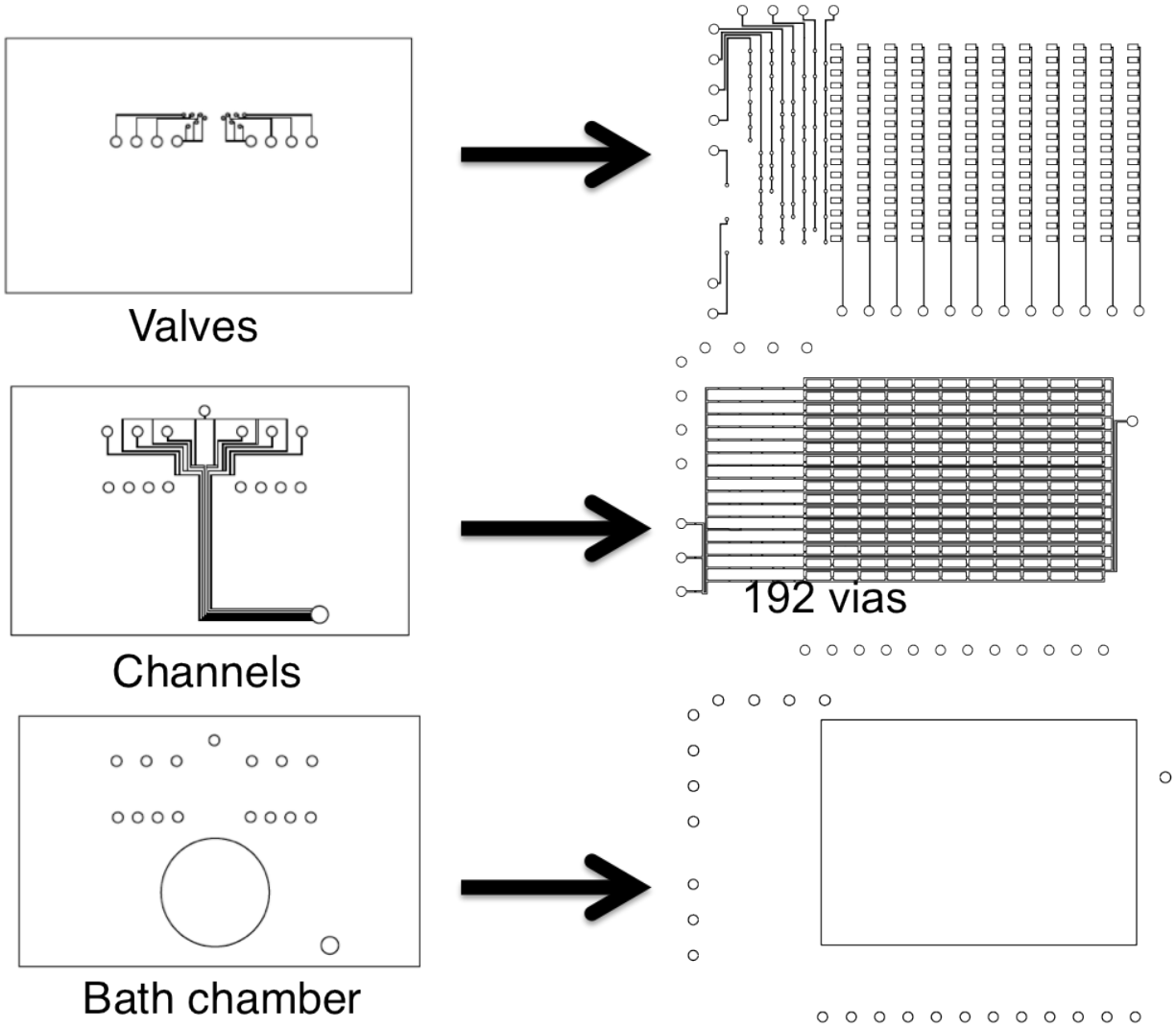

Figure 4.2 While the expanded ACDD appears to be much different than the original ACDD, the separate layers perform the same function. The valves control the fluid flow through the channels placed above, and the vias provide access to the surface where brain tissue is placed. The bath chamber provides inlets for fluid, air, and vacuum and can house buffer or media to maintain the tissue.

and was placed at 65°C for 5 minutes and 95°C for 11 minutes. The wafer was developed, and the final master resulted in channels with posts in areas were vias would be in the PDMS membrane. The master was also silanzed for 30 minutes for PDMS removal.

4.2.1.2 Fabrication of the PDMS layers and device assembly

The bottom PDMS layer of the device served as a base for the subsequent valve and channel membrane layers. A PDMS prepolymer (Sylgard 184, Dow Corning, IL) was mixed 10:1(polymer:curing agent) and poured into a square polystyrene petri dish (08-757-11A, Fisher Scientific, MA) to a ~4mm thickness and degassed. The PDMS was baked at 85°C for 90 minutes. Approximately 20g of PDMS was mixed, degassed, and placed aside for 2 hours for a thicker consistency. The master for the valve layer was spincoated with a quarter-sized deposit of PDMS at 800 RPM for 30 seconds and cured at 85°C for 90 minutes. The membrane was gently cut and removed from the wafer and placed on a cutting mat. A 14 gauge hole punch (6710A42, McMaster-Carr, PA) was used create the inlet and outlet ports for the valves. The membrane was plasma treated with a corona discharge device (BD-20AC, Electro-Technic, IL) and bonded to the 4 mm PDMS slab. Great care was taken to limit the number of bubbles between the two layers.

From the same 20 g premixed PDMS, the channel layer was spincoated at 1000 RPM for 30 seconds. Before curing, compressed air was used to remove PDMS covering the posts and placed aside for 30 minutes to allow for PDMS reflow for a uniform layer. The PDMS membrane was cured at 85°C for 90 minutes. Once cured, the wafer was silanized. The wafer was placed in the desiccator surrounded by four glass slides on each side and 50 μL of the silane

was placed on each slide and was silanized for 30 minutes. The wafer was placed into a petri dish with double-sided tape. About 70 g of the PDMS was mixed, degassed, and poured onto the channel membrane. It was degassed and baked at 85^{o}C for 90 minutes. Once cured, both layers of PDMS were removed together from the wafer with care to prevent the membrane from separating from the larger PDMS slab. With the slab side down, the inlets and outlets were punched with a 14 gauge hole puncher. The membrane side of the channel layer and the top of valve+PDMS base construct was plasma treated, aligned, and bonded under a macroscope (MVX10, Olympus, PA). Once bonded, the device was quickly attached to a 24-solenoid valve construct (detailed in the next section) that corresponded to each on-chip PDMS valve and was connected to a vacuum to deflect the valves downwards and prevent bonding. The device was placed on a 55^{o}C hotplate with a 3kg weight for 20 minutes to aid bonding. The vacuum was cycled on and off every for 30 minutes for the first 3 hours to prevent the valve from bonding with the bottom of the device in addition to the top. Lastly, the device was left undisturbed overnight. Next, the device was removed from the vacuum and solenoid valve construct. Slowly, compressed air was directed in between the thick PDMS layer and channel layer for separation. Once removed, inlets, outlets, and a bath chamber were made in thick PDMS layer. The top of the channel layer and the bottom of the PDMS bath chamber was plasma treated and bonded. As before, the device was placed on a 55^{o}C hotplate for 20 minutes with the chamber side down, and a weight was placed on top. After 24 hours, the device was cut into a desired rectangular shape and was ready to use.

4.2.2 Assembly of the 24-solenoid valve controller

Due to the increase in the number of on-chip PDMS valves, a different solenoid valve configuration was used to actuate the valves on the device. The USB-based controller developed by Rafael Gómez-Sjöberg at Lawrence Berkeley National Laboratory (LBNL) was constructed accordingly. This controller operates 3 valve manifolds which each house 8 solenoid pneumatic valves for a total of 24 valves. A custom-designed printed circuit board (PCB) was provided by the foundry. The controller box houses a commercial USB-based digital input/output (I/O) card connected to the PCB with 24 amplifiers, which converts the 0-5V low power outputs from the USB card to the high-current signals required to drive the solenoid valves. The PCB required resistors, capacitors, diodes, and other components for operation. The extensive list of all the components needed for the PCB is listed in Appendix B. The required parts were carefully soldered with a 25-watt solder iron (SP23LK, Weller) to prevent damage to the PCB. Ribbon cable (MC10M-5-ND, Digi-Key, MN) were used to connect the PCB to the USB I/O card, which was connected to a USB port on the computer. The controller required a 24V power source to drive the valves, and connectors were needed on the end of the solenoid valve cables to connect to the controller box. The solenoid valves (Festo, IL) have high switching times (4ms) and this specific PCB was designed to accommodate the fast speed of these valves. To connect a vacuum and air source, 1/4" OD x 0.17" ID polyurethane tubing (PU-250PB, Pneumadyne, MN) was connected to the side ports for each valve manifold. To connect the solenoid valves to the PDMS valves, 5/32" OD x 3/32" ID polyurethane tubing (PU-156F-0, Pneumadyne, MN) was cut to a length of 50 mm and attached to the output of each solenoid valve, and a male luer lock to barb for 3/32" ID tubing (51525K272, McMaster-Carr, PA) was connected. A corresponding

disposable Needle, 23 Gauge (75165A684, McMaster-Carr, PA) was inserted into the male luer lock, and 0.06" OD x 0.02" ID Tygon microbore tubing (EW-06418-02, Cole-Parmer, IL) connected the needle to the PDMS valve to deliver either air or vacuum.

4.2.3 Matlab software for valve actuation

Software to operate the valves was developed by Dr. Rafael Gómez-Sjöberg at Lawrence Berkeley National Laboratory. The software provided a base to build a MATLAB GUI for easier control over all the valves on the device. Detailed MATLAB code is presented in Appendix B.

4.3 Results and Discussion

4.3.1 The development of the expanded ACDD

When designing the large array device shown in Figure 4.3, there were several issues that had to be addressed concerning the device fabrication. First, the membrane used to create the valves on ACDD was very thin and while the membrane was appropriate for that device since the valves occupied a small area, this expanded device had a much larger area that was occupied by the valves. This increase made the membrane more susceptible to tearing, and this became more of an issue during alignment since it required multiple tries before the layers were aligned correctly. Therefore, there was a need to create a membrane that was thin enough for the valves to deflect but robust enough so as to not be susceptible to tearing.

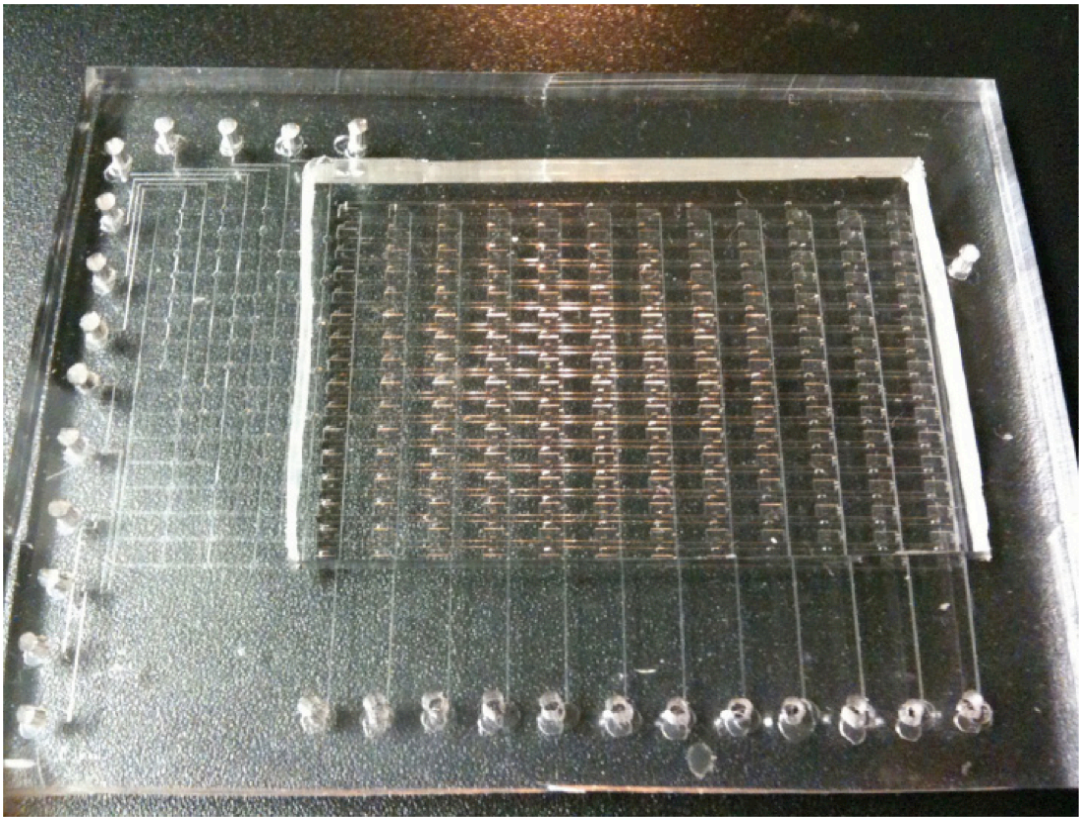

Figure 4.3 The expanded ACDD is a large array of 192 vias for the delivery of chemicals to brain slices and other tissue. The device contains 3 separate fluid inputs to deliver multiple chemicals or buffer, and any fluid that does not exit through a via exits from the outlet port on the right side. A multiplexer of valves on the right controls the row in which the fluid is delivered, and the valves on the bottom controls the column to which fluid is delivered.

In addition, a method to align the channel layer with the valve layer was needed since both were large thin membranes. Second, the purpose of the device was to create a large array of vias, ideally over 100. However, the one to one configuration with solenoid valve to PDMS valve in ACDD was not practical since 100 solenoid valves would be required for 100 vias, and it would be a very expensive and complicated setup. Therefore, a different approach was needed to reduce the number of valves while maintaining a large array. Third, the degree of alignment for the posts on the channel layer SU8 master for the large array was much higher, and standard alignment by hand during would not be sufficient to precisely align all the posts on the channels to create in the correct location of via in the device. Lastly, different software was explored to develop a quicker method to actuate to accommodate the increased number of vias requiring control. Each of these issues was carefully addressed to develop the expanded ACDD.

4.3.2 Redesigning the PDMS layers of the large array device

In the previous chapter, the ACDD was constructed with four PDMS layers. A thin ~3 mm thick patterned PDMS layer was inverted on the device with the patterned side facing up, and a thin PDMS-hexane layer covered the circular patterns created the valves. This allowed the membrane the ability to deflect downward into the patterned void and allowed fluid to flow underneath the channel layer placed above. However, the valves were only 300 μm in diameter, and there were 12 in total. Therefore, most of the membrane was bonded to the PDMS layer underneath except for the void patterned valve areas, and there were no issues with the membrane tearing. This configuration was not appropriate for the large array since it was mostly composed of valves.

To circumvent this issue, the 2 layer PDMS valves were modified to create a membrane that had the valve features patterned as shown in Figure 4.2. The SU8 master was patterned with the valves to a height of 50 μm and spincoated with PDMS. The SU8 height provided a sufficient area for the valves to collapse into the space beneath when deflected downward and the areas where the valves were patterned were thinner than the overall membrane due to the 50 μm structures, which was important to maintain the ability to actuate. However, the overall thickness of the membrane was about 120 μm making this layer more robust and easier to handle when bonding. When bonded to the PDMS base, it created a valve platform that was less susceptible to delamination or distortion of the valves due to the increased thickness.

The next step was to develop a method to align and bond two large membranes together. The ACDD only required the alignment of 12 valves so bonding the channel layer to the bath chamber/port layer first provided a sturdy substrate to keep membrane taut for aligning with the valve layer. This method was not applicable for the large array since the majority of the membrane would not be bonded to the PDMS due to the larger chamber area. Therefore, the area not bonded to the PDMS would still be able to warp making it difficult to align. To solve this problem, the channel layer was silanized and a thicker layer of PDMS was poured and cured on top. This provided stability of the membrane when aligned with the valve layer. After bonding, the silanized membrane was separated from the thick PDMS layer by spraying compressed air between the layers, and this was used to create the final layer for the inlets, outlets, and bath chamber.

4.3.3 Multiplexor utilized to increase the number of vias

To increase the number of vias on the device without requiring a large number of solenoid valves, a multiplexer was used for the delivery of fluids. A multiplexer takes a set of inputs and scales the number of possible outputs. In this case, eight valve lines were able to control fluid to 16 different channels. This was achieved by creating a pair of valve lines with binary behavior where only one was allowed to be open at a given instant[37]. Figure 4.4 shows an example of how a multiplexer composed of valves controls the fluid in the device. Shown in red are two set of valves: a set that controls fluid access to every other channel and another set that controls every other two channels. Only one valve in a set is allowed to be open at a time. To deliver fluid to channels 4 and 8, the first valve in the first set must be closed, and the first valve in the second set is also closed. If a 0 is assigned for a closed valve and a 1 for an opened valve, this can be represented as 0,1,0,1. This representation was used when coding for the MATLAB GUI.

For the placement of the valves on the channels, the valves were designed with increasing specificity with each subsequent valve. The valves were arranged perpendicular to the channels from left to right. For example, the first valve line in set 1 controlled the first eight channels (1-8) and the second valve line controlled the last eight channels (9-16). Valve set 2 had the first valve line control channels 1-4 and 9-12 where as the second valve line in the set controlled channels

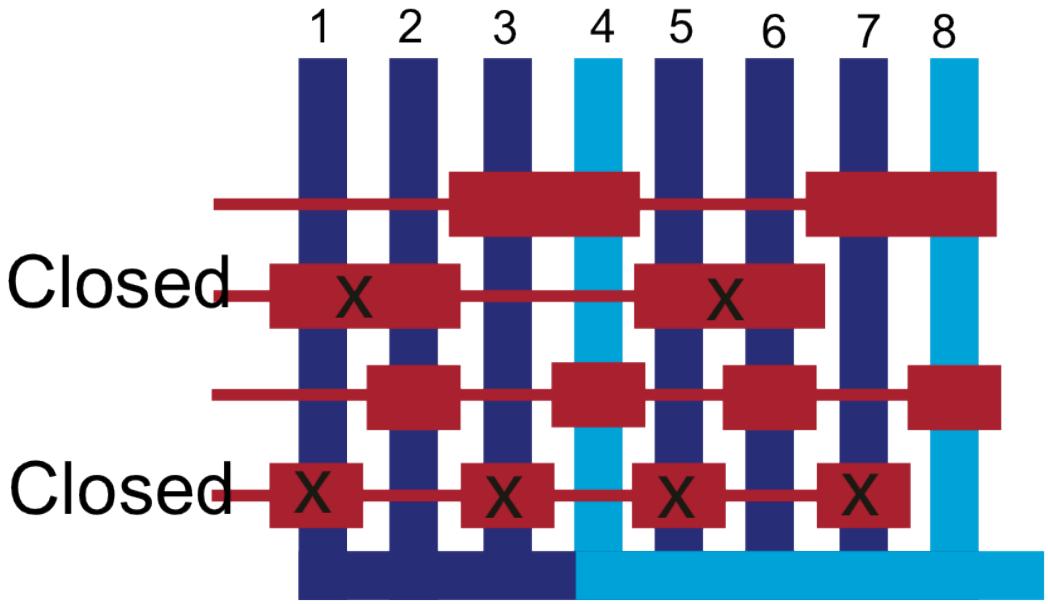

Figure 4.4 An example of a valve multiplexer to control fluid flow through channels. The valve were organized in pairs where only one could be open at a time. Binary numbers, 0 and 1, was assigned to a closed and open state respectively. Fluid flow was dependent on the state of the valves. A multiplexor reduces the number of solenoids needed to control the vias.

5-8 and 12-16. The first valve line in set three controlled 1,2,5,6,9,10,13,14, and the second valve line controlled 3,4,7,8,11,12,15,16. Lastly, the set 4 had the first valve line control 1,3,5,7,9,11,13,15, and second valve line in the set controlled 2,4,6,8,10,12,14,16. The second set of valves at the bottom of the device directed the fluid to a specific via in a row and one valve line connected to one solenoid valve. A valve multiplexer for controlling air and vacuum would be difficult to control. However, the representation of each valve remained the same with each line either being 0 for closed or 1 for an open state. Therefore, a string of 20 numbers (8 for fluid control valves and 12 via controlled valves) composed of ones and zeros could direct fluid to a specific via. Figure 4.5 shows the valves associated with the multiplexer to the left, and the valves to control the dispensing of fluid through vias at the bottom.

4.3.3 MicroPG is an essential tool for SU8 alignment

The channel SU-8 master requires alignment of the patterns between the first and second SU-8 layers to create posts for the vias in the PDMS membrane. The number and size of the area where the posts were patterned was too difficult to hand align especially since the thin SU-8 layer made it difficult to see the pattern on the first layer. The MicroPG is a maskless photolithography system that was able to expose and pattern SU-8 with UV light without the need for a transparency mask. The MicroPG alleviated this issue by locating the position of the alignment marks on the first layer and offsetting the pattern position of the second layer for the alignment. This produced posts that were placed precisely on the 125 μm wide fluid channels. This step was essential since any errors in alignment would produce a channel PDMS layer that

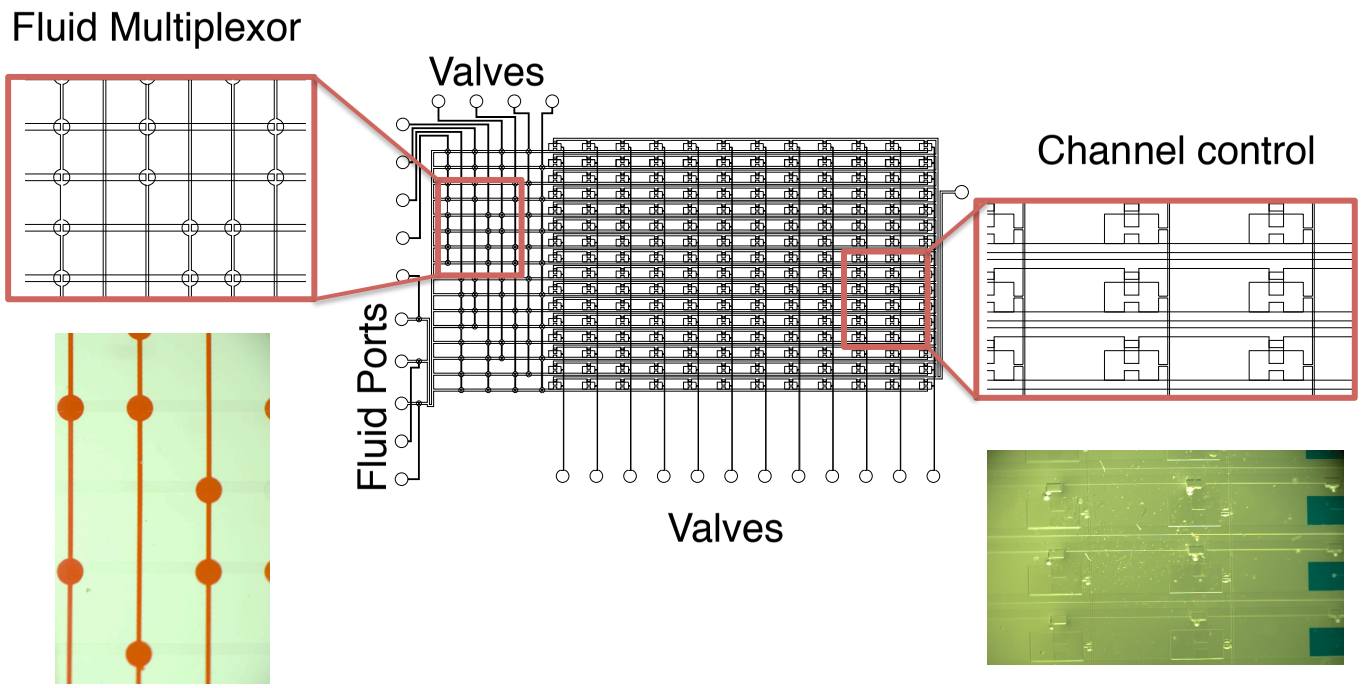

Figure 4.5 An image of the expanded ACDD shows the AutoCAD and its corresponding brightfield image of the different sets of valves. The valve multiplexer determines which row the fluid flows through and the bottom valve lines determine which column the fluid is directed.

may not be able to puff fluids due to incorrect via positioning. Figure 4.6 shows the device puffing blue food coloring through the vias at various positions.

4.3.4 MATLAB utilized for device operation

The USB-controller developed by LBNL foundry provided MATLAB code to actuate the individual valves. As described earlier, fluid is directed to a via depending on the state of valves in a manifold. However, listing the states of the 20 valves for each via becomes a cumbersome process. To simplify this, a MATLAB GUI that implemented the established code was developed. The GUI related a via's position to the binary states of the individual valves. For example, to direct fluid to via in position 1,1, a pushbutton on the GUI was connected to the binary states the valves for that position, which were 0,1,0,1,0,1,0,1,1,0,0,0,0,0,0,0,0,0,0,0. Essentially, a grid of pushbuttons (Figure 4.7) corresponded with each via on the device. This avoided the need to directly enter a string of numbers to operate the valves. The second aspect of the MATLAB coding was to control the timing of when fluid was puffed from a via. It is thts aspect that separates this device from other microfluidic devices that control the delivery of chemicals to a brain slice. The GUI was programmed to determine how when and where fluid was delivered to a via using the time kept on the computer's processor. This was sufficient for temporal control.

4.4 Discussion

The expanded ACDD is a platform that is able to deliver chemicals of interest to cells, tissues, and other constructs. The size of the vias (120 x 125 μm) restricts the area of chemical release, which increases the precision when targeting chemicals of interest to specific areas on tissues or specific regions

on a cell monolayer. The design of the device is an improvement over enclosed microfluidic devices since the targeting of these devices are dependent on the location of streamlines. In the example of chemical targeting on a brain slice with laminar flow [], a relatively large area of the brain slice is still activated since the streamlines run the length of the slice. In addition, other issues such as shear stress from fluid flow and the loss of soluble factors are avoided with the open bath design. The cells and tissues are delivered chemical mostly through diffusion, and any soluble factors or signaling molecules that are produced by the cells are retained in the environment. It is important to maintain this paracrine signaling between cells since it is another component in the over all cellular behavior.

The ability to temporally control the delivery of chemicals could be used to create a dynamic substrate for cells where chemical are delivered in a variety of areas over time. This could be particular useful for delivering chemicals of interest to a 3D culture of cells in a hydrogel. A hydrogel seeded with cells could be placed on the vias of the device and, depending on the experimental parameters, different chemicals could be puffed into the construct. The is particularly appealing for stem cell differentiation since multiple differentiation factors can be delivered to precise areas on the construct on precise time scale. The automation allows for the timing of the delivery to be another factor to test to determine if changes in the time of delivery can effect over all differentiation. Where as the cell patterning mentioned in the introduction focused primarily on static spatial control, the expanded ACDD provides dynamic spatial and temporal control of chemical delivery to cells and essentially patterns cells with chemicals.

As for tissue, specifically brain tissue, the ability to pattern neurotransmitters or drugs is very important for brain slice studies. A previous device utilized ports to focus chemical release to a slice, but the expanded ACDD greatly increases the available area for chemical delivery and can control the timing of release, which is an often overlooked component. The ability to have this control is and future experiments in characterizing this device for brain slice work is detailed in the next section.

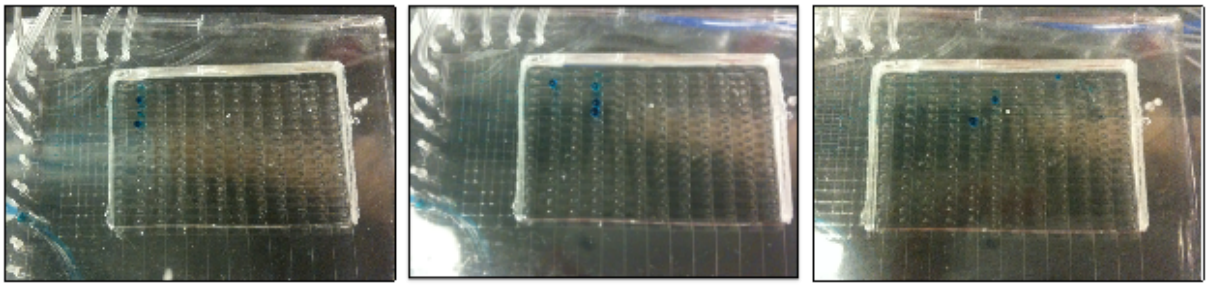

Figure 4.6 The expanded ACDD is able to deliver fluid (blue food coloring) to multiple areas on the device.

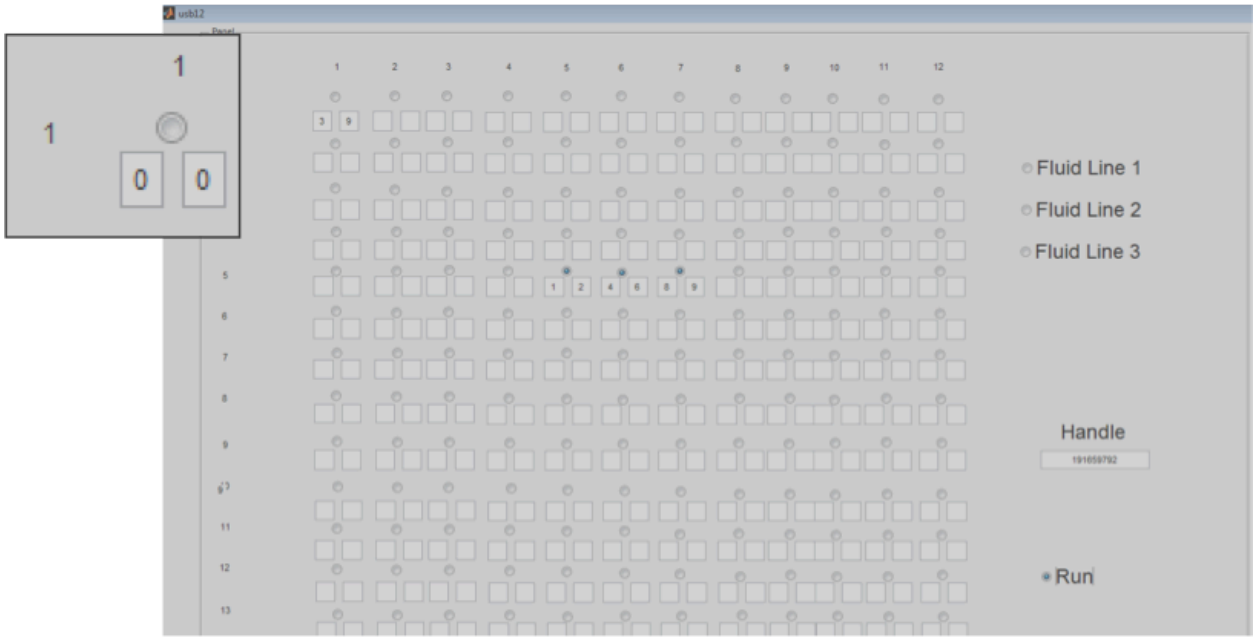

Figure 4.7 A screenshot of the MATLAB GUI used to control fluid delivery on to the vias. A different valve was also connected to each of the fluid lines to have control over which chemical of interest was delivered.

4.5 Future direction

The development of the expanded ACDD provides a new tool to deliver chemicals of interest to brain slices. The introduction stated the importance of creating tools to study neural circuits since behavior is related to how an organism processes external cues and its resulting actions.

As a proof of concept to test the device, activity on a brain slice will be artificially generated with the delivery of potassium, and a FURA-2, a calcium-sensitive fluorescent dye, will be used to measure the activity. FURA-2 was chosen since it will be able to detect the activity of cells that are exposed to K+ simultaneously in multiple areas, which is difficult to achieve with FSCV. Coronal brain slices, 300 to 400 um in thickness, will be dissected from CD-1 mice that are less than p21, since mice older than p21 are difficult to use for optical measurements. Areas on the slice that receive a bolus of potassium should have an increase fluorescent intensity at the corresponding sites. Different potassium concentrations can be perfused to different sites on the slice, and it can be determined if the dye intensity is correlated with potassium concentration. For these electrophysiology studies, a peristaltic pump will be required to perfuse artificial cerebral spinal fluid (ACSF) over the slice to maintain cell viability. Two 20.5 gauge needles will be inserted through the left and right sides of the device until the ends are just in the bath chamber to deliver ACSF.

To determine the precision of the chemical delivery timing, FSCV will be used to measure the change in concentration over time. Persistent activity is derived from the spatio-temporal changes in DA release. To mimic this phenomenon, the device must be able to quickly deliver varying patterns of a particular neurotransmitter to a slice. Alternating the delivery of K+

and buffer to a slice in quick succession will test this. For example, the device could deliver a 1μL bolus of K+ every 100 ms and a 1 μL subsequent bolus of buffer. The goal is to see a rapid change in the K+ concentration in the brain slice as measured by the FSCV with the puffing of K+ by the device. These studies will verify if the expanded ACDD is suitable for better simulating the in vivo activity of chemical release in the brain slice.

4.6 Conclusion

The current microfluidic devices that deliver chemicals to a brain slice focus on the spatial delivery, but do not address the time dependent delivery of neurotransmitters. The expanded ACDD addresses both of these aspects. In addition, since a MATLAB GUI controls the device, the ability to create a variety of profiles is a fairly simple process. The expanded ACDD will be different method for studying neural activity on brain slices in the area of electrophysiology.

References

1. Griffith, L.G. and G. Naughton, *Tissue Engineering--Current Challenges and Expanding Opportunities.* Science, 2002. **295**(5557): p. 1009-1014.
2. McBeath, R., et al., *Cell shape, cytoskeletal tension, and RhoA regulate stem cell lineage commitment.* Dev Cell, 2004. **6**(4): p. 483-95.
3. Thomas, C.H., et al., *Engineering gene expression and protein synthesis by modulation of nuclear shape.* Proceedings of the National Academy of Sciences, 2002. **99**(4): p. 1972-1977.
4. Rodríguez Fernández, J.L. and A. Ben-Ze'ev, *Regulation of fibronectin, integrin and cytoskeleton expression in differentiating adipocytes: inhibition by extracellular matrix and polylysine.* Differentiation, 1989. **42**(2): p. 65-74.
5. DeLong, S.A., J.J. Moon, and J.L. West, *Covalently immobilized gradients of bFGF on hydrogel scaffolds for directed cell migration.* Biomaterials, 2005. **26**(16): p. 3227-3234.
6. Chung, B.G., et al., *Human neural stem cell growth and differentiation in a gradient-generating microfluidic device.* Lab on a Chip, 2005. **5**(4): p. 401-406.
7. Cheng, S.Y., et al., *A hydrogel-based microfluidic device for the studies of directed cell migration.* Lab Chip, 2007. **7**(6): p. 763-9.
8. Whitesides, G.M., *The origins and the future of microfluidics.* Nature, 2006. **442**(7101): p. 368-373.
9. Chiu, D.T., et al., *Patterned deposition of cells and proteins onto surfaces by using three-dimensional microfluidic systems.* Proceedings of the National Academy of Sciences, 2000. **97**(6): p. 2408-2413.

10. Kung, L.A., et al., *Patterning Hybrid Surfaces of Proteins and Supported Lipid Bilayers.* Langmuir, 2000. **16**(17): p. 6773-6776.

11. James, C.D., et al., *Patterned Protein Layers on Solid Substrates by Thin Stamp Microcontact Printing.* Langmuir, 1998. **14**(4): p. 741-744.

12. Kim, Y.-D., C.B. Park, and D.S. Clark, *Stable sol-gel microstructured and microfluidic networks for protein patterning.* Biotechnology and Bioengineering, 2001. **73**(5): p. 331-337.

13. Thiébaud, P., et al., *PDMS device for patterned application of microfluids to neuronal cells arranged by microcontact printing.* Biosensors and Bioelectronics, 2002. **17**(1–2): p. 87-93.

14. Suh, K.Y., et al., *A simple soft lithographic route to fabrication of poly(ethylene glycol) microstructures for protein and cell patterning.* Biomaterials, 2004. **25**(3): p. 557-563.

15. Mrksich, M. and G.M. Whitesides, *Using self-assembled monolayers to understand the interactions of man-made surfaces with proteins and cells.* Annu Rev Biophys Biomol Struct, 1996. **25**: p. 55-78.

16. Xia, Y. and G.M. Whitesides, *SOFT LITHOGRAPHY.* Annual Review of Materials Science, 1998. **28**(1): p. 153-184.

17. Zhang, S., et al., *Biological surface engineering: a simple system for cell pattern formation.* Biomaterials, 1999. **20**(13): p. 1213-20.

18. Takayama, S., et al., *Patterning cells and their environments using multiple laminar fluid flows in capillary networks.* Proceedings of the National Academy of Sciences, 1999. **96**(10): p. 5545-5548.

19. Khademhosseini, A., et al., *Co-culture of human embryonic stem cells with murine embryonic fibroblasts on microwell-patterned substrates.* Biomaterials, 2006. **27**(36): p. 5968-5977.

20. Bhatia, S.N., et al., *Microfabrication of Hepatocyte/Fibroblast Co-cultures: Role of Homotypic Cell Interactions.* Biotechnology Progress, 1998. **14**(3): p. 378-387.

21. Rhee, S.W., et al., *Patterned cell culture inside microfluidic devices.* Lab Chip, 2005. **5**(1): p. 102-7.

22. Dekker, L.V. and A.W. Segal, *Signals to Move Cells.* Science, 2000. **287**(5455): p. 982-985.

23. Parent, C.A. and P.N. Devreotes, *A Cell's Sense of Direction.* Science, 1999. **284**(5415): p. 765-770.

24. Wadhams, G.H. and J.P. Armitage, *Making sense of it all: bacterial chemotaxis.* Nat Rev Mol Cell Biol, 2004. **5**(12): p. 1024-1037.

25. Raballo, R., et al., *Basic Fibroblast Growth Factor (Fgf2) Is Necessary for Cell Proliferation and Neurogenesis in the Developing Cerebral Cortex.* The Journal of Neuroscience, 2000. **20**(13): p. 5012-5023.

26. Ashe, H.L. and J. Briscoe, *The interpretation of morphogen gradients.* Development, 2006. **133**(3): p. 385-94.

27. Song, H.J. and M.M. Poo, *Signal transduction underlying growth cone guidance by diffusible factors.* Curr Opin Neurobiol, 1999. **9**(3): p. 355-63.

28. Zheng, J.Q., M.M. Poo, and J.A. Connor, *Calcium and chemotropic turning of nerve growth cones.* Perspect Dev Neurobiol, 1996. **4**(2-3): p. 205-13.

29. Kamholz, A.E., et al., *Quantitative Analysis of Molecular Interaction in a Microfluidic Channel: The T-Sensor.* Analytical Chemistry, 1999. **71**(23): p. 5340-5347.

30. Holden, M.A., et al., *Generating fixed concentration arrays in a microfluidic device.* Sensors and Actuators B: Chemical, 2003. **92**(1–2): p. 199-207.

31. Hatch, A., et al., *A rapid diffusion immunoassay in a T-sensor.* Nat Biotechnol, 2001. **19**(5): p. 461-5.

32. Herculano-Houzel, S., *The remarkable, yet not extraordinary, human brain as a scaled-up primate brain and its associated cost.* Proceedings of the National Academy of Sciences, 2012.

33. Yamamoto, C., *Activation of hippocampal neurons by mossy fiber stimulation in thin brain sections <i>in vitro</i&gt.* Experimental Brain Research, 1972. **14**(4): p. 423-435.

34. Blake, A.J., et al., *Multilayer PDMS microfluidic chamber for controlling brain slice microenvironment.* Lab on a Chip, 2007. **7**(7): p. 842-849.

35. Mohammed, J.S., et al., *Microfluidic add-on for standard electrophysiology chambers.* Lab on a Chip, 2008. **8**(7): p. 1048-1055.

36. Tang, Y.T., et al., *Development and characterization of a microfluidic chamber incorporating fluid ports with active suction for localized chemical stimulation of brain slices.* Lab on a Chip, 2011. **11**(13): p. 2247-2254.

37. Thorsen, T., S.J. Maerkl, and S.R. Quake, *Microfluidic Large-Scale Integration.* Science, 2002. **298**(5593): p. 580-584.

V. CONCLUSION

As stated previously, the motivation to control the microenvironment through microfabricated devices is the ability to selectively test and understand how different components in the environment affect cell behavior. Understanding what occurs in the cell in addition to outside the cell can help to develop in vitro models that better mimic the in vivo setting. This was best represented in the oxygen-sensitive microwells, where the ability to have real-time oxygen measurements is particularly important when conducting hypoxia experiments. An oxygen level of 10% may be considered hypoxic when compared to ambient air but in certain areas in the body, 10% could be considered normoxic or even hyperoxic. This example shows the importance of understanding the conditions cells are exposed to in vivo and then mimicking these conditions as close as possible on the bench top. Here, the oxygen was both delivered in a controlled manner and monitored to understand how different concentrations of oxygen affect cell behavior. This device could be useful to test highly oxygen-sensitive cells such as islets and monitor their behavior such as insulin secretion in response to a variety of oxygen tensions.

The ACDD was another device that exerted better control over the cell microenvironment by delivering a stable artificial pheromone gradient in agarose. While in microfluidics there is the tendency to completely overhaul standard biological platforms, many of these platforms have been optimized over many years to perform the necessary experiments and in some cases it is better to adapt them. Since the delivery of pheromones was completely through the diffusion of the pheromones through the agarose, this avoided many problems that normally are presented in microfluidic devices such as absorption of small molecules and shear forces from flowing media. The device was still able to create directed shmooing towards the gradient. However, since the

cells are exposed in the open well format, any assay that is performed in agarose can also be performed in the ACDD. This widens the possibility of experiments that were hindered by agarose-only or microfluidic-only platforms.

This ability to deliver chemicals in an open format can be accommodated to a variety of experimental conditions in addition to yeast biology. The most relevant application is the delivery of chemicals to brain slices. The expanded ACDD addresses several issues that usually have been overlooked in experiments utilizing brain slices: timing and location of delivery. Since an array of vias is possible in the expanded device, it is possible to have better control over when and where the chemical of interest is delivered. This is important to better simulate the delivery of neurotransmitters in the brain since it is a spatiotemporal process. As with the yeast, the open well format allows for standard electrophysiology procedures to be performed on the slice without any interference. The expanded ACDD allows the study of multiple chemicals to determine how their combined interactions affect neural activity.

These very different devices show the importance of creating platforms to understand and relate cell behavior with its environment. With the devices, the ability precisely control the environment allows for a wide range of experimental conditions that were previously difficult to achieve.

APPENDIX A

LabVIEW code developed to operate the solenoid valves.

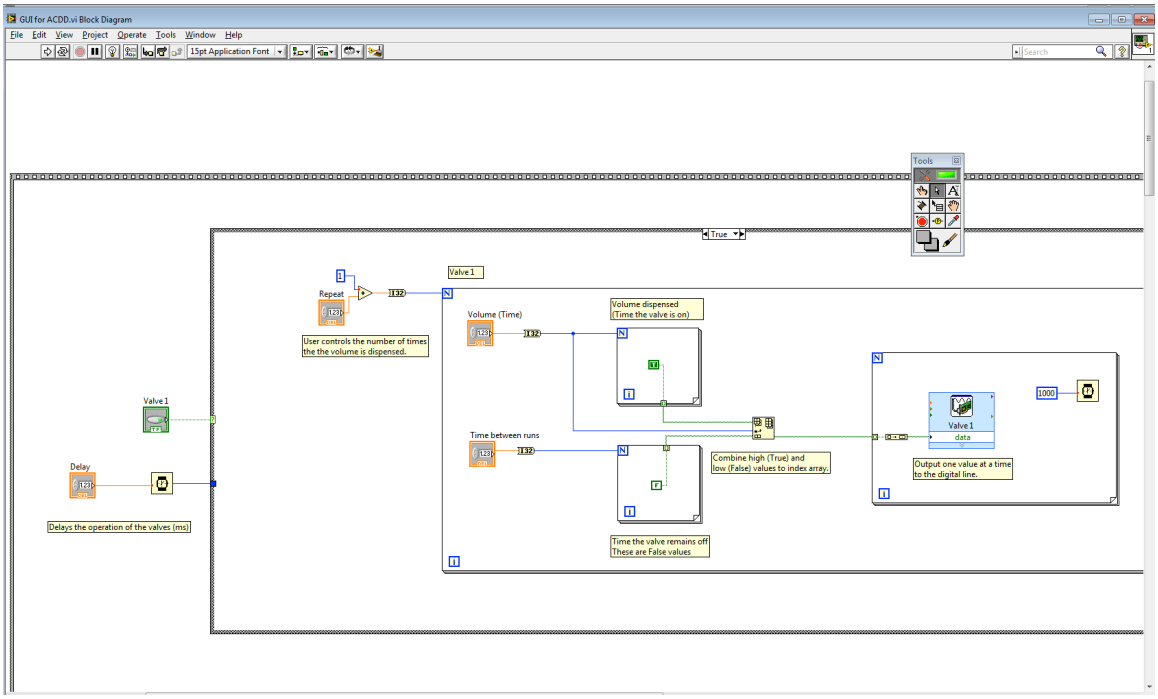

Valve 1.

This is the graphical code to operate valve 1. The four gray boxes outlined with orange are all user input variables. Information from the user is processed to actuate the solenoid valve. Starting from the left, the green true/false (TF) button determines whether the valve is on or off. If true, the sequence will run. If false, the system is halted. The delay user input delays the operation of the valve in milliseconds. This value is converted to a time constant. The repeat button determines the number of times a valve cycle is run. To insure a valve cycle is run at least once, the one is added to the user input. Therefore, if the user inputs a repetition of zero, the valves will cycle for one run and stop. This number is sent into a limited while loop to determine when the valves are on and off. The time the user inputs is translated to a true statement for the time the valve is on and a false statement for the time the valve is off. These statements are

combined into an index array that is sent to the DAQ card to determine when a 5V signal is sent. The 5V actuates the solenoid valves and 0V keeps the solenoid at rest. This process is the same for valves 2-6.

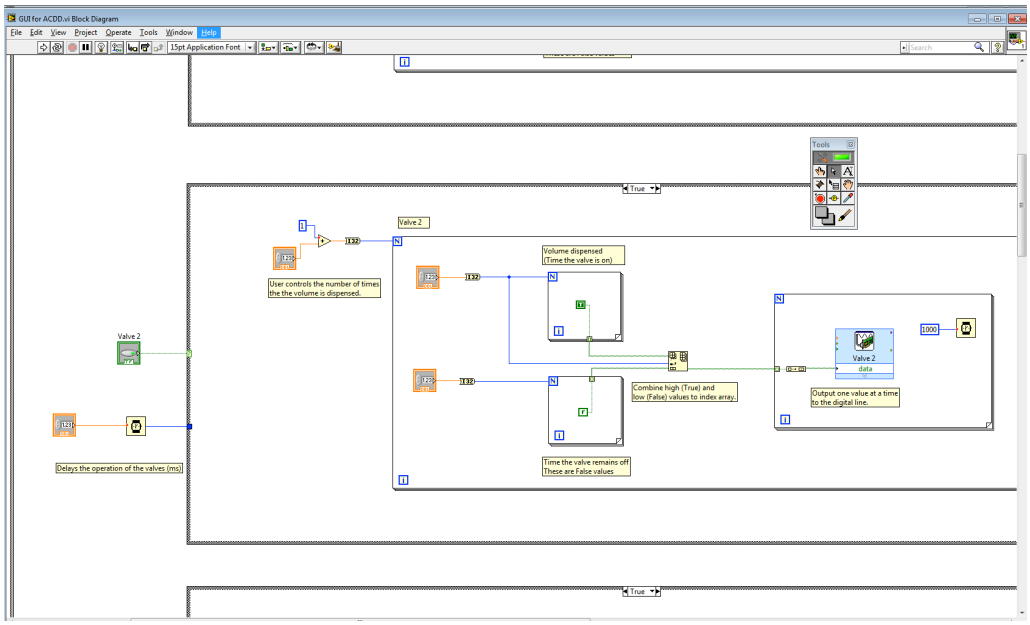

Valves 2 and 3

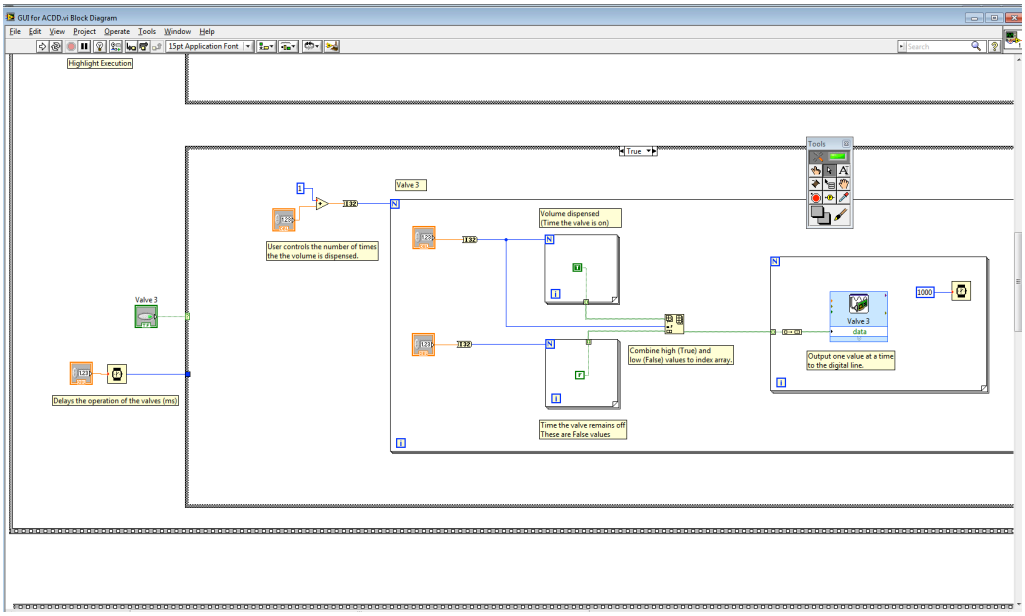

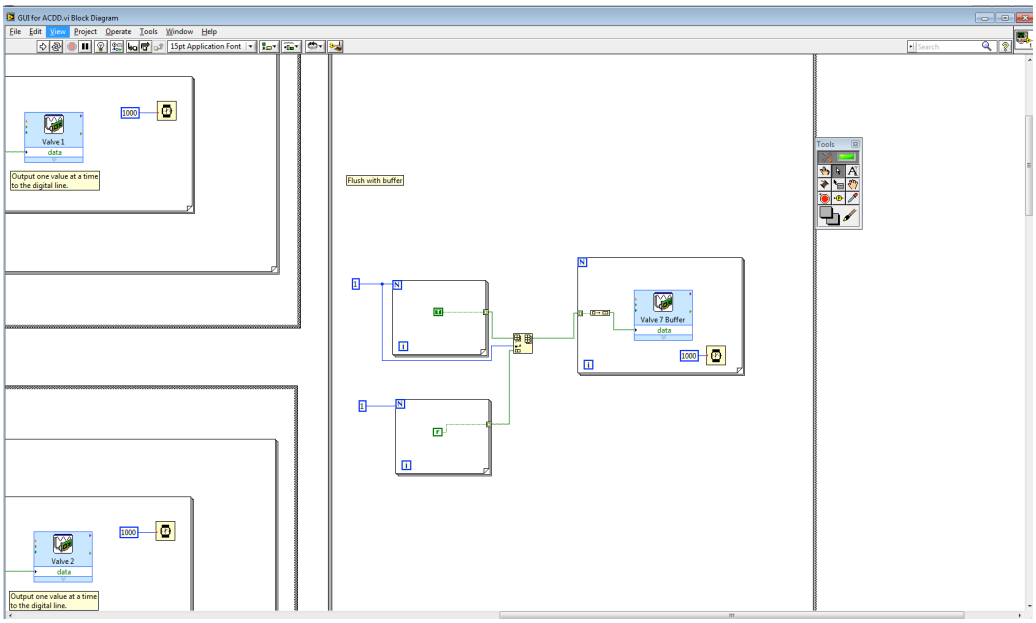

Valve 7

Valves 7 and 8 require different code since these control the buffer channels on the device. Valve 7's coded is connected to valves 1-3, and valve 8's code is connected to valves 4-6. When the last valve in a set has finished a cycle, either valve 7 or 8 become active to open the buffer channels and rinse any fluid that was previously in the channel. The length of time these valves are on is 1 second. This does not have a user input in the main GUI, but this can be easily changed in the block diagram for different times.

APPENDIX B

MATLAB code to actuate the valves of the expanded ACDD

A MATLAB GUI was constructed to easily actuate the valves. A detailed explanation to create the GUI and the required code is presented below.

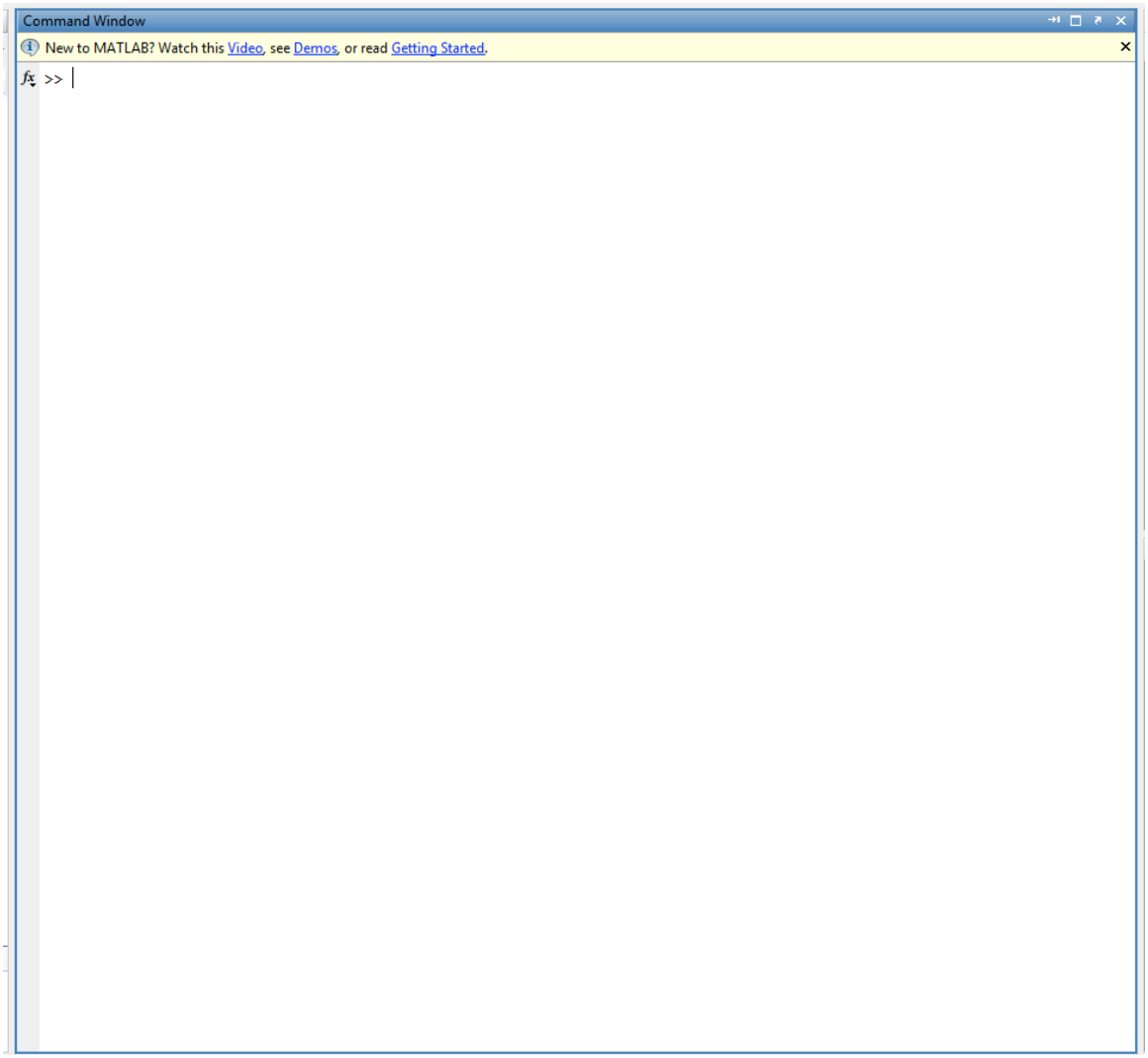

1. Open Matlab. The command window should be in the center. If not, check the side panels on the right to locate the command window.

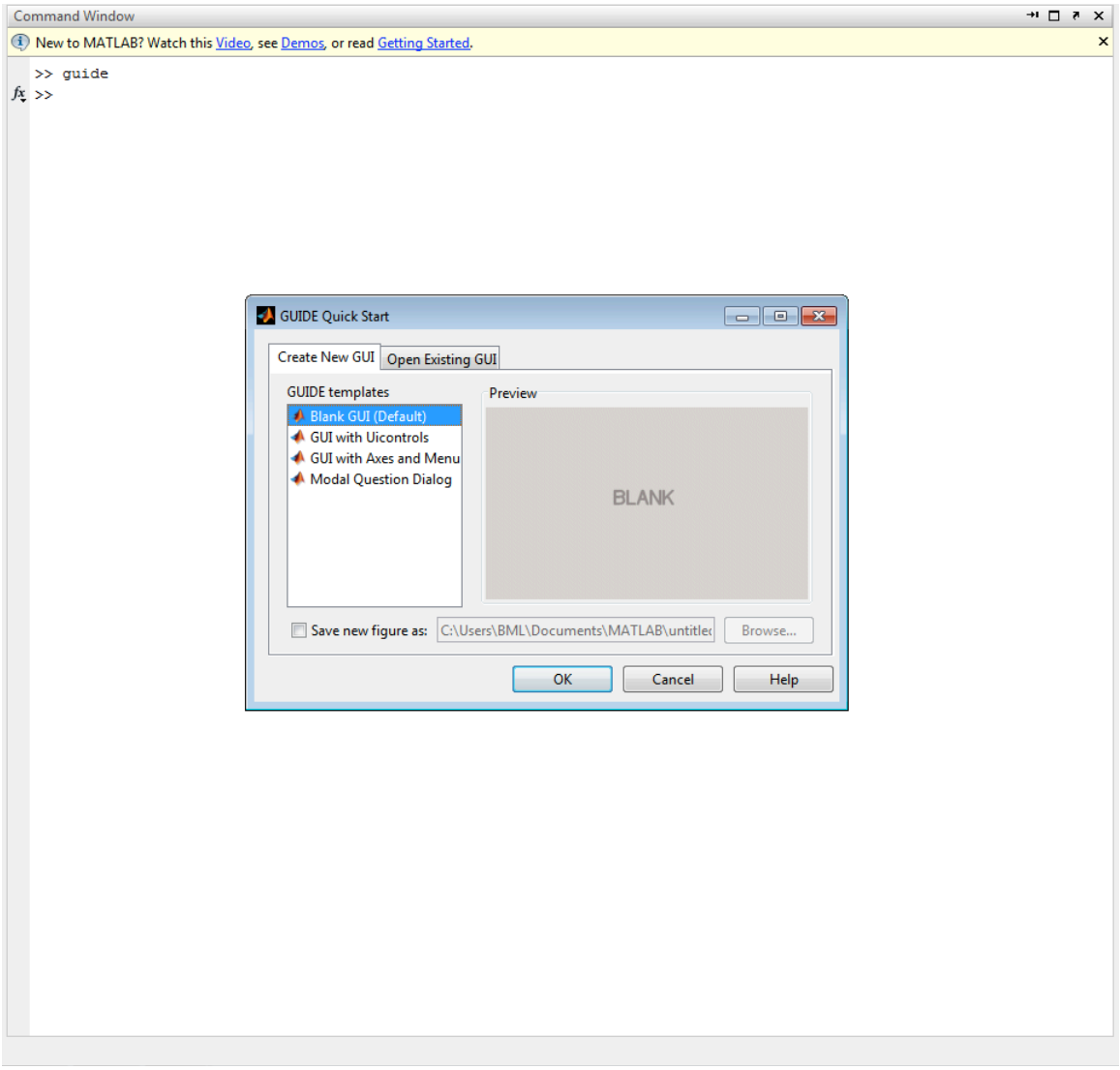

2. Type guide into the command window. A GUIDE Quick Start window should appear. Click the Create New GUI tab and select Blank GUI (Default). Click OK.

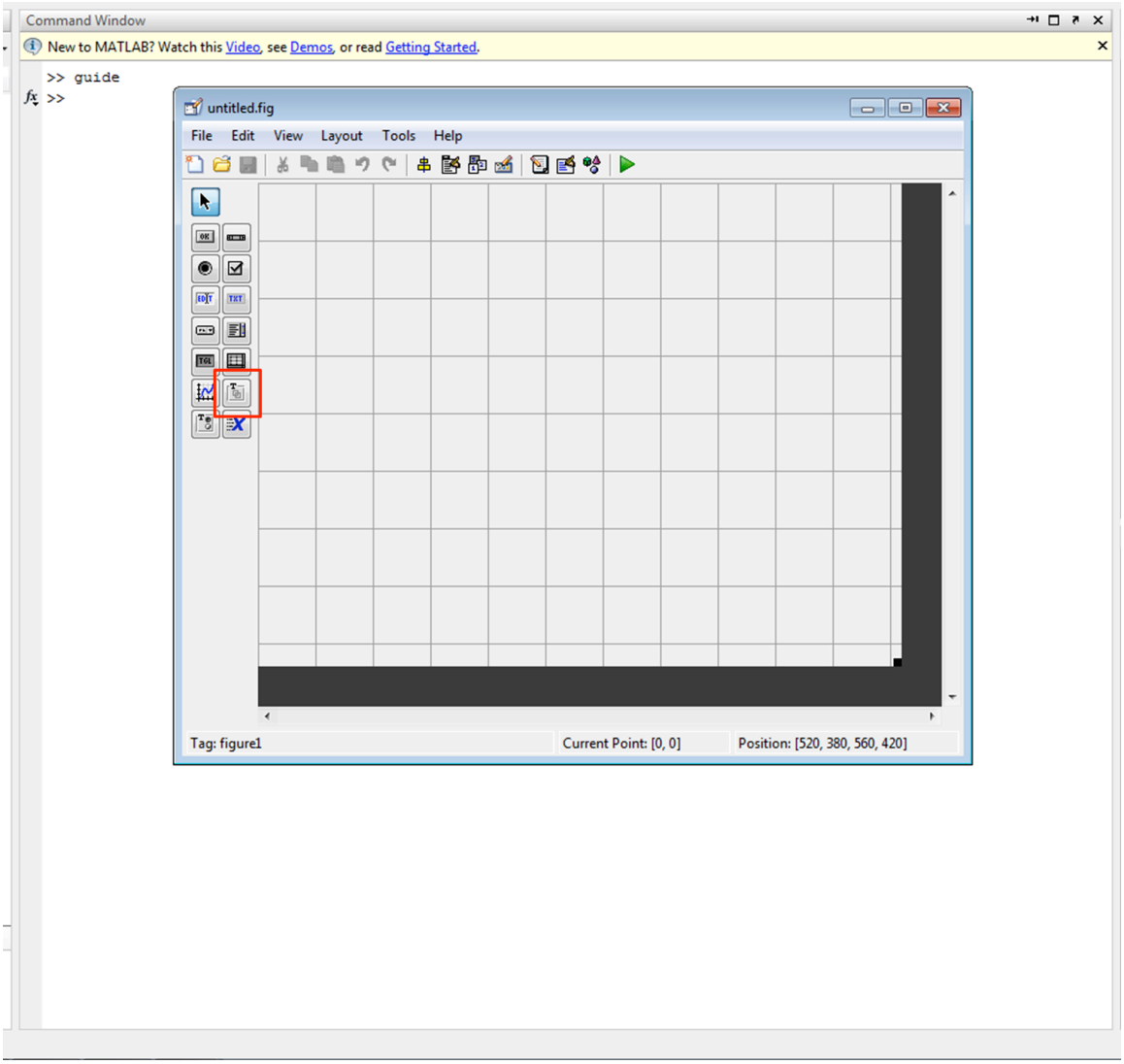

3. Another window with a grid and a panel of tools on the left side should appear. Click on the panel tool as highlighted in the red box.

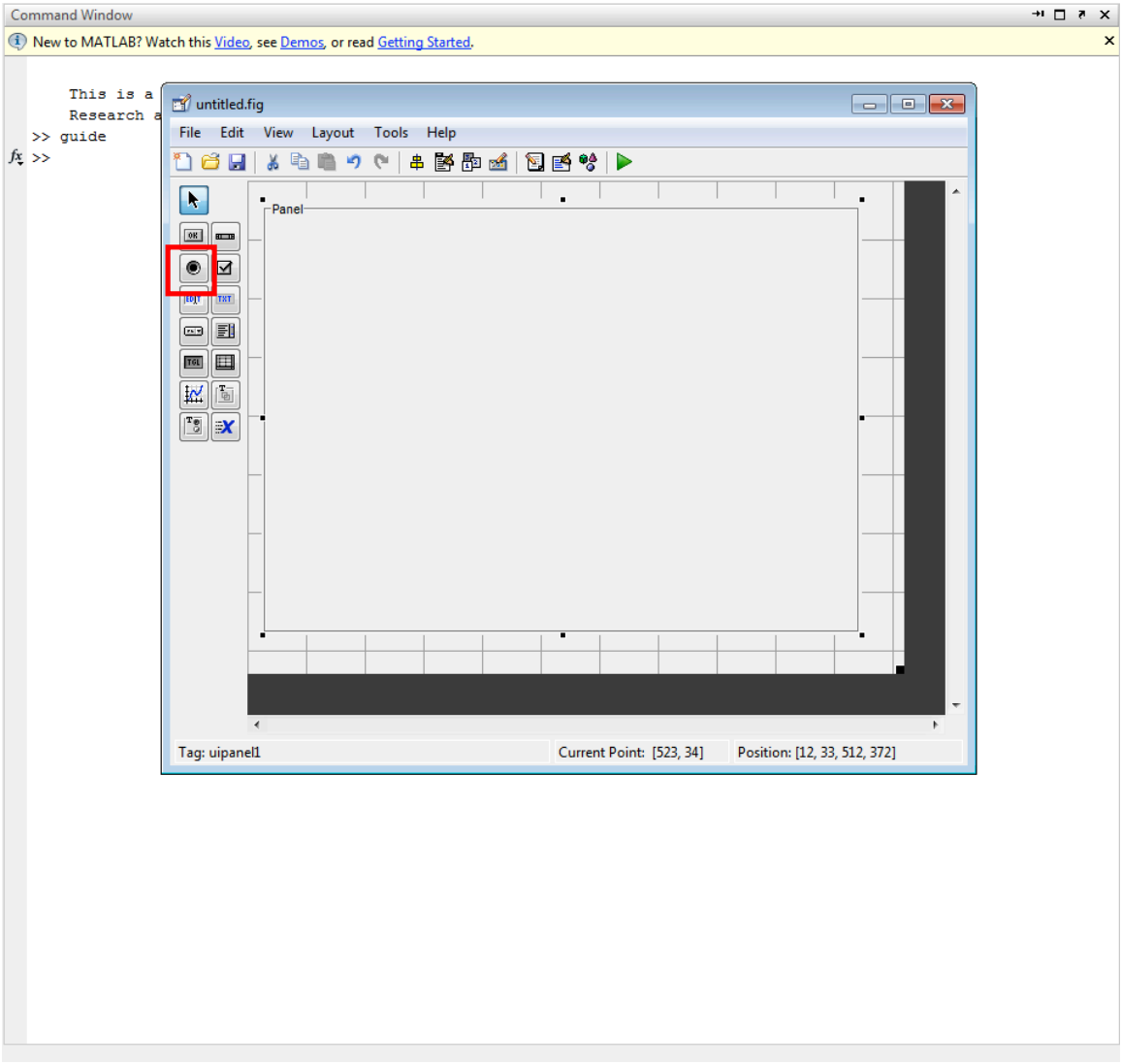

4. Click and drag the panel to a size appropriate to you application. Since the expanded ACDD requires a large number of buttons, it is best to create a panel the maximum size of your screen. You can adjust the size of the panel by clicking and dragging one of the eight small black boxes at the on the outside of the panel. Next, click on the radio button highlighted in red.

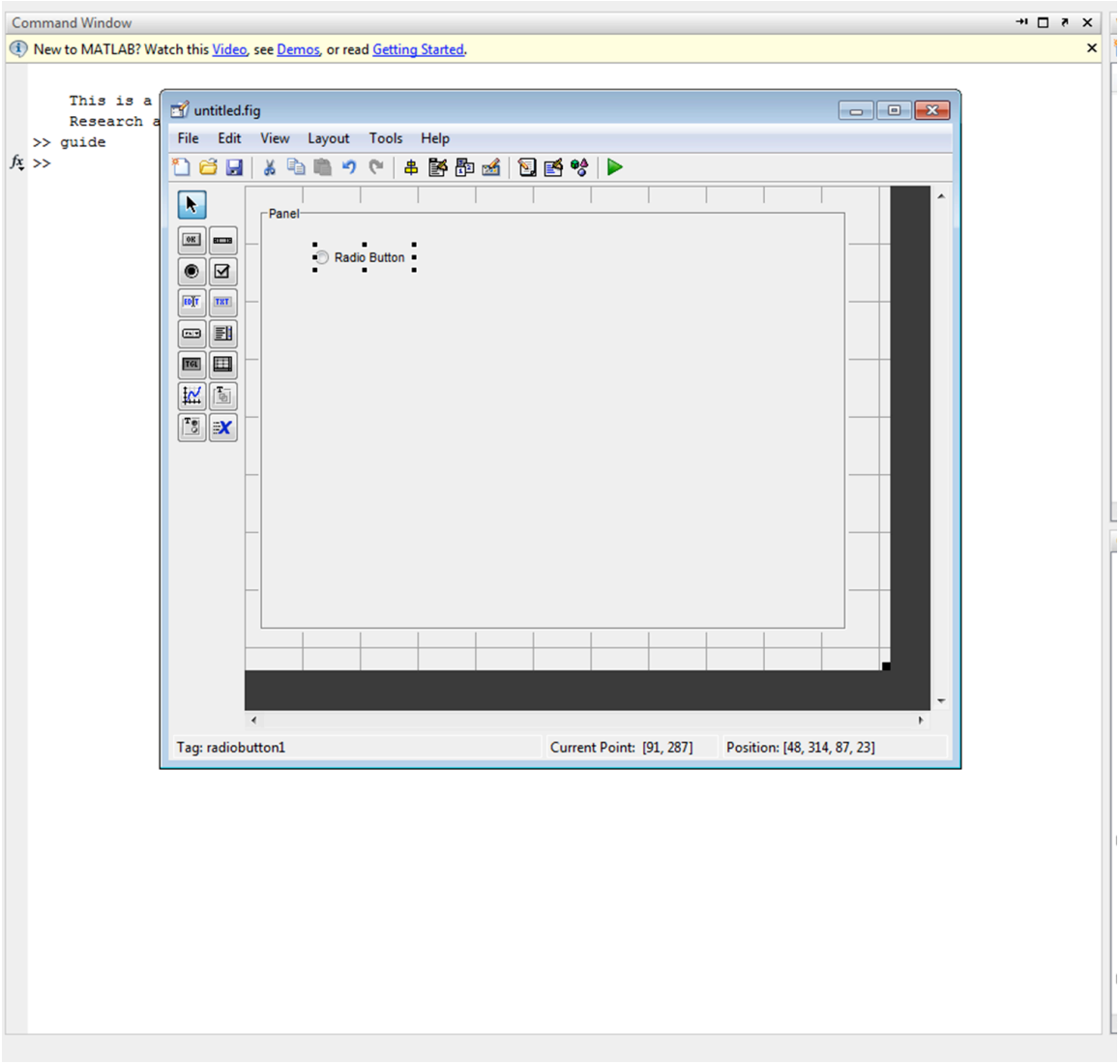

5. First, we need a radiobutton to signal the valves to direct fluid to the selected via. Click on the panel to place a radio button.

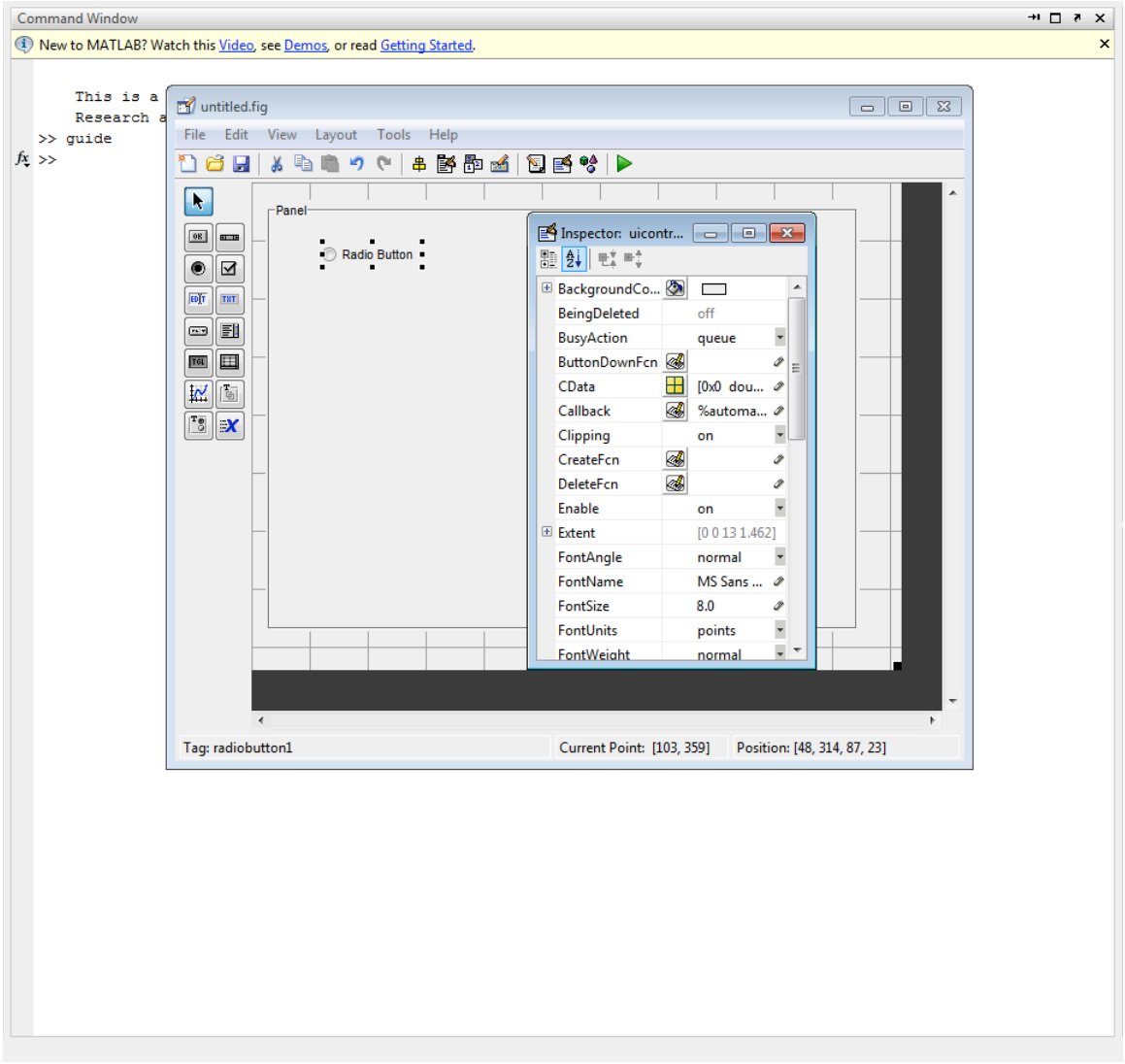

6. To change the name of the radiobutton, double click on the button to bring up the inspector. You can also right click and specifiy the inspector.

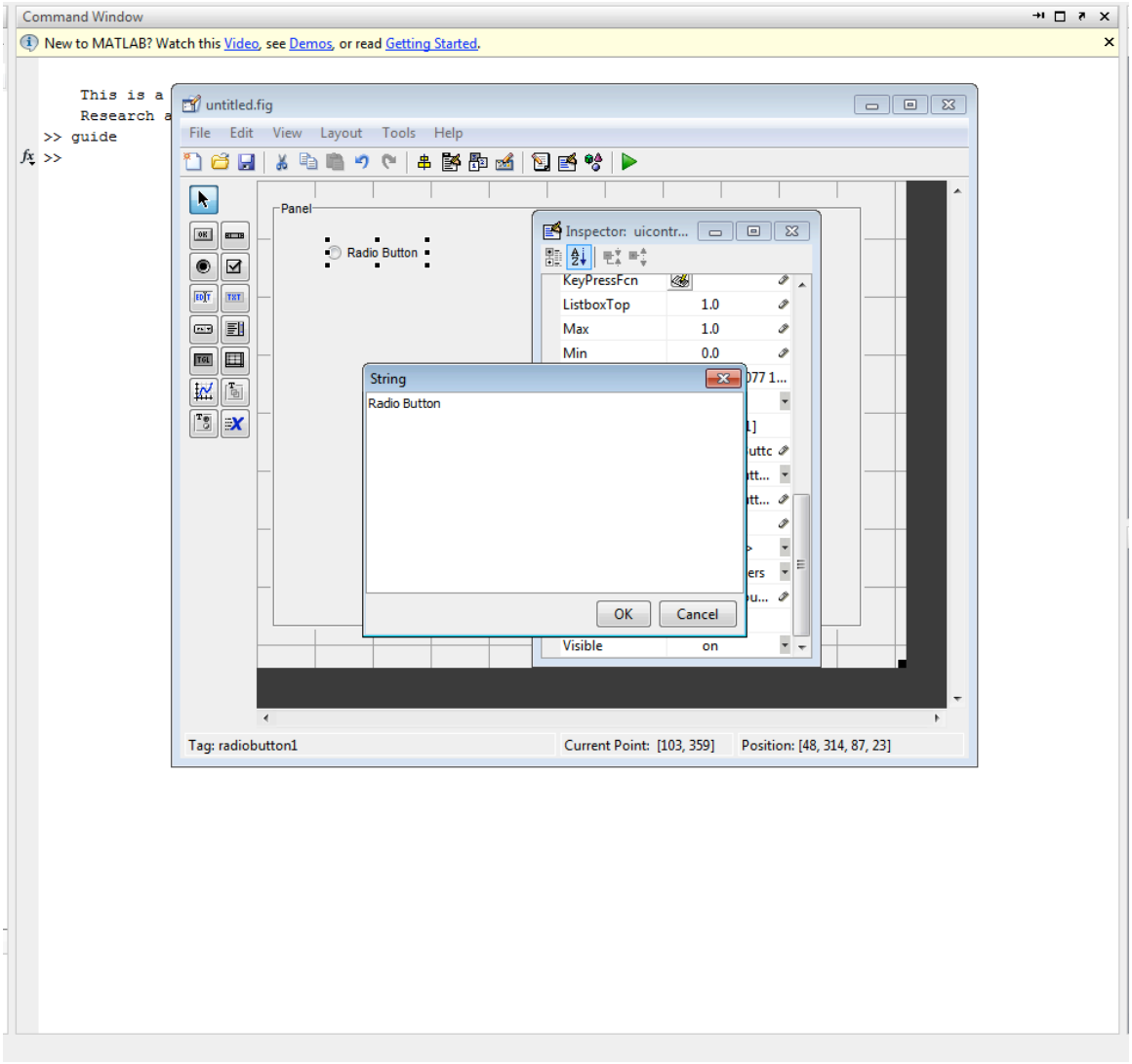

7. Scroll down until you see the word string. Double clicking on the string will bring up another window. In here, you can change the name of the button.

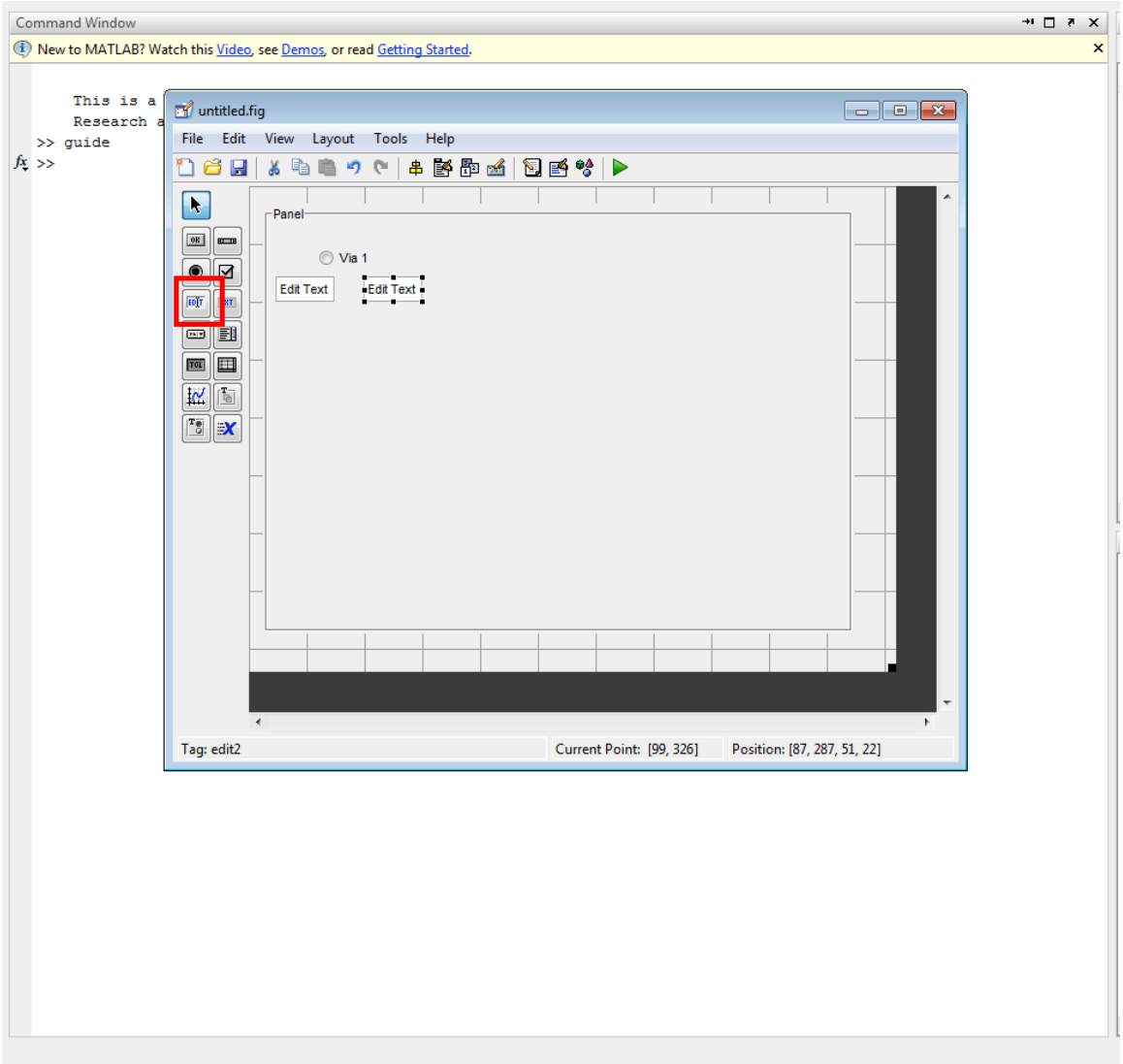

8. Here, radiobutton was renamed to via 1. Next, insert two edit text buttons by clicking on the highlighted red box and placing them on the panel. The first box will determine how long the fluid is delayed before exiting the via, and the second box how long the valves are open to control the amount of fluid exiting the via.

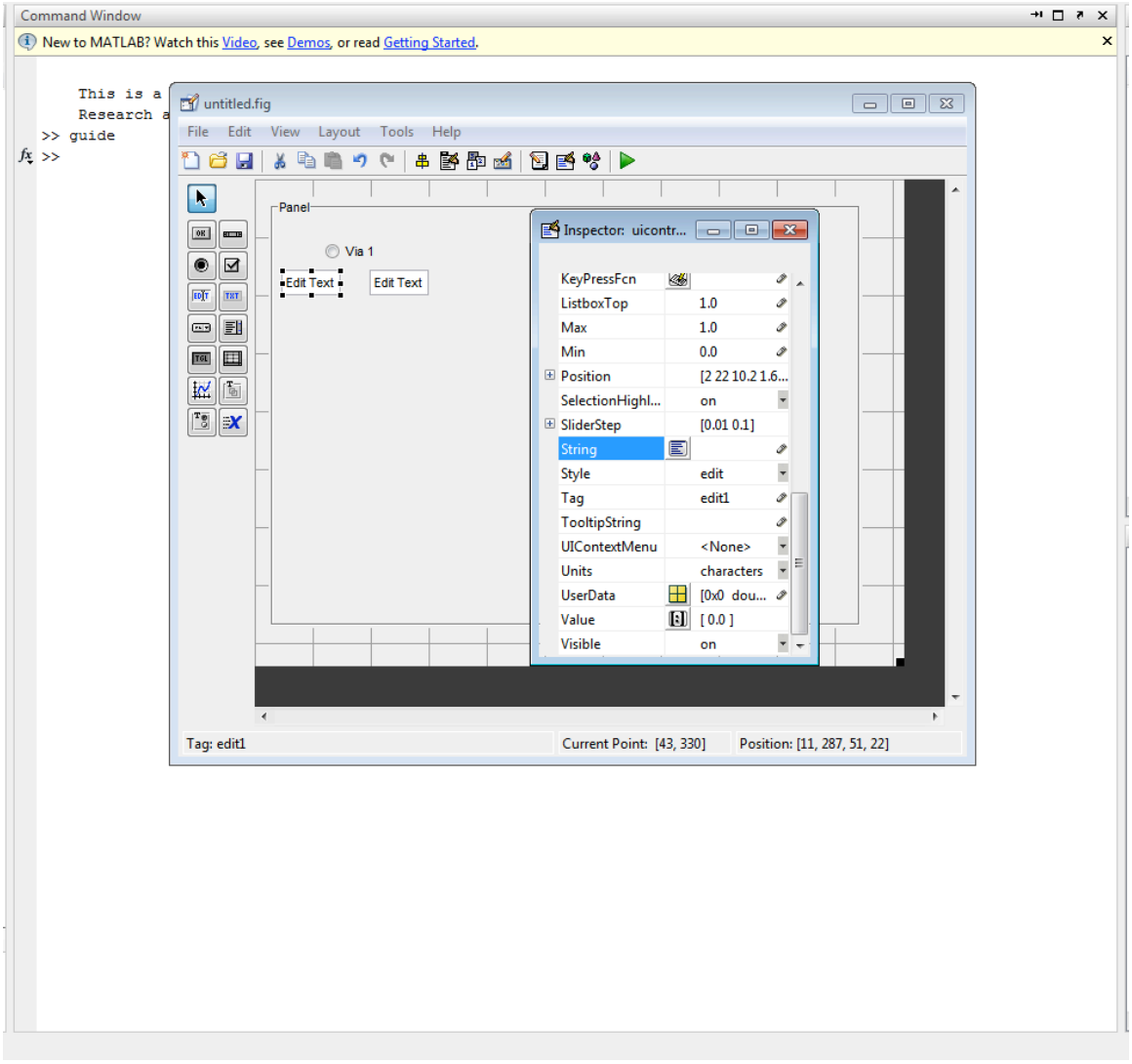

9. As before, double click on each edit box to bring up the inspector. Delete the string so that the field is empty. This domain must be empty for user input.

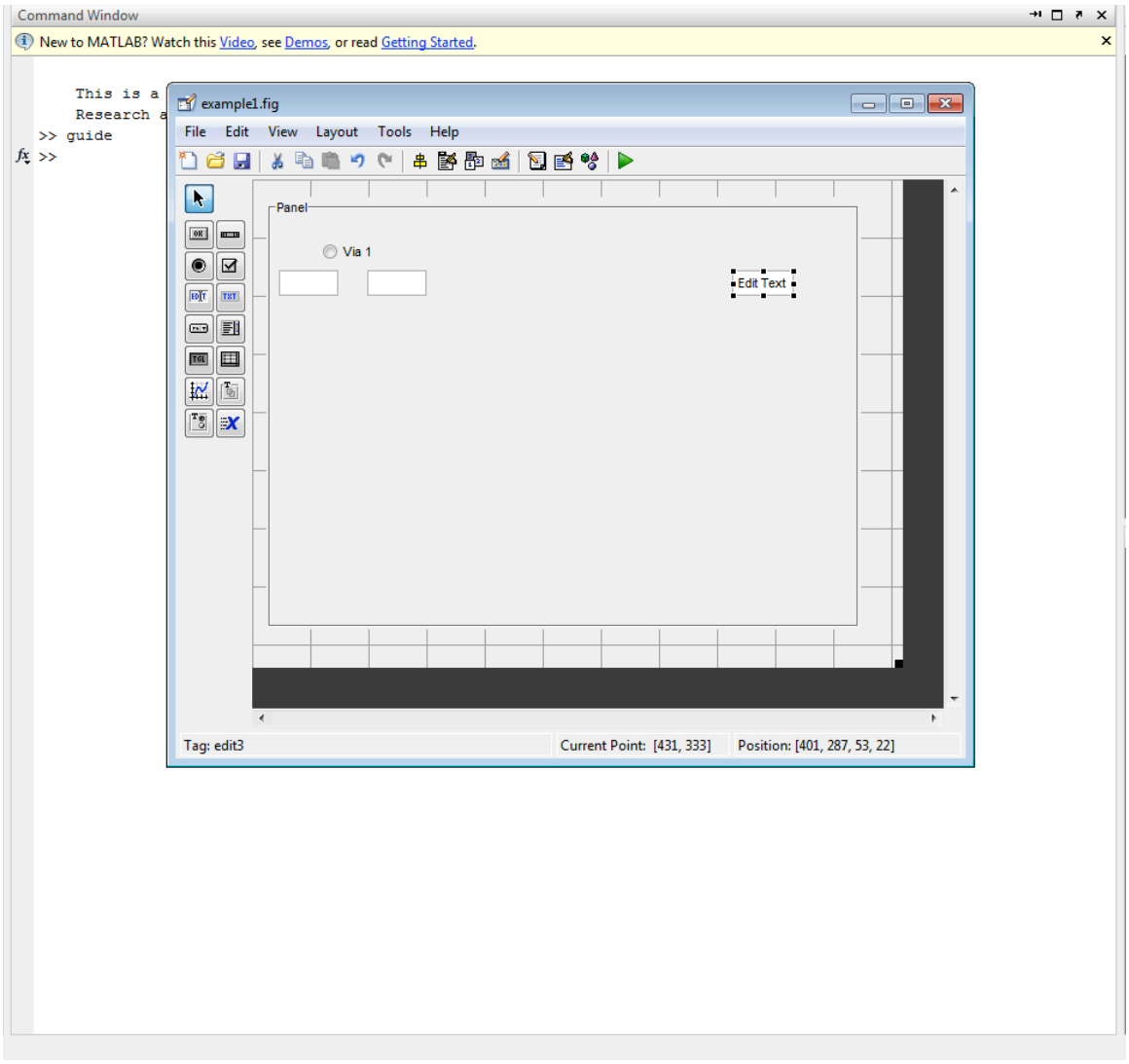

10. Place another edit text box for to enter the handle from the controller box. The handle is a series of numbers that identifies the controller box for the valves. This number changes every time the controller box is turned on so it is important update it. The edit text in the box should also be deleted.

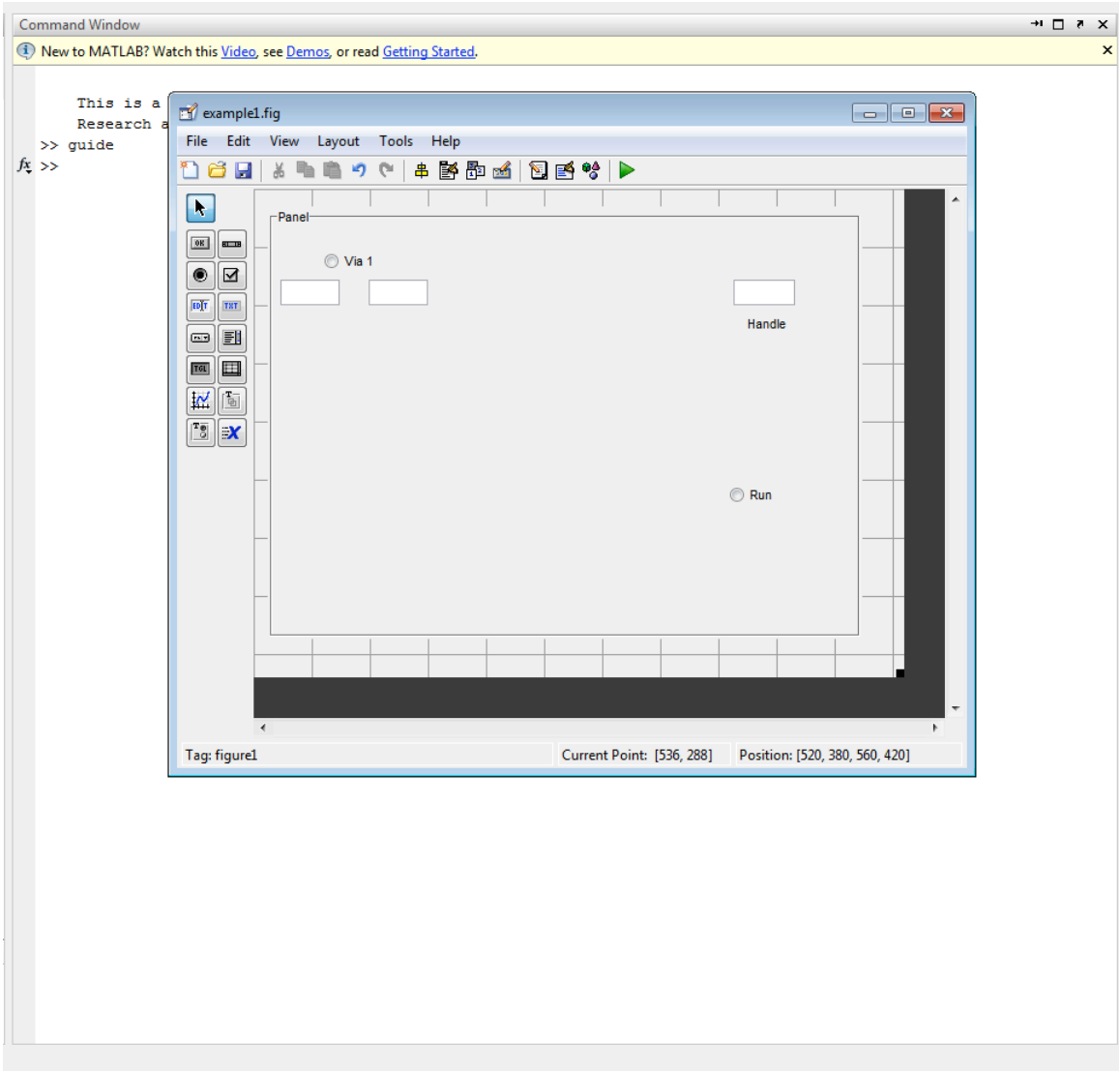

11. A label was placed on the edit text box by selecting the Text label on the left (symbolized as TXT). Another radiobutton was relabeled as run to start the GUI.

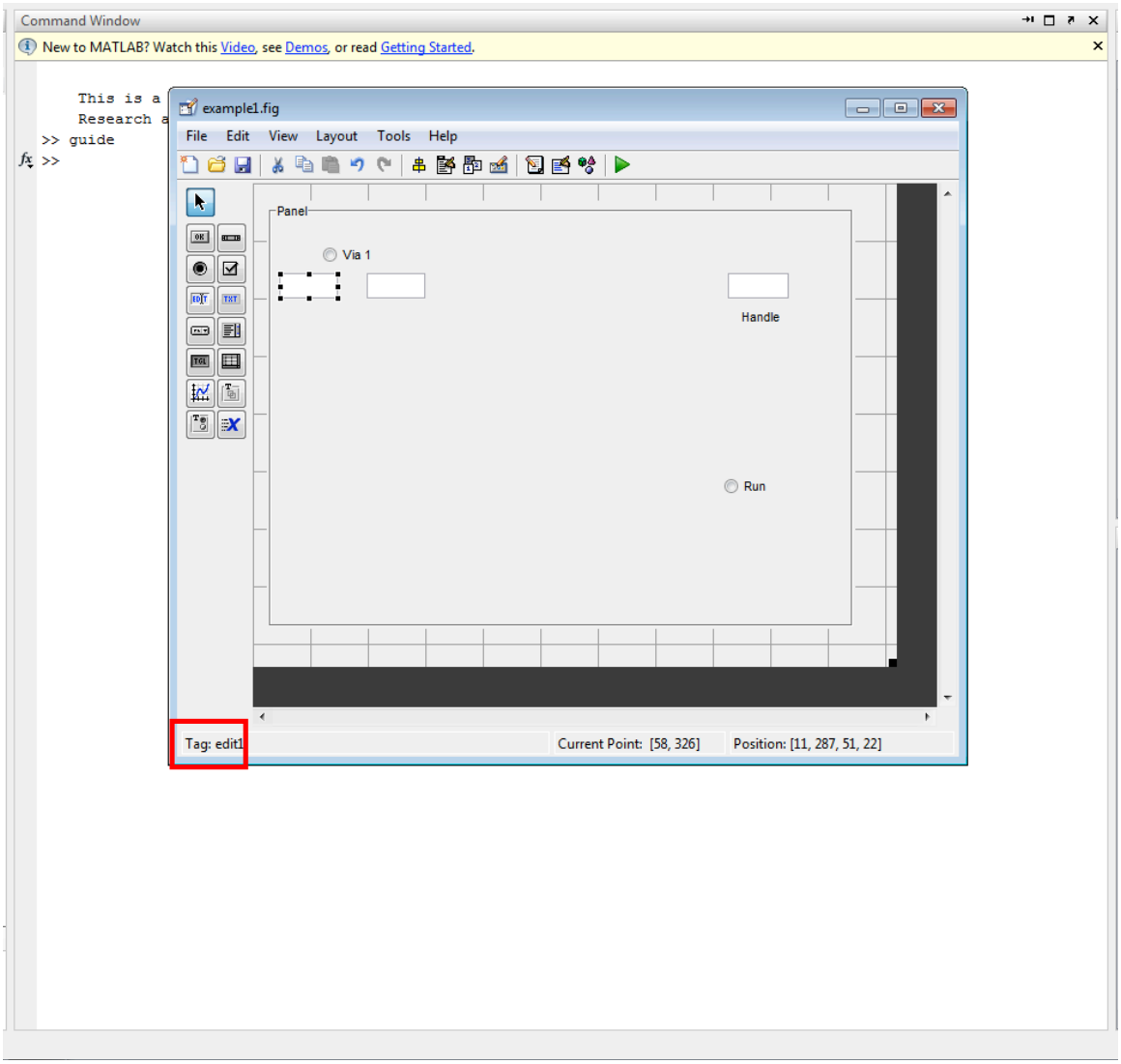

12. Next, the code to control the action of the buttons is written. It is important to note the name of the button in order to correctly match the code to the button. The name of an object on the panel can be determined by highlighting the object, and its name will be presented in the lower left hand side, which is highlighted in red. It is important to check this before writing code. In this case, code will first be written for the radiobutton via 1.

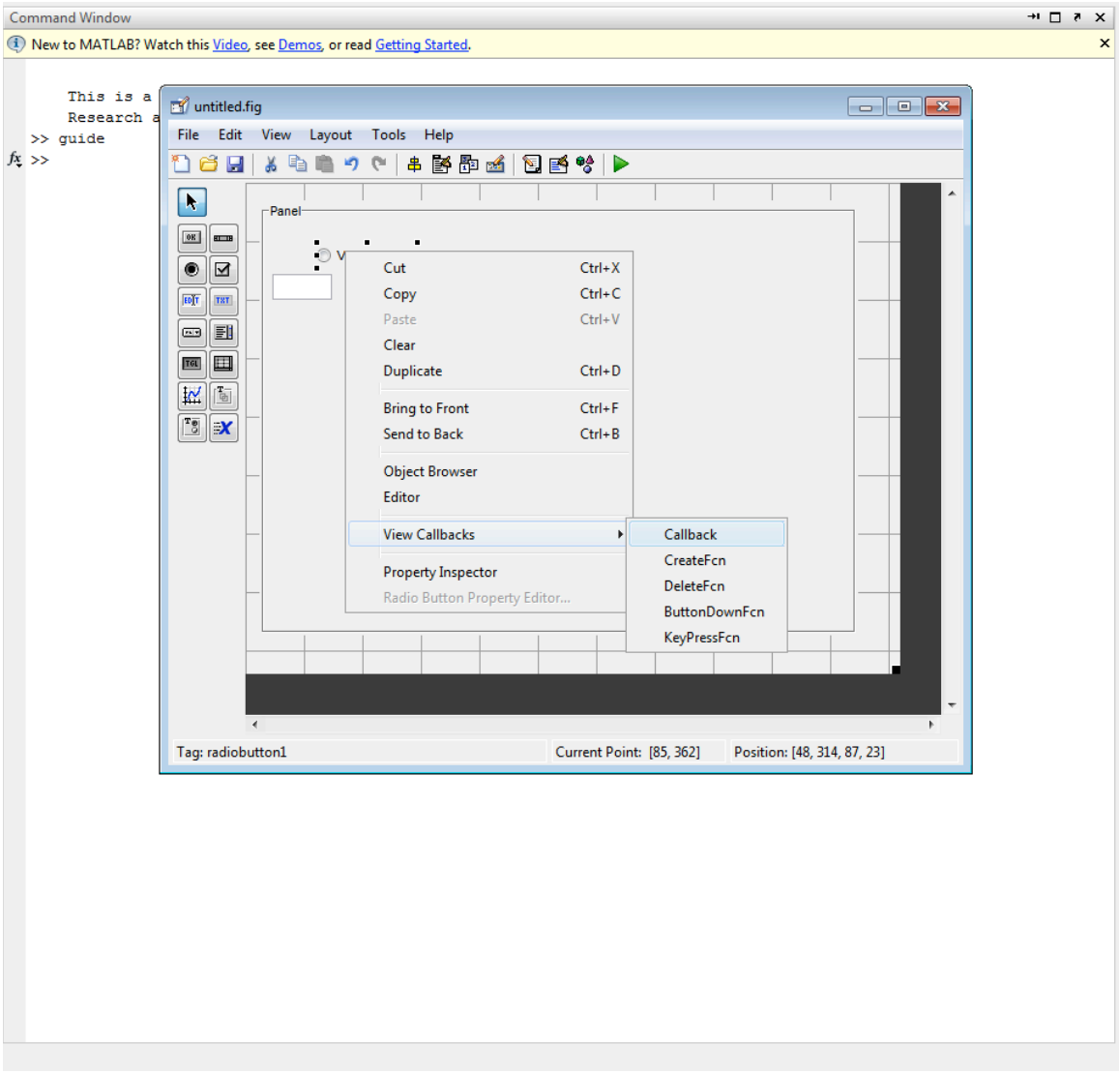

13. To write code for via 1, right click on the button and select view callbacks and then callback.

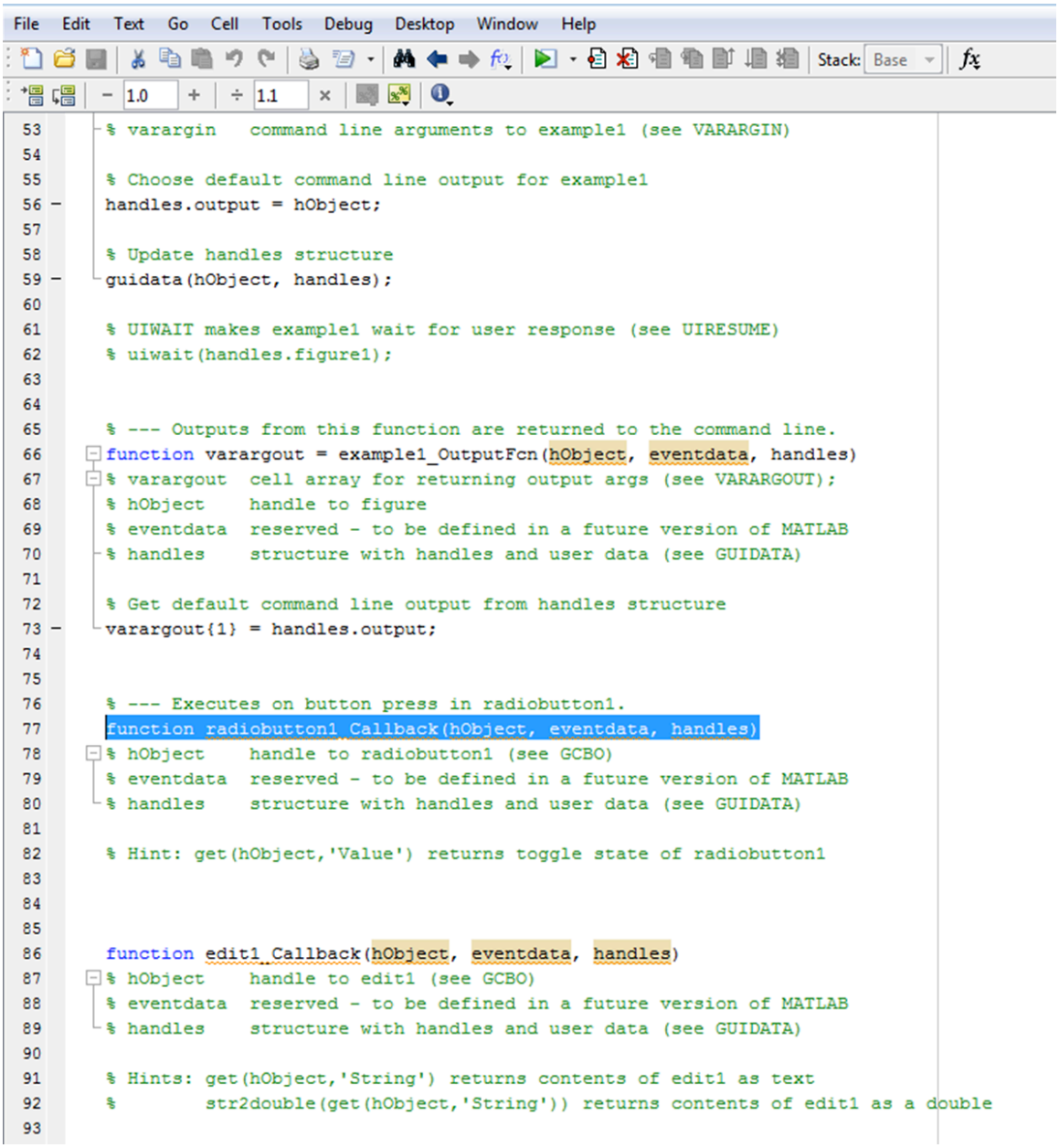

14. After clicking the callback, the code for the entire GUI appears and the specific code for the radiobutton is highlighted. Within the code, there is sub-code for each individual object on the GUI. It is important to make the correct code is written for each object. The
15. code to initiate fluid delivery is shown on the next page.

```
% --- Executes on button press in radiobutton1.
function radiobutton1_Callback(hObject, eventdata, handles)
% hObject    handle to radiobutton1 (see GCBO)
% eventdata  reserved - to be defined in a future version of MATLAB
% handles    structure with handles and user data (see GUIDATA)

% Hint: get(hObject,'Value') returns toggle state of radiobutton1
waitfor(handles.radiobutton376,'Value',1) – Waits to run code until the run button on the GUI is activated

%Time valve is delayed
pause on
pause1_1 = str2num(get(handles.edit1,'String'))
pause(pause1_1)

% Time valve is on
numbers = [0:19];
values = zeros(1,20);
values1_1 = [0,1,0,1,0,1,0,1,1,0,0,0,0,0,0,0,0,0,0,0]; - The string of binary numbers to specify a via
ontime = str2num(get(handles.edit2,'String'));
handle = str2num(get(handles.edit427, 'String'));

t0 = clock;
while etime(clock, t0) < ontime;
                [ft_status] = usbio24_set_bits(handle, numbers, values1_1); - This turns the valves off and restores them to their original state
end
[ft_status] = usbio24_set_bits(handle, numbers, values);
```

The multiplexor used to control which channel the flow was directed is displayed below. A 0 represents a closed valve line and a 1 represents an open valve line.

	Valve Lines							
Fluid Channel	**1**	**2**	**3**	**4**	**5**	**6**	**7**	**8**
1	0	1	0	1	0	1	0	1
2	0	1	0	1	0	1	1	0
3	0	1	0	1	1	0	0	1
4	0	1	0	1	1	0	1	0
5	0	1	1	0	0	1	0	1
6	0	1	1	0	0	1	1	0
7	0	1	1	0	1	0	0	1
8	0	1	1	0	1	0	1	0
9	1	0	0	1	0	1	0	1
10	1	0	0	1	0	1	1	0
11	1	0	0	1	1	0	0	1
12	1	0	0	1	1	0	1	0
13	1	0	1	0	0	1	0	1
14	1	0	1	0	0	1	1	0
15	1	0	1	0	1	0	0	1
16	1	0	1	0	1	0	1	0

Since one solenoid valve drives one column of valves, a simple 0 or 1 was need to direct flow of fluid to a specific column. The pause1_1 value grabs the user input and a delay occurs for switching the valves until after the pause has ended. For actuating the valves, the numbers value serves as a placeholder. Values are all zeros to reset and turn off the valves. Ontime value grabs the user input to set the length of time the valves are on. To create a grid of vias, this process is repeated with each via making sure the code

While there is code for the edit boxes, there is no need to edit the existing code. The contents in the edit text are simply pulled for the code in the radiobutton for the via.

```
function edit77_Callback(hObject, eventdata, handles)
% hObject    handle to edit77 (see GCBO)
% eventdata  reserved - to be defined in a future version of MATLAB
% handles    structure with handles and user data (see GUIDATA)

% Hints: get(hObject,'String') returns contents of edit77 as text
%        str2double(get(hObject,'String')) returns contents of edit77 as a double


% --- Executes during object creation, after setting all properties.
function edit77_CreateFcn(hObject, eventdata, handles)
% hObject    handle to edit77 (see GCBO)
% eventdata  reserved - to be defined in a future version of MATLAB
% handles    empty - handles not created until after all CreateFcns called

% Hint: edit controls usually have a white background on Windows.
%       See ISPC and COMPUTER.
if ispc && isequal(get(hObject,'BackgroundColor'), get(0,'defaultUicontrolBackgroundColor'))
    set(hObject,'BackgroundColor','white');
end
```

Lastly, the last three valves in the controller are dedicated to fluid delivery. They are decoupled from the multiplexer so they are able to remain on while the valves are actuating. Otherwise, the code is the same as the first set presented for fluid control without the delay and timing components.

```
% --- Executes on button press in radiobutton375.
function radiobutton375_Callback(hObject, eventdata, handles)
% hObject    handle to radiobutton375 (see GCBO)
% eventdata  reserved - to be defined in a future version of MATLAB
% handles    structure with handles and user data (see GUIDATA)

% Hint: get(hObject,'Value') returns toggle state of radiobutton375
% Time valve is on
numbers = [0:23];
values = zeros(1,24);
values_fluidline3 = [0,0,0,0,0,0,0,0,0,0,0,0,0,0,0,0,0,0,0,0,0,0,1,0];
handle = str2num(get(handles.edit427, 'String'));
[ft_status] = usbio24_set_bits(handle, numbers, values_fluidline3);
```

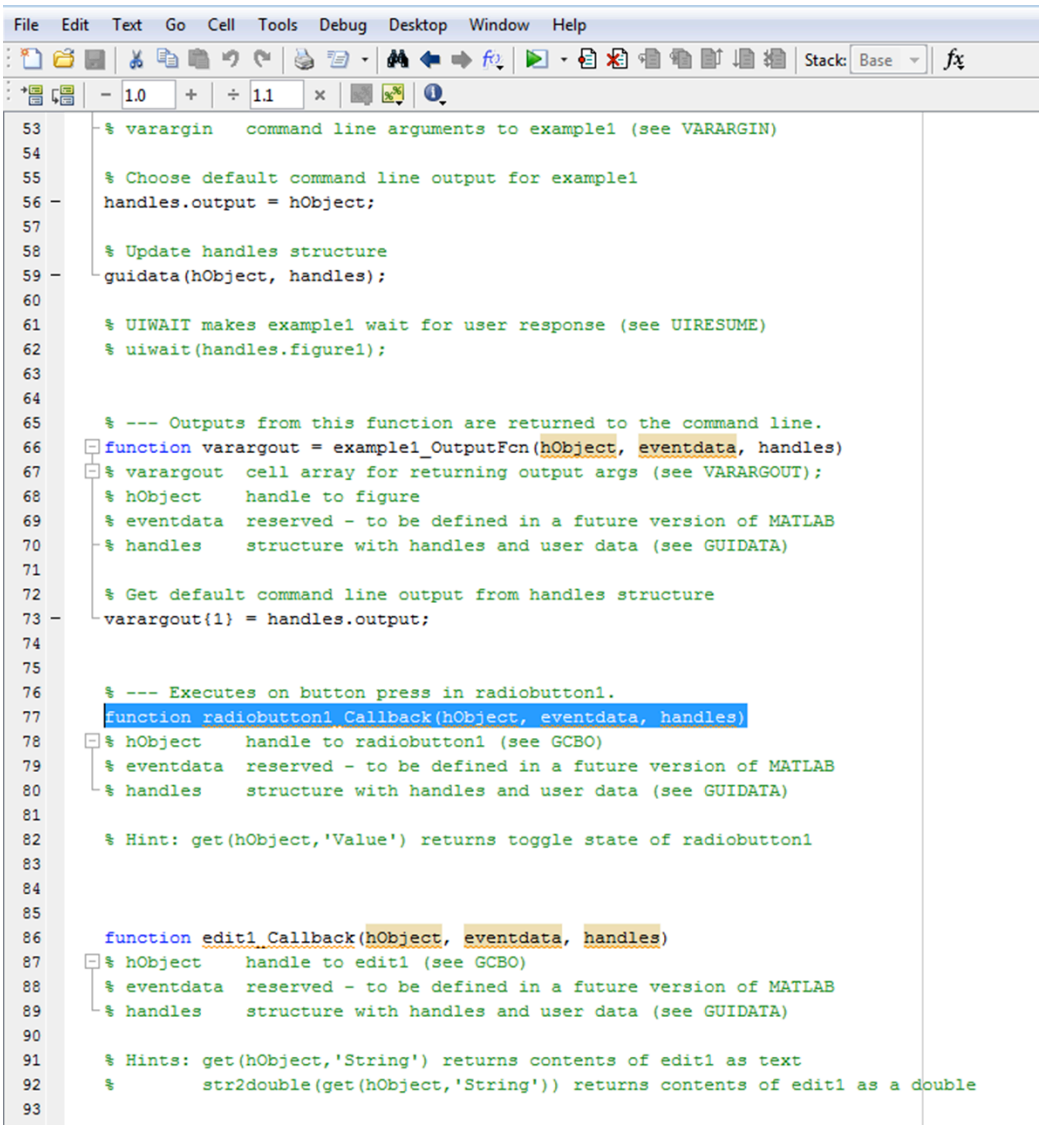

16. Once the coding is finished, press the green play button in the top tool bar to run the GUI.

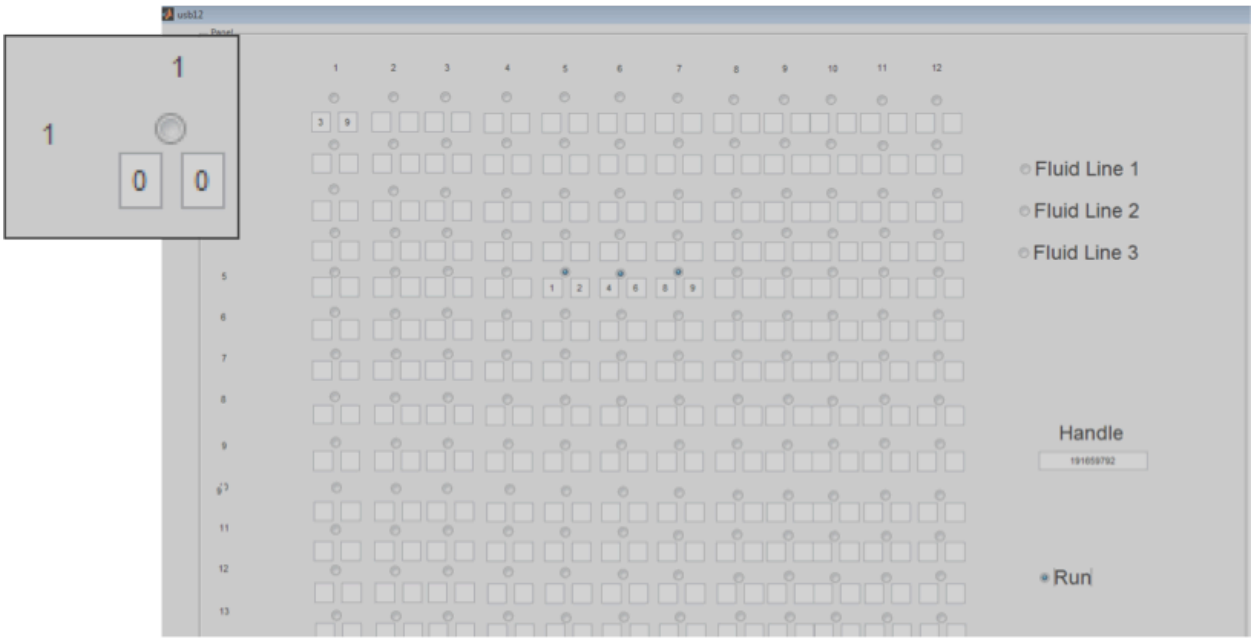

17. Now you are able to start the program. First configure which fluid valves and vias are active and also configure the timing. To activate the valve controller, enter usbio24_open_setup_by_idx.m(0) in the command window. In the workspace, a number will be assigned to the handle. Copy and paste that number into the Handle edit text on the GUI. Once everything is configured, click run to start the valves.

APPENDIX C

Fabrication of the expanded ACDD

1. Mix 35 gram/3.5 grams of the PDMS polymer:curing agent (10:1)and pour into a square polystyrene petri dish (08-757-11A, Fisher Scientific, MA) to a ~4 mm thickness and degas in desiccator. A black sharpie is used to mark the 4 mm mark on the petri dish.

2. Bake the PDMS at 85^{o}C for 90 minutes. This will be the base of the device.

3. Mix 20g/2g of PDMS polymer:curing agent degas and place aside for 1 hour for a thicker consistency.

4. Spincoat the master for the valve layer by placing a quarter-size deposit of PDMS and set the spinner at 1000 RPM with an acceleration of 1 for 30 seconds and cure at 85^{o}C for 90 minutes. It is important that there is a even thin coating of PDMS over the features on the wafer.

5. Cut the whole membrane and gently remove from the wafer and placed on a cutting mat. Be careful not to tear or warp the membrane. A clear transparency can be placed on the membrane before moving for better handling.

6. Use a 14 gauge hole punch to create the inlet and outlet ports for the valves. Flip the membrane over and plasma treated with a corona discharge device. Also plasma treat the previous made 4 mm PDMS slab and bond together. Take care to eliminate the bubbles between the two layers by gently pushing on the bubbles to press the air out.

7. Place bonded valves on hotplate at 85^{o}C for 30 minutes to aid in bonding and then set aside.

8. From the same 20 g premixed PDMS, spincoat the channel layer at 1000 RPM at an acceleration of 1 for 30 seconds.

9. Before curing, use compressed air to remove the PDMS covering the posts and place aside for 30 minutes to allow for the PDMS to reflow for a uniform layer. You will need to check and see if the post are visibly above the PDMS layer before curing to ensure through holes will be made.

10. Cure the PDMS membrane at 85^{o}C for 90 minutes.

11. Silanize the wafer with the channel PDMS membrane. Place the wafer in the desiccator surrounded by four glass slides on each side. Place 50 μL of the silane on each slide and was silanized for 30 minutes. Do not go over the 30 minutes limit since the membrane will become too silanized, and it will be difficult to bond subsequent layers on top.

12. Place the wafer was placed into a petri dish with double-sided tape. Mix, degas, and pour 60 g/6g of the PDMS onto the channel membrane. Degas and bake at 85^{o}C for 90 minutes. Mix another 60 g of PDMS and degas and cure at 85^{o}C for 90 minutes and set aside.

13. Once cured, remove both layers of PDMS together from the wafer with care to prevent the membrane from separating from the larger PDMS slab.

14. With the slab side down, create the inlets and outlets with a 14 gauge hole puncher and set aside.

15. Before plasma treating, take the 24-solenoid valve construct and detach the power source and USB cord from the controller box and valves. Attach a vacuum to all three valve manifold to the

normally open (bottom) port. There should be a vacuum now pulling through all the solenoid valves.

16. Take the second 60g PDMS slab and create all the inlets and outlets with the 14 gauge hole puncher. Use wafers as a guide. Connect the tubing from the valve controller into the PDMS slab. This will quicken the process of establishing a vacuum on the bonded device and skip the process on inserting tubing into each inlet and outlet.

15. Plasma treat the membrane side of the channel layer and the top of valve+PDMS base construct.

16. Align under a macroscope. When aligning, start at the bottom left corner were the multiplexor and the via valves are in view. systematically align up the device and across. Also check to see if the fluid valves on the left side are aligned. Since PDMS is flexible, you can slightly stretch or contract the PDMS slab + membrane to line up with the valve features on the bottom. Align as quick as possible to prevent the valves from bonding.

17. Quickly attach the PDMS slab connected to the vacuum to deflect the valves downwards and prevent bonding.

18. Place the device on a 55^{o}C hotplate with a 3kg weight for 20 minutes to aid bonding.

19. Cycle the vacuum on and off every for 30 minutes for the first 3 hours to prevent the valve from bonding with the bottom of the device. Leave the device was undisturbed overnight.

20. Next, remove the device from the valve controller. Slowly begin to separate the top thick PDMS layer from the channel membrane. Once a small area has been lifted, direct compressed air into this pocket between the thick PDMS layer and channel layer for separation.

21. Once removed, make the inlets, outlets, and a bath chamber in the thick PDMS layer.

22. Plasma treat the top of the channel layer and the bottom of the PDMS bath chamber.

23. As before, the device was placed on a 55^{o}C hotplate for 20 minutes with the chamber side down, and a weight was placed on top. After 24 hours, the device was cut into a desired rectangular shape and was ready to use.

VITA

ELLY SINKALA

EDUCATION

Ph.D. (May 2013) in Bioengineering, The University of Illinois at Chicago, Chicago, IL
Specialty Areas: Microfabrication, Microfluidics, Cell and Tissue Engineering.

B.S. in Biomedical Engineering (2008), Vanderbilt University, Nashville, TN

RESEARCH EXPERIENCE

08/2008 – 3/2013 **The University of Illinois at Chicago**, Chicago, IL

NSF/LSAMP Graduate Research Fellow (2008-2010), Biological Microsystems Laboratory

- Produced a multi-layer automated device for the spatial and temporal control of chemical delivery to cells, tissues, and other constructs.
- Designed a multi-layer microfluidic device for the automated delivery of pheromone for yeast chemotropism studies, producing artificial pheromone gradients to induce directed yeast projections.
- Collaborated with a psychology laboratory to produce a microfluidic flow cell that simplified and improved electrode calibrations for in vivo neurobiology studies and is currently used at eight different institutions with continued interest.
- Developed a simple but novel method to quickly measure oxygen tension of isolated cell clusters in culture.
- Advised several undergraduate students in their own independent projects.

01/2007 – 05/2008 **Vanderbilt University,** Nashville, TN

Undergraduate Research Assistant, Systems Biology and Bioengineering Undergraduate Research Experience

- Utilized microfabrication, microscopy, paramagnetic beads, and MATLAB to measure the adhesion forces of breast cancer cell lines to study the role of E-cadherin cancer metastasis.
- Received 3rd place award for the area of engineering at the Tennessee Academy of Science Research Symposium. Advised several undergraduate students in their

TEACHING EXPERIENCE

08/2012 – 12/2012 **The University of Illinois at Chicago**, Chicago, IL
Teaching Assistant, Introduction to Bioengineering

06/2012 – 07/2012 **Early Outreach Program**, Chicago, IL
Science Teacher, High School Enrichment Program (HSEP)

NATION-WIDE NON-PROFIT MANAGEMENT & LEADERSHIP EXPERIENCE

The Society of Women Engineers, Chicago, IL (10,000+ members)

Graduate Student Conference Committee Member:

- SWE Conference, Houston TX, 2012 – Coordinated and moderated a panel discussion with successful industry-based engineers.
- SWE Conference, Chicago IL, 2011 – Moderated and paneled for several meetings geared towards graduate students at the national conference.

PUBLICATIONS

- **E.Sinkala**, M.E. Brett, M. Sukumar, D. Stone, D.T. Eddington, "A Fully Automated Microfluidic Platform for Gradient Generation in an Agarose Pad for the Study of Yeast Chemotropism" Yeast, In preparation.
- **E.Sinkala**, J.E. McCutcheon, E. Schimdt, M. Schuck, M.F. Roitman, D.T. Eddington (2012) "Electrode Calibration with a Microfluidic Flow Cell for Fast Scan Cyclic Voltammetry", Lab on a Chip, 2(13), 2403-2408.
- J.F. Lo, **E. Sinkala**, and D.T. Eddington (2010) "Oxygen Gradient for Open Well via Microfluidic Substrates", Lab on a Chip, 10(18): 2394-2401.
- **E. Sinkala** and D.T. Eddington (2010) "Oxygen Sensitive Microwells", Lab on a Chip, 10 (23): 2394-2401.
- S.C. Oppegard, **E. Sinkala**, D.T. Eddington (2010) "Fabrication and Operation of an Oxygen Insert for Adherent Cell Cultures." J. Visualized Exp. 35. http://www.jove.com/index/details.stp?id=1695, doi:10.3791/1695.

CONFERENCES

- E. Sinkala, D.T. Eddington, "A microfluidic device for the automated delivery of chemicals to brain slices and other tissues", Biomedical Engineering Society (BMES), Atlanta, GA October 24-27, 2012.
- E. Sinkala, J.E. McCutcheon, M.F. Roitman, D.T. Eddington "Electrode Calibration with a Microfluidic Flow Cell for Fast Scan Cyclic Voltammetry", Society for Lab Automation and Screening (SLAS), San Diego, CA February 5-8, 2012.
- E. Sinkala, D.T. Eddington "Oxygen-Sensitive Microwells" Biomedical Engineering Society (BMES), Austin, TX, October 7-10, 2010.
- E. Sinkala, D.T. Eddington "Polystrene Microwells for Cellular Isolation" Lab Automation, Palm Springs, CA, January 23-27, 2010.
- E. Sinkala, D.T. Eddington "Micropatterned Thin Polystyrene Films for Single Cell Culture", Biomedical Engineering Society, Pittsburgh, PA, October 7-10, 2009.

FELLOWSHIPS, SCHOLARSHIPS, & AWARDS

NATIONAL SCIENCE FOUNDATION
Bridge to the Doctorate Fellowship (2008-2010)

SCREENING AND LABORATORY AUTOMATION SOCIETY
Tony B. Academic Travel Award (2011)

THE UNIVERSITY OF ILLINOIS AT CHICAGO
Graduate College Academic Travel Award(2012)
Outstanding Achievement in Academics and Research – BD Program (2011)

Graduate College Academic Travel Award (2010)

SKILLS

LABORATORY & ANALYTICAL:
Microfabrication
Microscopy: fluorescence,
Mammalian cell culture
Animal models (mice): IACUC protocols, brain slice preparation

SOFTWARE:
MATLAB, AutoCAD, ProE, LabVIEW